

# Occupied Processes: Going with the Flow

Valentin Tissot-Daguette\*

Quantitative Research, Office of the CTO, Bloomberg

October 14, 2025

## Abstract

A stochastic process  $X$  becomes *occupied* when it is enlarged with its occupation flow  $\mathcal{O}$ , which tracks the time spent by the path at each level. Crucially, the occupied process  $(\mathcal{O}, X)$  enjoys a Markov structure when  $X$  is Markov. We develop a novel Itô calculus for occupied processes that lies midway between Dupire's functional Itô calculus and the classical version. We derive a surprisingly simple Itô formula and, through Feynman-Kac, unveil a broad class of path-dependent PDEs where  $\mathcal{O}$  plays the role of time. The space variable, given by the current value of  $X$ , remains finite-dimensional, thereby paving the way for standard elliptic PDE techniques and numerical methods.

In the financial applications, we demonstrate that occupation flows provide unified Markovian lifts for exotic options and variance instruments, allowing financial institutions to price and manage derivatives books with a single numerical solver. We then explore avenues in financial modeling where volatility is driven by the occupied process. In particular, we propose the local occupied volatility (LOV) model which not only calibrates to European vanilla options but also offers the flexibility to capture stylized facts of volatility or fit other instruments. We also present an extension of forward variance models that leverages the entire forward occupation surface.

**Keywords:** Occupation flow, Itô calculus, exotic derivatives, variance instruments, path-dependent volatility

**MSC (2020):** 60J55, 60J25, 60H30, 60G40, 91G20

**Acknowledgments.** I would like to thank Bruno Dupire, Ibrahim Ekren, Julien Guyon, Yuxing Huang, Thibault Jeannin, Bryan Liang, Jin Ma, Alexandre Pannier, Mete Soner, Nizar Touzi, Jianfeng Zhang, and Xin Zhang for stimulating discussions. My gratitude goes also to two anonymous referees for their feedback and interesting ideas.

---

\*Email: vtissotdague@bloomberg.net. Research supported by the 2022-2023 and 2023-2024 Bloomberg Quantitative Finance Ph.D. Fellowship.

# Contents

<b>1</b>	<b>Introduction</b>	<b>3</b>
1.1	Contributions . . . . .	4
1.2	Applications . . . . .	5
<b>2</b>	<b>Occupied Processes</b>	<b>6</b>
2.1	Calendar Time Occupation Flow . . . . .	7
2.2	Occupation Flow Dynamics . . . . .	7
2.3	Occupation Functional and Markov Property . . . . .	8
2.4	Metrics on Space of Measures . . . . .	9
<b>3</b>	<b>Itô Calculus</b>	<b>9</b>
3.1	Occupation Derivative . . . . .	9
3.2	Itô's Formula . . . . .	12
3.3	Feynman-Kac's Formula for the Backward Heat Equation . . . . .	14
3.4	Occupied SDEs and Dirichlet Problems . . . . .	15
<b>4</b>	<b>Unified Markovian Lift of Financial Instruments</b>	<b>18</b>
4.1	Exotic Options and Structured Products . . . . .	18
4.2	Variance Derivatives . . . . .	21
<b>5</b>	<b>Occupied Volatility</b>	<b>23</b>
5.1	Simulation of Occupied SDEs . . . . .	25
5.2	Local Occupied Volatility (LOV) Model . . . . .	26
5.3	Market Implied Occupation Sensitivity . . . . .	31
5.4	Joint Calibration . . . . .	35
<b>6</b>	<b>Forward Occupation Models</b>	<b>36</b>
6.1	Dynamics of Forward Occupation Flows . . . . .	37
<b>7</b>	<b>Stopping Spot Local Time</b>	<b>39</b>
7.1	Optimal Stopping . . . . .	39
7.2	Spot Local Time and Early Exercise Premium . . . . .	40
7.3	Numerical Resolution in the case $\mathcal{T} = [0, T]$ . . . . .	42
7.4	Shrinking the Corridor . . . . .	43
<b>A</b>	<b>Chronology Invariance</b>	<b>45</b>
<b>B</b>	<b>Proofs</b>	<b>47</b>
B.1	Theorem 3.1 . . . . .	47
B.2	Proposition 4 . . . . .	48
B.3	Theorem 3.2 . . . . .	48
B.4	Theorem 3.3 . . . . .	49
B.5	Proposition 7 . . . . .	51
B.6	Proposition 8 . . . . .	51

<b>C</b>	<b>Algorithms</b>	<b>52</b>
	C.1 Least Square Monte Carlo for Spot Local Time . . . . .	52

## 1 Introduction

This work originates from an identity in Revuz and Yor [75, Chapter VI],

$$\sup_x L_T^x = \sup_{t \leq T} L_t^{X_t}, \quad (1)$$

where  $X$  is Brownian motion and  $L^x$  its local time process at  $x$ . We refer to  $L_t^{X_t}$  as the *spot local time*. To prove (1), let  $x^*$  be a maximizer<sup>1</sup> of  $x \mapsto L_T^x$  and define the random time  $\tau^* = \sup\{t \leq T \mid X_t = x^*\}$ . Then  $\sup_x L_T^x = L_{\tau^*}^{X_{\tau^*}}$ , which shows that  $\sup_x L_T^x \leq \sup_{t \leq T} L_t^{X_t}$ . The reversed inequality is immediate. One question arises: what if the anticipative strategy  $\tau^*$  is replaced by stopping times? I.e., what is the optimal rule and value of the optimal stopping (OS) problem,

$$\sup\{\mathbb{E}[L_{\tau}^{X_{\tau}}] : \tau = \text{stopping time}\} \quad (2)$$

To our best knowledge, there is no definitive approach in the literature to tackle stochastic control or optimal stopping problems involving local times as in (2). Our work addresses this by recovering a Markovian framework in these situations, classically leading to considerable simplifications [45, 72]. This is achieved by exploiting the fact that for continuous semimartingales, the local time field  $(L_t^x)_{x \in \mathbb{R}}$  is the Radon-Nikodym derivative of the occupation measure of  $X$ ,

$$\mathcal{O}_t(A) = \int_0^t \mathbb{1}_A(X_s) d\langle X \rangle_s, \quad A = \text{Borel set of } \mathbb{R}. \quad (3)$$

See [50], [75, Chapter VI], and Section 2. The *occupation flow*  $\mathcal{O} = (\mathcal{O}_t)_{t \geq 0}$  is a measure-valued process adapted to the filtration of  $X$ . Moreover, the *occupied process*  $(\mathcal{O}, X)$  is Markov provided that  $X$  is Markov.

The goal of this work is to develop a differential calculus for occupied processes and demonstrate its relevance and practicality. The study of occupied processes strikes a middle ground between the classical Itô calculus and the fully path-dependent setting introduced by Dupire [40] (see also [25, 26]). We shall see throughout that numerous examples in mathematical finance and stochastic analysis fit into our framework. Moreover, the occupation measure gives rise to nice structural and regularity properties otherwise unavailable in pathwise calculi.

Introduced by Dawson [32, 33] and Fleming and Viot [47], measure-valued processes have gained increasing attention recently, e.g., in mean field games and McKean-Vlasov controls [21, 22, 66, 79, 80], robust pricing and hedging [27, 28], and infinite-dimensional polynomial diffusions [30, 31]. The measure may represent the marginal law of a process or a conditional distribution which concentrates as the filtration unfolds [27, 28]. Either way, the process takes values in a suitable subspace of probability measures. In contrast,  $\mathcal{O}$  evolves in the convex cone  $\mathcal{M}$  of finite positive measures. The meaning behind the occupation measure also greatly differs from flows of distributions: it is a pathwise object whose total mass increases

---

<sup>1</sup>The maximum is achieved since  $x \mapsto L_T^x$  has compact support and admits a continuous version [75, Chapter VI].

with the passage of time. Besides, occupation measures can be added to one another. To study occupation functionals, this presents a clear advantage over working in the path space, deprived of vector space structure.

The study of functionals of occupied processes and their dynamics appears to be new. In fact, the occupation flow is rarely the main object of interest and comes rather as a tool. Let us mention the use of the expected occupation measures to formulate relaxed optimal stopping or stochastic control problems [13, 18, 46]. In contrast, the occupation flow is herein given at the outset, and may directly appear in the objective function of control problems as exemplified by the optimal stopping problem (2). Moreover, local times may control the dynamics of the system, as shown in the recent work by Béthencourt et al. [12] which adopted the framework developed here. The control problem considered therein relates to the evolution of filamentous fungi [83, 16] offering another promising line of application for occupied processes. For the theoretical foundation of controlled occupied processes, we refer the interested reader to our companion paper [78]

## 1.1 Contributions

In Theorem 3.1, we generalize Itô's formula to *occupation functionals*  $f(\mathcal{O}_t, X_t)$  and discover, to our fortunate surprise, that the expression is almost identical to the classical case. The only difference is that the time derivative in Itô's formula for functions  $f(t, X_t)$  is replaced by the *occupation derivative*  $\partial_{\mathfrak{o}}f(\mathcal{O}_t, X_t) = \delta_{\mathfrak{o}}f(\mathcal{O}_t, X_t)(X_t)$  where  $\delta_{\mathfrak{o}}$  is the linear derivative [21, Chapter 2] and  $\mathfrak{o}$  is the occupation flow variable which takes values in the space  $\mathcal{M}$  of finite measures. The projection of  $\delta_{\mathfrak{o}}f(\mathcal{O}_t, X_t) \in \mathcal{C}(\mathbb{R})$  onto the spot  $X_t$  comes from the singular dynamics of the occupation measure  $d\mathcal{O}_t = \delta_{X_t}d\langle X \rangle_t$ , where  $\delta_x$  denotes the Dirac mass at  $x$ . We are then able to extend Itô's formula in Theorem 3.1 to occupied continuous semimartingales, namely

$$df(\mathcal{O}_t, X_t) = \left( \partial_{\mathfrak{o}} + \frac{1}{2} \partial_{xx} \right) f(\mathcal{O}_t, X_t) d\langle X \rangle_t + \partial_x f(\mathcal{O}_t, X_t) dX_t. \quad (4)$$

To compare the above formula with other Itô calculi, we shall introduce the *calendar time occupation flow*  $\tilde{\mathcal{O}}(A) = \int_0^{\cdot} \mathbb{1}_A(X_s) ds$ , leading to the more familiar expression

$$df(\tilde{\mathcal{O}}_t, X_t) = \partial_{\mathfrak{o}}f(\tilde{\mathcal{O}}_t, X_t) dt + \frac{1}{2} \partial_{xx}f(\tilde{\mathcal{O}}_t, X_t) d\langle X \rangle_t + \partial_x f(\tilde{\mathcal{O}}_t, X_t) dX_t. \quad (5)$$

We can then show that (5) is consistent with Dupire's *functional Itô formula* [40] and the classical one. Precisely, the occupation derivative  $\partial_{\mathfrak{o}}$  replaces the (functional) time derivative. We then apply Itô's formula in the case where  $(\mathcal{O}, X)$ ,  $(\tilde{\mathcal{O}}, X)$  is solution of *occupied* stochastic differential equations (OSDEs),

$$dX_t = b(\mathcal{O}_t, X_t) dt + \sigma(\mathcal{O}_t, X_t) dW_t, \quad d\mathcal{O}_t = \delta_{X_t} \sigma(\mathcal{O}_t, X_t)^2 dt \quad (6)$$

$$dX_t = b(\tilde{\mathcal{O}}_t, X_t) dt + \sigma(\tilde{\mathcal{O}}_t, X_t) dW_t, \quad d\tilde{\mathcal{O}}_t = \delta_{X_t} dt \quad (7)$$

where their wellposedness is proved in Section 3.4. OSDE (7) shares similarities with *self-interacting diffusions* [41, 29, 73, 9, 6, 7, 8] where the drift uses the calendar time occupation flow to create mean reversion of repulsion. See also the discussion in Section 3.4.

If  $f$  in (5) is given by  $f(\tilde{\mathcal{O}}_t, X_t) = \mathbb{E}^{\mathbb{Q}}[\varphi(\tilde{\mathcal{O}}_T, X_T) | \mathcal{F}_t]$  where  $(\tilde{\mathcal{O}}, X)$  evolves according to (7), we then obtain by Feynman-Kac's formula (Theorem 3.6) that  $f$  solves the backward

PDE (possibly in a weak sense)

$$\left(\partial_{\mathfrak{o}} + b\partial_x + \frac{\sigma^2}{2}\partial_{xx}\right)u(\mathfrak{o}, x) = 0, \quad \mathfrak{o}(\mathbb{R}) < T, \quad u(\mathfrak{o}, x) = \varphi(\mathfrak{o}, x), \quad \mathfrak{o}(\mathbb{R}) = T. \quad (8)$$

Under the stochastic clock  $\mathcal{O}_t(\mathbb{R}) = \langle X \rangle_t$ , one obtains a Dirichlet problem instead; see Theorem 3.5. We can therefore recast a large class of path-dependent PDEs involving the occupation derivative  $\partial_{\mathfrak{o}}$  in lieu of the usual time derivative  $\partial_t$ . As the space derivatives in (8) are the classical ones, classical results in viscosity theory can be leveraged to study a large class of (possibly nonlinear) path-dependent PDEs; see the accompanying paper [78].

Proving the regularity of solutions of path-dependent PDEs is notoriously hard [44, 71] (see also [85, Chapter 11]) and still a subject of active research. In a recent work, Bouchard and Tan [17] study linear parabolic PPDEs for functionals depending on  $X_t$  and  $I_t = \int_0^t X_s dA_s$  for some continuous function  $A$  of finite variation. Note that their setting relates to ours as the integral process  $I$  can be retrieved from the occupation measure in some situations. Indeed, if  $A_t := \langle X \rangle_t$  is deterministic (e.g., when  $X$  is a Gaussian martingale) and fulfills the conditions in [17], then  $I_t = \int_{\mathbb{R}} x \mathcal{O}_t(dx)$ .

The choice of state enlargement is critical for path-dependent problems as it determines whether the resulting Markovian representation of conditional expectations is both regular and numerically tractable; see, e.g., Viens and Zhang [84] for Gaussian Volterra processes or the *Better Asian PDE* example in Dupire [40]. While one may introduce the path functional,

$$v(t, \omega) = \mathbb{E}^{\mathbb{Q}}[\varphi(\mathcal{O}_T, X_T) | \mathcal{F}_t](\omega), \quad \omega \in \mathcal{D}([0, T], \mathbb{R}),$$

which trivially induces a Markovian framework, this approach is often impractical. Moreover, the continuity in  $\omega$  of  $v$  is typically not guaranteed: we shall see in Example 6, related to spot local times, that  $v$  is discontinuous in the input path while  $v$  is smooth. This further supports choosing a more adequate Markovian lift, such as  $(\mathcal{O}, X)$ .

## 1.2 Applications

Sections 4, 5, and 6 are dedicated to financial applications. We shall see that the occupation measure is ever-present, particularly in the eponymous occupation time derivatives [34, 62, 24], timer options, and corridor variance swaps. Other examples include Asian options contingent upon the running average, or Parisian options depending on the time spent by the asset above/below a barrier [24, 62]. It is a challenge for financial institutions to consistently price and manage complex derivatives books, and we show in 4 that occupation flows offer a unified framework for this task.

We then explore application of occupied processes in volatility modeling. In Section 5, we introduce the *local occupied volatility* (LOV) model that lies conveniently between local volatility [38] and path-dependent volatility [52, 53, 56, 59]. By design, this model guarantees a perfect fit to market prices of European vanilla options while providing additional flexibility to capture stylized facts of volatility or calibrate to other instruments such as VIX, barrier, and American options. We also propose a generalization of forward variance models in Section 6, opening the doors to *nonlinear* variance instruments contingent on the floating leg of corridor variance swaps.

The spot local time OS problem (2) is at last analyzed in Section 7. After extending standard tools in optimal stopping to our context, we shed light in Section 7.3 on the numerical resolution of (2) by demonstrating a least square Monte Carlo approach similar to

[69]. The stopping of spot local time reveals great numerical challenges and comes as a novel benchmark for numerical methods solving path-dependent OS problems such as [2, 3, 4].

## 2 Occupied Processes

We restrict ourselves to one space dimension to simplify the exposition. Let  $\lambda$  be the Lebesgue measure on  $\mathbb{R}$ . We may write  $\int f d\lambda$  or  $\int f(x)dx$ , whichever is more convenient. We also write  $\mathcal{B}(\mathbb{R})$  for the Borel  $\sigma$ -algebra on  $\mathbb{R}$  and  $\mathcal{M}$  for the set of finite, positive Borel measures on  $\mathbb{R}$ . Given  $\mu \in \mathcal{M}$ ,  $\int_A f d\mu = \frac{1}{\mu(A)} \int_A f d\mu$  denotes the average of  $f$  with respect to  $\mu$  inside  $A \in \mathcal{B}(\mathbb{R})$ . We write  $B_\varepsilon = (-\varepsilon, \varepsilon)$  for the open ball of radius  $\varepsilon$  centered at the origin and  $B_\varepsilon(x) = x + B_\varepsilon$ . Finally,  $\text{int}A$ ,  $\partial A$ ,  $\bar{A}$  denote the interior, boundary, and closure of a set  $A$ , respectively.

Let  $X$  be a real-valued continuous semimartingale on a probability space  $(\Omega, \mathcal{F}, \mathbb{F}, \mathbb{Q})$  where  $\mathbb{F} = (\mathcal{F}_t)_{t \geq 0}$  is the natural filtration of  $X$ . The *occupation measure of  $X$*  at  $t \geq 0$  is defined as

$$\mathcal{O}_t(\omega) : \mathcal{B}(\mathbb{R}) \rightarrow \mathbb{R}, \quad \mathcal{O}_t(\omega)(A) = \int_0^t \mathbf{1}_A(X_s) d\langle X \rangle_s(\omega), \quad A \in \mathcal{B}(\mathbb{R}), \quad \omega \in \Omega. \quad (9)$$

Unless stated otherwise, we omit the dependence on  $\omega$  throughout and write  $\mathcal{O}_t(A)$  for the random variable  $\omega \mapsto \mathcal{O}_t(\omega)(A)$ .

**Definition 1.** The collection of occupation measures  $\mathcal{O} = (\mathcal{O}_t)_{t \geq 0}$  is called the *occupation flow of  $X$* . Moreover, the pair  $(\mathcal{O}, X)$  is an *occupied process*, and takes values in the product space  $\mathcal{D} := \mathcal{M} \times \mathbb{R}$ .

The occupation flow can also be regarded as a measure-valued process; see [32, 33, 47].

**Proposition 1.** *The occupation flow  $\mathcal{O}$  satisfies the following properties.*

I. (Strong Time Additivity) *For all stopping times  $\varsigma \leq \tau$  and  $A \in \mathcal{B}(\mathbb{R})$ ,*

$$\mathcal{O}_\tau(A) = \mathcal{O}_\varsigma(A) + \mathcal{O}_{\varsigma, \tau}(A), \quad \mathbb{Q} - a.s., \quad (10)$$

*with the incremental flow  $\mathcal{O}_{\varsigma, \tau}(A) := \int_\varsigma^\tau \mathbf{1}_A(X_s) d\langle X \rangle_s$ .*

II. (Absolute Continuity)  $\mathcal{O}_t \ll \lambda$   $\mathbb{Q} - a.s.$ , *where  $\lambda$  is the Lebesgue measure on  $\mathbb{R}$ .*

III. (Occupation Time Formula) *For every Borel function  $\phi : \mathbb{R} \rightarrow \mathbb{R}_+$ ,*

$$\int_0^t \phi(X_s) d\langle X \rangle_s = \int_{\mathbb{R}} \phi(x) \mathcal{O}_t(dx). \quad (11)$$

*Proof.* See I. [75, X]; II. [75, VI] or [50]; III. [75, VI]. □

The Radon-Nikodym derivative of  $\mathcal{O}_t$  is the *local time field*  $L_t = (L_t^x)_{x \in \mathbb{R}}$ ,

$$L_t^x = \frac{d\mathcal{O}_t}{d\lambda}(x) = \lim_{\varepsilon \rightarrow 0} \frac{1}{2\varepsilon} \int_0^t \mathbf{1}_{B_\varepsilon(x)}(X_s) d\langle X \rangle_s. \quad (12)$$

Evidently, the (strong) time additivity of  $\mathcal{O}$  carries over to  $L$ , that is  $L_\tau = L_\varsigma + L_{\varsigma, \tau}$  with  $L_{\varsigma, \tau} := \frac{d\mathcal{O}_{\varsigma, \tau}}{d\lambda}$  for all stopping times  $\varsigma \leq \tau$ . The local time is in fact central in the theory

of *additive functionals* [14], [75, Chapter X]. For local martingales, it is well-known that the process  $L_t = (L_t^x)_{x \in \mathbb{R}}$  (indexed by  $x$ ) admits a version that is  $\alpha$ -Hölder continuous for all  $\alpha < 1/2$ . For general semimartingales,  $x \mapsto L_t^x$  may only be shown to be càdlàg [75, Chapter VI]. Finally, note that  $\mathcal{O}_t(\mathbb{R}) = \langle X \rangle_t$ , i.e., the total mass of  $\mathcal{O}$  coincides with the stochastic clock of  $X$ .

Introduce also the space of compactly supported, absolutely continuous Borel measures,

$$\mathcal{M}^\lambda = \left\{ \mathfrak{o} \in \mathcal{M} : \mathfrak{o} \ll \lambda \text{ and } \frac{d\mathfrak{o}}{d\lambda} : \mathbb{R} \rightarrow \mathbb{R} \text{ has compact support} \right\}. \quad (13)$$

Clearly,  $\mathcal{O}_t \in \mathcal{M}^\lambda$   $\mathbb{Q}$ -a.s. from Proposition 1 II. and the compactness of  $\{X_s : s \leq t\} = \text{supp}(\mathcal{O}_t)$  as  $X$  is continuous. Note that  $\mathcal{M}^\lambda$  and  $\mathcal{M}$  are convex cones. In particular, occupation measures can be added to one another. This vector space structure is advantageous over a pathwise setting where the addition of paths on different horizons cannot be reasonably defined.

## 2.1 Calendar Time Occupation Flow

Let us also introduce the *calendar time occupation flow*,

$$\tilde{\mathcal{O}}_t(A) := \int_0^t \mathbf{1}_A(X_s) ds, \quad A \in \mathcal{B}(\mathbb{R}), \quad t \in [0, T], \quad (14)$$

and *calendar time occupied process*  $(\tilde{\mathcal{O}}, X)$ . Note that  $\tilde{\mathcal{O}}$  also satisfies properties I., III. in Proposition 1, but not II (absolute continuity). Indeed,  $\tilde{\mathcal{O}}$  may generate atoms if  $X$  is constant on a time interval of positive length. Hence  $\tilde{\mathcal{O}}_t \in \mathcal{M} \setminus \mathcal{M}^\lambda$  in general, so there may not exist an associated local time process. On the other hand, the calendar time occupation measure is well-defined for paths of any roughness and nontrivial for smooth trajectories. Therefore,  $\tilde{\mathcal{O}}$  is more universal than  $\mathcal{O}$  and may be preferred in some applications; see Sections 4.1 and Section 5.

## 2.2 Occupation Flow Dynamics

By definition, the flows  $\mathcal{O}$ ,  $\tilde{\mathcal{O}}$  gradually accumulate some mass at the levels visited by  $X$ . As the latter is assumed to be continuous, the flow is therefore expected to only increase in a neighborhood the current value  $X_t$  (or in financial terms, the *spot*) within a short time window. Indeed, for all  $s > t$ , the incremental flow  $\mathcal{O}_{t,s}(A) = \int_t^s \mathbf{1}_A(X_u) d\langle X \rangle_u$  is supported on the range  $\{X_u : u \in [t, s]\}$  which shrinks to  $\{X_t\}$  as  $s \downarrow t$ . Consequently, the probability measures

$$A \mapsto \frac{\mathcal{O}_{t,s}(A)}{\mathcal{O}_{t,s}(\mathbb{R})} = \frac{\int_t^s \mathbf{1}_A(X_u) d\langle X \rangle_u}{\int_t^s d\langle X \rangle_u} \in [0, 1],$$

converge weakly to the Dirac mass  $\delta_{X_t}$  when  $s \downarrow t$ . Hence  $\mathcal{O}_{t,s} \approx \delta_{X_t} \int_t^s d\langle X \rangle_u$ , leading finally to the dynamics

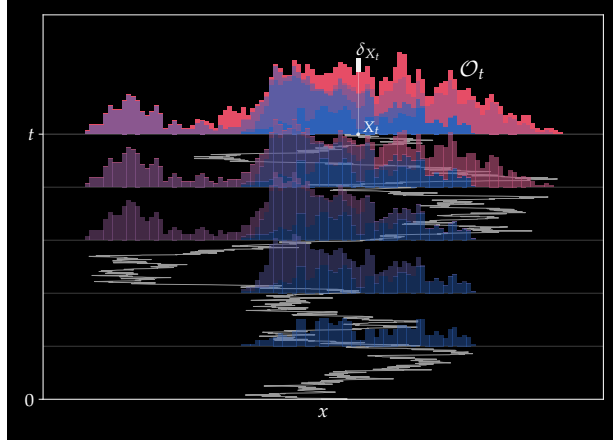
$$d\mathcal{O}_t = \delta_{X_t} d\langle X \rangle_t. \quad (15)$$

Alternatively, observe that  $d\mathcal{O}_t(A) = \mathbf{1}_A(X_t) d\langle X \rangle_t$  from the definition of  $\mathcal{O}$  and  $\mathbf{1}_A(X_t) = \delta_{X_t}(A)$  for all  $A \in \mathcal{B}(\mathbb{R})$ . Similarly, the calendar time occupation flow evolves according to

$$d\tilde{\mathcal{O}}_t = \delta_{X_t} dt, \quad (16)$$

Occupation flows thus admit singular dynamics that involves a Dirac impulse at the current level. See Fig. 1.

Figure 1: Occupation flow  $\mathcal{O}$  and its dynamics  $d\mathcal{O}_t = \delta_{X_t} d\langle X \rangle_t$ .



### 2.3 Occupation Functional and Markov Property

An *occupation functional* is a map  $f : \mathcal{D} \rightarrow \mathbb{R}$ ,  $(\mathfrak{o}, x) \mapsto f(\mathfrak{o}, x)$ . Naturally, we are interested in plugging in occupied processes and studying properties of  $f(\mathcal{O}_t, X_t)$  or  $f(\tilde{\mathcal{O}}_t, X_t)$ . We stress that occupation functionals do not explicitly depend on the time variable. This is because occupation flows play the same role as time. This simplification will reveal its grace in Section 3.

**Proposition 2.** *Let  $X$  be a strong Markov process. Then the occupied processes  $(\mathcal{O}, X)$ ,  $(\tilde{\mathcal{O}}, X)$  are strong Markov as well.*

*Proof.* This follows from the strong time additivity of the occupation measure (Proposition 1 I): for all stopping times  $0 \leq \tau \leq \varsigma \leq T$  and occupation functional  $f : \mathcal{D} \rightarrow \mathbb{R}$ ,

$$\mathbb{E}^{\mathbb{Q}}[f(\mathcal{O}_{\varsigma}, X_{\varsigma}) \mid \mathcal{F}_{\tau}] = \mathbb{E}^{\mathbb{Q}}[f(\mathcal{O}_{\tau} + \mathcal{O}_{\tau, \varsigma}, X_{\varsigma}) \mid \mathcal{F}_{\tau}] = \mathbb{E}^{\mathbb{Q}}[f(\mathcal{O}_{\varsigma}, X_{\varsigma}) \mid (\mathcal{O}_{\tau}, X_{\tau})],$$

noting that  $\mathcal{O}_{\tau, \varsigma}$  (and  $X_{\varsigma}$ ) is conditionally independent of  $\mathcal{F}_{\tau}$  given  $X_{\tau}$ . The same arguments apply to the calendar time occupied process.  $\square$

**Remark 1.** Suppose that  $X$  is a continuous local martingale with Dambins-Dubins-Schwartz (DDS) Brownian motion

$$W_{\theta} := X_{\tau_{\theta}}, \quad \tau_{\theta} = \inf\{t \in [0, T] : \langle X \rangle_t > \theta\}, \quad \theta \leq \Theta := \langle X \rangle_T,$$

or conversely  $X_t = W_{\theta_t}$ ,  $\theta_t := \langle X \rangle_t$ . If  $\mathcal{O}^X$  (respectively  $\mathcal{O}^W$ ) denotes the occupation flow of  $X$  (resp.  $W$ ), it is easily seen that  $\mathcal{O}_t^X(\omega) = \mathcal{O}_{\theta_t}^W(\omega)$  for all  $\omega \in \Omega$ . In particular, for every  $\mathbb{F}$ -stopping time  $\tau$ , and functional  $f : \mathcal{D} \rightarrow \mathbb{R}$ ,

$$f(\mathcal{O}_{\tau}^X, X_{\tau}) = f(\mathcal{O}_{\theta_{\tau}}^W, W_{\theta_{\tau}}). \quad (17)$$

Note that  $\theta_{\tau}$  is a stopping time under the Brownian filtration  $\mathbb{F}^W = (\mathcal{F}_{\tau_{\theta}})_{\theta \leq \Theta}$ . This observation will be particularly useful in Section 7 to derive simple formulation of optimal stopping problems. See also [72, Chapter IV].

## 2.4 Metrics on Space of Measures

In connection with local time, we introduce

$$\mathbf{m}_p(\mathfrak{o}, \mathfrak{o}') := \|\mathfrak{o} - \mathfrak{o}'\|_p, \quad \|\mathfrak{o}\|_p := \left\| \frac{d\mathfrak{o}}{d\lambda} \right\|_{L^p(\mathbb{R})}, \quad \mathfrak{o}, \mathfrak{o}' \in \mathcal{M}^\lambda, \quad p \in [1, \infty]. \quad (18)$$

Since  $\frac{d\mathfrak{o}}{d\lambda}$  is bounded and compactly supported for each  $\mathfrak{o} \in \mathcal{M}^\lambda$ , we gather that  $\|\mathfrak{o}\|_p < \infty \forall p \in [1, \infty]$ . Note that the distance between any two measures  $\mathcal{M}^\lambda$  makes sense irrespective of their respective total mass. This is particularly convenient when comparing the occupation measure at different times, to wit,

$$\mathbf{m}_p(\mathcal{O}_s, \mathcal{O}_t) = \|\mathcal{O}_{s,t}\|_p = \|L_{s,t}\|_{L^p(\mathbb{R})}, \quad s < t.$$

Important values for  $p$  are  $p \in \{1, \infty\}$ . First,  $\mathbf{m}_1$  coincides with the total variation distance of finite measures, so it can be extended to  $\mathcal{M}$  and used for the calendar time occupation flow as well. Moreover, for all  $s \leq t$ ,  $\mathbf{m}_1(\mathcal{O}_s, \mathcal{O}_t) = \|\mathcal{O}_{t-s}\|_1$  is conveniently the total mass of  $\mathcal{O}_{t-s}$ . For these reasons, we shall endow  $\mathcal{M}^\lambda$  (and  $\mathcal{M}$ ) with  $\mathbf{m}_1$  when establishing Itô's formula in Section 3. Second, the supremum distance  $\mathbf{m}_\infty$  is pivotal to the spot local time in Section 7. Indeed, a strong metric is required to guarantee the continuity of  $\mathfrak{o} \mapsto \varphi(\mathfrak{o}, x) = \frac{d\mathfrak{o}}{d\lambda}(x)$  (hence  $\varphi(\mathcal{O}_t, X_t) = L_t^{X_t}$ ). We also note that  $\|\mathcal{O}_t\|_\infty = \sup_{x \in \mathbb{R}} L_T^x$ , which admits well-known bounds in  $L^p(\mathbb{Q})$ ; see [75, XI], [1], and references therein.

Besides, we shall use in Section 3.4 the *bounded Lipschitz distance* [58] to prove the existence and uniqueness of solutions of *occupied* stochastic differential equations SDEs. This metric proves more suitable than  $\mathbf{m}_p$  due to its dual representation.

## 3 Itô Calculus

### 3.1 Occupation Derivative

We seek a suitable differential operator, say  $\delta_{\mathfrak{o}} : \mathcal{C}^1(\mathcal{M}) \rightarrow \mathcal{C}(\mathbb{R})$ , with the class  $\mathcal{C}^1(\mathcal{M})$  still to be defined, such that  $f(\mathcal{O}_t)$  satisfies the chain rule

$$df(\mathcal{O}_t) = \delta_{\mathfrak{o}} f(\mathcal{O}_t) \cdot d\mathcal{O}_t, \quad f \in \mathcal{C}^1(\mathcal{M}), \quad (19)$$

where  $\cdot$  denotes the dual pairing

$$\phi \cdot \mathfrak{o} := \int_{\mathbb{R}} \phi(x) \mathfrak{o}(dx), \quad \phi : \mathbb{R} \rightarrow \mathbb{R}, \quad \mathfrak{o} \in \mathcal{M}. \quad (20)$$

From the occupation flow dynamics  $d\mathcal{O}_t = \delta_{X_t} d\langle X \rangle_t$  (Section 2.2), note that

$$df(\mathcal{O}_t) = \delta_{\mathfrak{o}} f(\mathcal{O}_t) \cdot d\mathcal{O}_t = \delta_{\mathfrak{o}} f(\mathcal{O}_t) \cdot \delta_{X_t} d\langle X \rangle_t = \delta_{\mathfrak{o}} f(\mathcal{O}_t)(X_t) d\langle X \rangle_t. \quad (21)$$

It is natural to impose that (21) holds for all linear maps  $f(\mathfrak{o}) = \phi \cdot \mathfrak{o}$ ,  $\phi \in \mathcal{C}(\mathbb{R})$ . From the occupation time formula (11),  $f(\mathcal{O}_t) = \int_0^t \phi(X_s) d\langle X \rangle_s$ , and together with (21),  $\delta_{\mathfrak{o}}$  must satisfy

$$\delta_{\mathfrak{o}}(\mathfrak{o} \mapsto \phi \cdot \mathfrak{o}) \equiv \phi, \quad \forall \phi \in \mathcal{C}(\mathbb{R}). \quad (22)$$

Hence  $\delta_{\mathfrak{o}}$  must be the *linear derivative* commonly used in mean field games [21, 22, 66, 79, 80]. Although typically used for probability measures, we effortlessly extend its definition to

arbitrary (finite) measures. In what follows, we endow  $\mathcal{M}$  with the total variation metric  $\mathfrak{m}_1$  in Section 2. We also extend the dual pairing in (20) to signed measures  $\mathfrak{o} = \mathfrak{o}^+ - \mathfrak{o}^-$  ( $\mathfrak{o}^+, \mathfrak{o}^- \in \mathcal{M}$ ) by setting  $\phi \cdot \mathfrak{o} = \phi \cdot \mathfrak{o}^+ - \phi \cdot \mathfrak{o}^-$ .

**Definition 2.** A functional  $f : \mathcal{M} \rightarrow \mathbb{R}$  is *continuously linearly differentiable* ( $f \in \mathcal{C}^1(\mathcal{M})$ ) if there exists  $\delta_{\mathfrak{o}}f : \mathcal{M} \rightarrow \mathcal{C}(\mathbb{R})$ , the *linear derivative of  $f$* , such that

- I.  $\mathcal{M} \times \mathbb{R} \ni (\mathfrak{o}, x) \mapsto \delta_{\mathfrak{o}}f(\mathfrak{o})(x)$  is continuous in the product topology,
- II.  $|\delta_{\mathfrak{o}}f(\mathfrak{o})(x)| \leq C(1 + |x|^2)$  for some  $C \in (0, \infty)$ , uniformly in  $\mathfrak{o}$ ,
- III. For all  $\mathfrak{o}, \mathfrak{o}' \in \mathcal{M}$  and  $\Delta = \mathfrak{o}' - \mathfrak{o}$ , then

$$f(\mathfrak{o}') - f(\mathfrak{o}) = \int_0^1 \delta_{\mathfrak{o}}f(\mathfrak{o} + \eta\Delta) \cdot \Delta \, d\eta. \quad (23)$$

In light of (23), we can regard  $\delta_{\mathfrak{o}}f(\mathfrak{o})(x)$  as the Gateaux derivative of  $f$  at  $\mathfrak{o}$  in the direction  $\delta_x$ , namely  $\frac{d}{dh}f(\mathfrak{o} + h\delta_x)|_{h=0}$ . In the mean field game literature [22, 21, 79], the linear derivative is defined up to an additive constant as it is restricted to probability measures. Herein, the total mass of the test measures  $\mathfrak{o}, \mathfrak{o}'$  may differ, which pins down  $\delta_{\mathfrak{o}}f$  uniquely.

We now introduce a notion of differential tailored to occupation measures.

**Definition 3.** The *occupation derivative*  $\partial_{\mathfrak{o}}f : \mathcal{M} \times \mathbb{R} \rightarrow \mathbb{R}$ , is defined as

$$\partial_{\mathfrak{o}}f(\mathfrak{o}, x) = \begin{cases} \delta_{\mathfrak{o}}f(\mathfrak{o})(x), & f \in \mathcal{C}^1(\mathcal{M}), \\ \delta_{\mathfrak{o}}f(\mathfrak{o}, x)(x), & f \in \mathcal{C}^{1,0}(\mathcal{M} \times \mathbb{R}), \end{cases} \quad (24)$$

where  $\mathcal{C}^{1,0}(\mathcal{M} \times \mathbb{R})$  denotes the space of continuous functions  $f : \mathcal{M} \times \mathbb{R} \rightarrow \mathbb{R}$  in the product topology such that  $f(\cdot, x) \in \mathcal{C}^1(\mathcal{M})$  for all  $x \in \mathbb{R}$ .

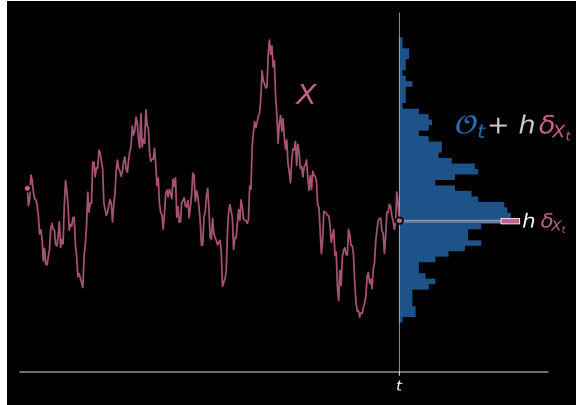
Evidently, the occupation derivative may be restricted to  $\mathcal{D}$ . When  $f = f(\mathfrak{o}, x)$ , we write  $f \in \mathcal{C}^{1,2}(\mathcal{D})$  if  $\delta_{\mathfrak{o}}f$ ,  $\partial_x f$ ,  $\partial_{xx}f$  exist and are jointly continuous.<sup>2</sup> The motivation behind introducing the occupation derivative becomes clear when plugging in the occupied process in (24). Given  $f \in \mathcal{C}^1(\mathcal{D})$ , then  $\partial_{\mathfrak{o}}f(\mathcal{O}_t, X_t)$  takes the linear derivative  $\delta_{\mathfrak{o}}f(\mathcal{O}_t, X_t)(\cdot)$  and evaluates it at  $X_t$ . In terms of directional derivative, this reads

$$\partial_{\mathfrak{o}}f(\mathcal{O}_t, X_t) = \frac{d}{dh}f(\mathcal{O}_t + h\delta_{X_t}, X_t)|_{h=0}.$$

See Fig. 2. The local nature of the occupation derivative comes directly from the dynamics of the occupation flow (15), whence the terminology. As we shall see in Section 3.2.1, the occupation derivative is intrinsically linked to the time derivative in the functional Itô calculus [40]. Similar to the functional derivatives,  $\partial_{\mathfrak{o}}$  and  $\partial_x$  do not commute. Hence, the *Lie bracket*  $[\partial_{\mathfrak{o}}, \partial_x]f := \partial_{x\mathfrak{o}}f - \partial_{\mathfrak{o}x}f$  may be nonzero for some  $f : \mathcal{M} \rightarrow \mathbb{R}$ . A simple example is  $f(\mathfrak{o}, x) = \int_{\mathbb{R}} y\mathfrak{o}(dy)$ , where  $[\partial_{\mathfrak{o}}, \partial_x]f = 1$ . Next, we see how the linear derivative and occupation measure interact with each other and provide a precise meaning of the chain rule (19).

<sup>2</sup>Note also that condition II. in Definition 2 is replaced by II'.  $|\delta_{\mathfrak{o}}f(\mathfrak{o}, x)(y)| \leq C(1 + |y|^2)$  for some constant  $C \in (0, \infty)$ , uniformly in  $(\mathfrak{o}, x) \in \mathcal{D}$ .

Figure 2: The occupation derivative  $\partial_{\circ}f(\mathcal{O}_t, X_t)$  gives the sensitivity of  $f$  with respect to a Dirac impulse at the spot  $X_t$ .



**Proposition 3.** *If  $X$  is a continuous semimartingale and  $f \in \mathcal{C}^1(\mathcal{M})$ , then*

$$df(\mathcal{O}_t) = \partial_{\circ}f(\mathcal{O}_t, X_t)d\langle X \rangle_t, \quad (25)$$

$$df(\tilde{\mathcal{O}}_t) = \partial_{\circ}f(\tilde{\mathcal{O}}_t, X_t)dt. \quad (26)$$

*Proof.* It is a byproduct of Theorem 3.1 below.  $\square$

**Example 1.** Consider the linear functional  $f(\circ) = \phi \cdot \circ$ . In light of the occupation time formula (11),  $f(\mathcal{O}_t) = \int_0^t \phi(X_u)d\langle X \rangle_u$ . Since  $\delta_{\circ}f(\circ) \equiv \phi$ ,

$$f(\mathcal{O}_t) - f(\mathcal{O}_0) = \int_0^t \delta_{\circ}f(\eta \mathcal{O}_t) \cdot \mathcal{O}_t d\eta = \int_{\mathbb{R}} \phi(x) \mathcal{O}_t(dx) = \int_0^t \phi(X_u)d\langle X \rangle_u,$$

which indeed yields (25).

**Example 2.** Consider the trivial but key example  $f(\circ) = g(\circ(\mathbb{R}))$  for some  $g \in \mathcal{C}^1([0, T])$ . Then  $f(\tilde{\mathcal{O}}_t) = g(t)$ , and as  $\circ(\mathbb{R}) = \mathbf{1} \cdot \circ$  with  $\mathbf{1}(x) \equiv 1$ , we obtain from Example 1 and the chain rule that

$$\partial_{\circ}f(\tilde{\mathcal{O}}_t, X_t) = \delta_{\circ}f(\tilde{\mathcal{O}}_t)(X_t) = g'(\tilde{\mathcal{O}}_t(\mathbb{R})) \underbrace{\delta_{\circ}(\mathbf{1} \cdot \tilde{\mathcal{O}}_t)(X_t)}_{=1} = g'(t).$$

Applying (26), we recover the fundamental theorem of calculus  $g(t) - g(0) = \int_0^t g'(u)du$ .

**Example 3.** (Running maximum) Consider the functional

$$M(\circ) = \sup \left\{ x \in \mathbb{R} : \frac{d\circ}{d\lambda}(x) > 0 \right\} = \sup \text{supp}(\circ). \quad (27)$$

Hence  $M(\mathcal{O}_t) = \sup_{s \leq t} X_s$  is the maximum of  $X$  on  $[0, t]$ . If  $t = 0$ , we use the convention that  $\text{supp}(\mathcal{O}_0) = \{X_0\}$ , i.e.,  $M(\mathcal{O}_0) = X_0$ . Note that  $M \notin \mathcal{C}^1(\mathcal{M})$  as its linear derivative is discontinuous at the maximum  $x = M(\circ)$  since  $\lim_{y \uparrow x} \delta_{\circ}M(\circ)(y) = 0 \neq 1 = \lim_{y \downarrow x} \delta_{\circ}M(\circ)(y)$ . We thus consider a mollified version of  $M$  to apply Proposition 3. Given  $\circ \in \mathcal{M}^{\lambda}$ ,  $\circ(\mathbb{R}) > 0$ , consider the smooth functional (akin to Laplace's principle in large deviations theory)

$$M^{\varepsilon}(\circ) = \varepsilon \log \int_{\mathbb{R}} e^{x/\varepsilon} \circ(dx). \quad (28)$$

where we recall that  $\int_A f d\mathfrak{o} = \frac{1}{\mathfrak{o}(A)} \int_A f d\mathfrak{o}$ . It is straightforward to see that  $M^\varepsilon \rightarrow M$  pointwise. Moreover, using Examples 1, 2, and the chain rule,

$$\partial_{\mathfrak{o}} M^\varepsilon(\mathfrak{o}, x) = \delta_{\mathfrak{o}} M^\varepsilon(\mathfrak{o})(x) = \frac{\varepsilon}{\mathfrak{o}(\mathbb{R})} \left( e^{[x - M^\varepsilon(\mathfrak{o})]/\varepsilon} - 1 \right). \quad (29)$$

Hence  $M^\varepsilon \in \mathcal{C}^1(\mathcal{M}^\lambda)$ , and  $M^\varepsilon(\mathcal{O}_t) = X_0 + \int_0^t \delta_{\mathfrak{o}} M^\varepsilon(\mathcal{O}_s) \cdot d\mathcal{O}_s$  using Proposition 3. Next, a straightforward calculation shows that  $\delta_{\mathfrak{o}} M^\varepsilon(\mathfrak{o})$  converges, as  $\varepsilon \rightarrow 0$ , to the Dirac mass at  $M(\mathfrak{o})$ . If  $M_t := M(\mathcal{O}_t)$ , we thus have that

$$M_t - X_0 = \lim_{\varepsilon \downarrow 0} M^\varepsilon(\mathcal{O}_t) - X_0 = \int_0^t \delta_{M_s}(X_s) d\langle X \rangle_s = L_t^0(M - X),$$

where  $L^0(M - X)$  is the local time at zero of  $M_t - X_t = \sup_{s \leq t} X_s - X_t$ . We thus recover the equality  $M_t = X_0 + L_t^0(M - X)$   $\mathbb{Q}$ -*a.s.* established by Dupire [40, Example 2], generalizing Lévy's distributional result.

### 3.2 Itô's Formula

**Theorem 3.1.** (Itô's formula) *Let  $X$  be a continuous semimartingale and  $\mathcal{O}$  its flow of occupation measures. If  $f \in \mathcal{C}^{1,2}(\mathcal{D})$ , then*

$$df(\mathcal{O}_t, X_t) = \left( \partial_{\mathfrak{o}} + \frac{1}{2} \partial_{xx} \right) f(\mathcal{O}_t, X_t) d\langle X \rangle_t + \partial_x f(\mathcal{O}_t, X_t) dX_t. \quad (30)$$

Similarly, if  $\tilde{\mathcal{O}}$  is the calendar time occupation flow of  $X$ , then

$$d f(\tilde{\mathcal{O}}_t, X_t) = \partial_{\mathfrak{o}} f(\tilde{\mathcal{O}}_t, X_t) dt + \frac{1}{2} \partial_{xx} f(\tilde{\mathcal{O}}_t, X_t) d\langle X \rangle_t + \partial_x f(\tilde{\mathcal{O}}_t, X_t) dX_t. \quad (31)$$

*Proof.* See B.1. □

**Example 4.** Let  $f(\mathfrak{o}, x) = g(\mathfrak{o}(\mathbb{R}), x)$ ,  $g \in \mathcal{C}^{1,2}([0, T] \times \mathbb{R})$ . Then  $f(\tilde{\mathcal{O}}_t, X_t) = g(t, X_t)$ . As in Example 2, we have  $\partial_{\mathfrak{o}} f = \partial_t g$ . As  $\partial_x g = \partial_x f$ ,  $\partial_{xx} g = \partial_{xx} f$ , so we recover from (31) the classical Itô formula,

$$dg(t, X_t) = \partial_t g(t, X_t) dt + \partial_x g(t, X_t) dX_t + \frac{1}{2} \partial_{xx} g(t, X_t) d\langle X \rangle_t.$$

**Remark 2.** Let  $X = (X^1, \dots, X^d)$  be a continuous semimartingale in  $\mathbb{R}^d$ ,  $d \geq 2$ , with covariation process  $\langle X \rangle = (\langle X^i, X^j \rangle) \in \mathbb{R}^{d \times d}$ . The occupation flow of  $X$  is given by  $\mathcal{O}_t = \int_0^t \delta_{X_s} \text{tr}(d\langle X \rangle_s)$ , taking values in the space  $\mathcal{M}_d$  of Borel measures on  $\mathbb{R}^d$ . Note that  $\mathcal{O}$  is still a single entity, akin to the time derivative. Theorem 3.1 is then easily generalized: if  $f \in \mathcal{C}^{1,2}(\mathcal{M}_d \times \mathbb{R}^d)$ ,

$$\begin{aligned} df(\mathcal{O}_t, X_t) &= \partial_{\mathfrak{o}} f(\mathcal{O}_t, X_t) \text{tr}(d\langle X \rangle_t) + \frac{1}{2} \text{tr}(\nabla^2 f(\mathcal{O}_t, X_t) d\langle X \rangle_t) \\ &\quad + \nabla f(\mathcal{O}_t, X_t) \cdot dX_t, \end{aligned}$$

where  $\nabla, \nabla^2$  denote the gradient and Hessian operator. The occupation derivative is again given by  $\partial_{\mathfrak{o}} f(\mathfrak{o}, x) = \delta_{\mathfrak{o}} f(\mathfrak{o}, x)(x)$ . A general Itô's formula with arbitrary stochastic clock can be found in [78, Proposition 3.3].

### 3.2.1 Connection with the Functional Itô Calculus

We first recall the functional Itô formula, established by Dupire [40] and further studied by Cont [25], Cont and Fournié [26]. Adopting the canonical setting, let  $\Omega_T$  be the space of càdlàg paths  $\omega : [0, T] \rightarrow \mathbb{R}$  for some  $T > 0$ , and introduce the coordinate process  $X_t(\omega) = \omega_t$ . Fix also a non-anticipative path functional  $f : [0, T] \times \Omega_T \rightarrow \mathbb{R}$  meaning that  $f(t, \omega)$  only depends on  $\omega$  up to time  $t$ . If  $f$  is regular enough, we then have from [40] that

$$df(t, \omega) = \Delta_t f(t, \omega) dt + \Delta_x f(t, \omega) dX_t(\omega) + \frac{1}{2} \Delta_{xx} f(t, \omega) d\langle X \rangle_t(\omega), \quad \mathbb{Q} - a.s., \quad (32)$$

where  $\Delta_t f(t, \omega) = \frac{d}{dh} f(t+h, \omega_{\cdot \wedge t})|_{h=0}$ ,  $\Delta_x f(t, \omega) = \frac{d}{dh} f(t, \omega + h\mathbf{1}_{[t, T]})|_{h=0}$ . To connect (32) with Theorem 3.1, fix  $f \in \mathcal{C}^{1,2}(\mathcal{M} \times \mathbb{R})$  and introduce the functional

$$f(t, \omega) = f(\tilde{\mathcal{O}}_t, X_t)(\omega) = f(\tilde{\mathcal{O}}_t(\omega), \omega_t).$$

First, note that  $\Delta_x f = \partial_x f$  and  $\Delta_{xx} f = \partial_{xx} f$  as a vertical bump of  $\omega$  at  $t$  does not affect the Lebesgue integrals  $\int_0^t \mathbf{1}(\omega_s) ds$ , therefore leaving  $\tilde{\mathcal{O}}_t$  unchanged. For the functional time derivative, we have for all  $h \in [0, T-t]$  that

$$f(t+h, \omega_{\cdot \wedge t}) = f(\tilde{\mathcal{O}}_{t+h}(\omega_{\cdot \wedge t}), \omega_t) = f(\tilde{\mathcal{O}}_t(\omega), \omega_t) + h \int_0^1 \delta_{\mathbf{o}} f(\tilde{\mathcal{O}}_t(\omega) + \eta h \delta_{\omega_t}, \omega_t) \cdot \delta_{\omega_t} d\eta,$$

using that  $\tilde{\mathcal{O}}_{t+h}(\omega_{\cdot \wedge t}) - \tilde{\mathcal{O}}_t(\omega) = h \delta_{\omega_t}$  since  $\omega$  is frozen on  $[t, t+h]$ . Taking derivative with respect to  $h$  and letting  $h \downarrow 0$  leads to

$$\Delta_t f(t, \omega) = \partial_{\mathbf{o}} f(\tilde{\mathcal{O}}_t, X_t)(\omega), \quad (33)$$

further confirming that  $\tilde{\mathcal{O}}$  plays the same role as time. All in all, we indeed obtain that

$$\begin{aligned} df(\tilde{\mathcal{O}}_t, X_t)(\omega) &= df(t, \omega) \\ &= \Delta_t f(t, \omega) dt + \Delta_x f(t, \omega) dX_t(\omega) + \frac{1}{2} \Delta_{xx} f(t, \omega) d\langle X \rangle_t(\omega) \\ &= \left( \partial_{\mathbf{o}} f(\tilde{\mathcal{O}}_t, X_t) dt + \partial_x f(\tilde{\mathcal{O}}_t, X_t) dX_t + \frac{1}{2} \partial_{xx} f(\tilde{\mathcal{O}}_t, X_t) d\langle X \rangle_t \right) (\omega). \end{aligned}$$

### 3.2.2 Connection with the Malliavin Calculus

This section regards terminal occupation functionals  $\mathcal{O}_T \mapsto f(\mathcal{O}_T)$  through the lens of Malliavin calculus; see, e.g., [35]. Suppose that  $\mathbb{Q}$  is the Wiener measure so that the canonical process  $X$  is Brownian motion. Then  $\mathcal{O}_T = \tilde{\mathcal{O}}_T = \int_0^T \delta_{X_t} dt$   $\mathbb{Q}$ -a.s. due to  $\langle X \rangle_t = t$ . We then obtain the following result.

**Proposition 4.** *Let  $f \in \mathcal{C}^1(\mathcal{M})$  such that  $x \mapsto \partial_{\mathbf{o}} f(\mathbf{o}, x)$  is differentiable for every  $\mathbf{o} \in \mathcal{M}^\lambda$ , and  $f(\omega) := f(\mathcal{O}_T(\omega))$ ,  $\omega \in \Omega_T$ , is Malliavin differentiable (see [35]). Then, the Malliavin derivative of  $f$  at  $t \in [0, T]$  admits the alternative expression*

$$D_t f(\omega) := \frac{d}{dh} f(\omega + h\mathbf{1}_{[t, T]}) \Big|_{h=0} = \int_t^T \partial_{x\mathbf{o}} f(\mathcal{O}_T(\omega), \omega_s) ds, \quad \mathbb{Q} - a.s. \quad (34)$$

*Proof.* See Section B.2. □

**Remark 3.** Introduce the Fréchet derivative  $\mathfrak{D}f \in L^2([0, T])$  of  $f(\omega) = f(\mathcal{O}_T(\omega))$ , defined via  $\frac{d}{dh}f(\omega + h\omega')|_{h=0} = (\mathfrak{D}f(\omega), \omega')_{L^2([0, T])} \forall \omega, \omega' \in \Omega_T$ . Then (34) implies that

$$\mathfrak{D}_t f(\omega) = -\partial_t D_t f(\omega) = \partial_{x\mathfrak{o}} f(\mathcal{O}_T(\omega), \omega_t).$$

Interpreting the path functional  $f$  as a lift of  $f$ , i.e.,  $f(\omega) = f(\mathfrak{o})$  if  $\mathcal{O}_T(\omega) = \mathfrak{o}$ , then the relation  $\mathfrak{D}f = \partial_{x\mathfrak{o}} f = \partial_x \delta_{\mathfrak{o}} f$  is analogous to the link between the Lions derivative and  $\delta_{\mathfrak{o}}$  in mean field games [21, 22, 66].

### 3.3 Feynman-Kac's Formula for the Backward Heat Equation

We first prove a Feynman-Kac theorem for occupied Brownian motion, while a more general result will be given in Section 3.4. Write  $\varphi \in \mathcal{C}^2(\mathcal{D})$  if  $\varphi \in \mathcal{C}^{2,2}(\mathcal{D})$  and  $(x, y) \mapsto \delta_{\mathfrak{o}} \varphi(\mathfrak{o}, x)(y)$ ,  $(y, y') \mapsto \delta_{\mathfrak{o}\mathfrak{o}} \varphi(\mathfrak{o}, x)(y, y')$  are twice continuously differentiable with bounded derivatives.

**Theorem 3.2.** (Feynman-Kac) *Let  $\varphi : \mathcal{D} \rightarrow \mathbb{R}$  such that  $\varphi(\mathcal{O}_T, X_T) \in L^1(\mathbb{Q})$  and consider the backward heat equation,*

$$\begin{cases} \left(\partial_{\mathfrak{o}} + \frac{1}{2}\partial_{xx}\right)u = 0, & \text{on } \mathcal{D}_T := \{(\mathfrak{o}, x) \in \mathcal{D} : \mathfrak{o}(\mathbb{R}) < T\}, \\ u = \varphi, & \text{on } \partial\mathcal{D}_T := \{(\mathfrak{o}, x) \in \mathcal{D} : \mathfrak{o}(\mathbb{R}) = T\}. \end{cases} \quad (35a)$$

$$\quad (35b)$$

If  $v \in \mathcal{C}^{1,2}(\mathcal{D})$  is a classical solution of (35a)–(35b), then

$$v(\mathfrak{o}, x) = \mathbb{E}_{\mathfrak{o}, x}^{\mathbb{Q}}[\varphi(\mathcal{O}_T, X_T)] := \mathbb{E}^{\mathbb{Q}}[\varphi(\mathfrak{o} + \mathcal{O}_{T-t}^x, x + X_{T-t})], \quad \mathfrak{o}(\mathbb{R}) = t, \quad (36)$$

where  $\mathcal{O}_{T-t}^x(A) = \mathcal{O}_{T-t}(A - x)$ . Conversely, if  $\varphi \in \mathcal{C}^2(\mathcal{D})$ , then  $v$  in (36) belongs to  $\mathcal{C}^2(\mathcal{D})$  as well and is the unique classical solution of (35a)–(35b).

*Proof.* See B.3. □

We finally discuss several examples where  $\varphi$  has little regularity while the value functional is still smooth. As we shall see, this is in contrast with other path-dependent calculi where the associated value functional typically fails to be even continuous.

**Example 5.** (Local time at zero) Let  $X$  be Brownian motion and  $\varphi(\mathfrak{o}, x) = \frac{d\mathfrak{o}}{d\lambda}(0)$ , irrespective of  $x$ . Hence  $\varphi(\mathcal{O}_T, X_T) = L_T^0$  is the local time at 0. If  $(\mathfrak{o}, x) \in \partial\mathcal{D}_t$ , a simple calculation shows that

$$v(\mathfrak{o}, x) = \mathbb{E}_{\mathfrak{o}, x}^{\mathbb{Q}}[L_T^0] = \mathbb{E}_{\mathfrak{o}, x}^{\mathbb{Q}}[L_t^0 + L_{t, T}^0] = \frac{d\mathfrak{o}}{d\lambda}(0) + \mathbb{E}^{\mathbb{Q}}[L_{T-t}^{|x|}].$$

The first term in the last equality is linear in  $\mathfrak{o}$  and Lipschitz continuous with respect to the metric  $\mathfrak{m}_{\infty}$  seen in Section 2. Moreover, the second term is continuous in  $x$  and even piecewise smooth on  $\mathbb{R} \setminus \{0\}$  for all  $t < T$ . From the pathwise setting in Section 3.2.1, we note that the functional

$$v(t, \omega) = \mathbb{E}^{\mathbb{Q}}[L_T^0 | \mathcal{F}_t](\omega) = L_t^0(\omega) + \mathbb{E}^{\mathbb{Q}}[L_{T-t}^{|x|}]_{x=\omega_t}, \quad \omega \in \Omega_T, \quad (37)$$

is *not* continuous in  $\omega$  (with respect to the supremum norm), regardless of the definition of  $L_t^0 : \Omega_T \rightarrow \mathbb{R}$ . First, one may set  $L_t^0(\omega) = \lim_{\varepsilon \rightarrow 0} \frac{1}{2\varepsilon} \int_0^t \mathbb{1}_{B_{\varepsilon}}(\omega_s) ds$  as the occupation measures  $\mathcal{O}, \tilde{\mathcal{O}}$  almost surely coincide under the Wiener measure. However, if  $(\omega^N)$  is a sequence of

piecewise linear paths that converges to  $\omega$  (e.g. using Schauder's theorem) it may happen that  $L_t^0(\omega^N) = \infty$  as the occupation measure of  $\omega^N$  is not absolutely continuous with respect to  $\lambda$ . Another possibility is  $L_t^0(\omega) := \lim_{\varepsilon \rightarrow 0} \frac{1}{2\varepsilon} \int_0^t \mathbb{1}_{B_\varepsilon}(X_s) d\langle X \rangle_s(\omega)$  when  $\langle X \rangle$  is well-defined. But  $L_t^0(\omega^N) = 0$  for the above sequence  $(\omega^N)$ , leading again to the discontinuity of  $L_t^0$  with respect to  $\omega$ . Finally, we could derive the local time at zero (or any other level) from Tanaka's formula [75, Chapter VI]. However, the expression would involve stochastic integrals which are infamously discontinuous with respect to the input path. This representation is thus subject to the same fate as the previous ones.

**Example 6.** (Spot Local time) Let  $\varphi(\mathfrak{o}, x) = \frac{d\mathfrak{o}}{d\lambda}(x)$ , that is  $\varphi(\mathcal{O}_t, X_t) = L_t^{X_t}$ . Then  $\varphi$  is continuous in  $x$ , since  $X$  is a continuous martingale, and also continuous in  $\mathfrak{o}$  with respect to  $\mathfrak{m}_\infty$ . However,  $\varphi$  is not differentiable in  $x$ . For every  $(\mathfrak{o}, x) \in \partial \mathcal{D}_t$ ,  $t < T$ , let us write the value function as

$$v(\mathfrak{o}, x) = \mathbb{E}_{\mathfrak{o}, x}^{\mathbb{Q}}[L_T^{X_T}] = \int_{\mathbb{R}} \frac{d\mathfrak{o}}{d\lambda}(y) \phi_{T-t}(x-y) dy + \mathbb{E}^{\mathbb{Q}}[L_{T-t}^{X_{T-t}}],$$

where  $\phi_\tau$  is the density of  $\mathcal{N}(0, \tau)$ . From  $\frac{d\mathfrak{o}}{d\lambda}(y) dy = \mathfrak{o}(dy)$  and Proposition 6 below, we obtain

$$v(\mathfrak{o}, x) = \int_{\mathbb{R}} \phi_{T-t}(x-y) \mathfrak{o}(dy) + \sqrt{\frac{2}{\pi}(T-t)}. \quad (38)$$

Since  $x \mapsto \phi_{T-t}(x-y)$  is smooth for all  $y \in \mathbb{R}$ ,  $t < T$ , and the second term is independent of  $x$ , then  $v$  is smooth in  $x$ . For the occupation derivative, recall that  $t = \mathfrak{o}(\mathbb{R})$  as  $(\mathfrak{o}, x) \in \partial \mathcal{D}_t$ , and  $\delta_{\mathfrak{o}}(\mathfrak{o} \mapsto \mathfrak{o}(\mathbb{R})) \equiv 1$ . Hence,

$$\begin{aligned} \partial_{\mathfrak{o}} v(\mathfrak{o}, x) &= \int_{\mathbb{R}} \partial_t \phi_{T-t}(x-y) \mathfrak{o}(dy) + \underbrace{\phi_{T-t}(0) - (2\pi(T-t))^{-1/2}}_{=0} \\ &= -\frac{1}{2} \int_{\mathbb{R}} \partial_{xx} \phi_{T-t}(x-y) \mathfrak{o}(dy), \end{aligned}$$

since  $\phi$  solves the heat equation  $\partial_\tau \phi_\tau = \frac{1}{2} \partial_{xx} \phi_\tau$ . We conclude that  $v$  belongs to  $\mathcal{C}^{1,2}(\mathcal{D})$  and is thus a classical solution of (35a)–(35b). On the other hand, the path functional  $v(t, \omega) = \mathbb{E}^{\mathbb{Q}}[L_T^{X_T} | \mathcal{F}_t](\omega)$  is discontinuous in  $\omega$  similar to Example 5.

### 3.4 Occupied SDEs and Dirichlet Problems

Consider the *occupied stochastic differential equation (OSDE)*,

$$\begin{cases} d\mathcal{O}_t = \delta_{X_t} d\langle X \rangle_t, & \mathcal{O}_0 \in \mathcal{M}, \end{cases} \quad (39a)$$

$$\begin{cases} dX_t = b(\mathcal{O}_t, X_t) dt + \sigma(\mathcal{O}_t, X_t) dW_t, & X_0 \in \text{supp}(\mathcal{O}_0), \end{cases} \quad (39b)$$

with coefficients  $b, \sigma : \mathcal{D} \rightarrow \mathbb{R}$ . Note that (39a) can be equivalently written as  $d\mathcal{O}_t = \delta_{X_t} \sigma(\mathcal{O}_t, X_t)^2 dt$ . Incorporating the occupation flow into stochastic differential equations is uncommon in the literature. A notable exception is [9] and subsequent papers [6, 7, 8] proving ergodic results for diffusions that are *self-interacting*, i.e., where the drift depends on the rescaled calendar time occupation flow  $t \mapsto \frac{1}{t} \tilde{\mathcal{O}}_t$ . We can also mention the recent papers [37, 23] connecting self-interacting diffusions with McKean-Vlasov SDEs.

We first discuss the wellposedness of (39a)–(39b). Similar to the classical theory of SDEs, we impose Lipschitz and growth assumptions on the coefficients  $b, \sigma$ . This necessitates an

appropriate metric for occupied processes. While the next theorem may be established for the metrics  $\mathfrak{m}_p$  seen in Section 2, it proves convenient to use a distance with explicit dual representation. In particular, the *bounded Lipschitz distance* [58] yields a somewhat simple proof. Let  $\phi : \mathbb{R} \rightarrow \mathbb{R}$  be a bounded Lipschitz function and  $[\phi]_{\text{Lip}}$  denote its Lipschitz constant. If  $\|\phi\|_{\text{BL}} = \|\phi\|_{L^\infty(\mathbb{R})} \vee [\phi]_{\text{Lip}}$  and  $\mathfrak{o}$  is a signed Radon measure on  $\mathbb{R}$ , define its bounded Lipschitz norm by

$$|\mathfrak{o}|_{\text{BL}} = \sup\{\phi \cdot \mathfrak{o} : \|\phi\|_{\text{BL}} \leq 1\}. \quad (40)$$

Also, introduce the parabolic norm  $\varrho(\mathfrak{o}, x) = \sqrt{|\mathfrak{o}|_{\text{BL}} + |x|^2}$ ,  $(\mathfrak{o}, x) \in \mathcal{D}$ .

**Theorem 3.3.** *Suppose that  $b, \sigma \in \mathcal{C}(\mathcal{D})$  satisfy the following Lipschitz and growth conditions: there exists  $K > 0$  such that for all  $(\mathfrak{o}, x), (\mathfrak{o}', x') \in \mathcal{D}$ ,*

$$|b(\mathfrak{o}, x)|^2 \leq K^2[1 + \varrho(\mathfrak{o}, x)^2], \quad |\sigma(\mathfrak{o}, x)|^2 \leq K^2[1 + \varrho(\mathfrak{o}, x)], \quad (41)$$

$$|f(\mathfrak{o}', x') - f(\mathfrak{o}, x)| \leq K\varrho(\mathfrak{o}' - \mathfrak{o}, x' - x), \quad f \in \{b, \sigma\}. \quad (42)$$

*Then the OSDE (39a)–(39b) admits a unique strong solution.*

*Proof.* See Section B.4. □

Notice the unusual linear growth condition for the *squared* diffusion coefficient  $\sigma^2$  in (41) instead of  $\sigma$  as in the classical case [75, Chapter IX]. This is because  $\sigma^2(\mathcal{O}, X)$  appears in the dynamics of the occupation flow.

**Remark 4.** Incorporating the occupation flow into stochastic differential equations is uncommon in the literature. A notable exception is the class of *self-attracting diffusions* of Cranston and Le Jan [29], inspired by the Brownian polymer model of Durrett and Rogers [41]. Therein, the drift is influenced by the the calendar time occupation flow so as to create ergodic behaviors. These diffusions were further studied by Raimond [73], and extended in [6, 7, 8, 9] to *self-interacting diffusions*, also including SDEs exhibiting self-repulsion. Whereas self-interacting diffusions use the occupation flow in the drift, note that OSDEs involve the occupation in the diffusion coefficient as well. Besides, let us mention the recent papers [23, 37] linking self-interacting diffusions to ergodic McKean-Vlasov SDEs.

**Theorem 3.4.** (Itô's formula for OSDEs) *Let  $(\mathcal{O}, X)$  be a strong solution of the OSDE (39a)–(39b) with coefficients  $b, \sigma$ . If  $f \in \mathcal{C}^{1,2}(\mathcal{D})$ , then*

$$df(\mathcal{O}_t, X_t) = (\sigma^2 \partial_{\mathfrak{o}} + b \partial_x + \frac{\sigma^2}{2} \partial_{xx}) f(\mathcal{O}_t, X_t) dt + (\sigma \partial_x) f(\mathcal{O}_t, X_t) dW_t, \quad (43)$$

*Proof.* This is a direct consequence of Theorem 3.1. □

Next, we extend Theorem 3.2 to OSDEs. If  $(\mathcal{O}^{\mathfrak{o}, x}, X^{\mathfrak{o}, x})$  denotes the solution of the OSDE (39a)–(39b) given  $(\mathcal{O}_t, X_t) = (\mathfrak{o}, x)$ , it is tempting to define  $v(\mathfrak{o}, x) = \mathbb{E}^{\mathbb{Q}}[\varphi(\mathcal{O}_T^{\mathfrak{o}, x}, X_T^{\mathfrak{o}, x})]$  as in (36). However, unlike Brownian motion or any continuous Gaussian martingale where  $\mathcal{O}_T(\mathbb{R}) = \langle X \rangle_T$  is deterministic, the total mass may well be random. Take for instance  $b \equiv 0$  and  $\sigma(\mathfrak{o}, x) = x$ . The terminal condition is therefore misspecified in general. A remedy is to replace the horizon  $T$  by the time at which the total mass  $\mathcal{O}(\mathbb{R})$  first exceeds a threshold, say

$\Theta > 0$ . With this new interpretation, the terminal date becomes stochastic and corresponds to the exit time

$$\tau_\Theta = \inf\{t \geq 0 : (\mathcal{O}_t, X_t) \notin \mathcal{D}_\Theta\} = \inf\{t \geq 0 : \langle X \rangle_t \geq \Theta\}. \quad (44)$$

This is precisely the logic behind the DDS transformation in Remark 1. We now state a Feynman-Kac's theorem for OSDEs. Its proof is almost identical to the first part in Theorem 3.2.

**Theorem 3.5.** (Feynman-Kac) *Let  $\varphi : \mathcal{D} \rightarrow \mathbb{R}$  such that  $\varphi(\mathcal{O}_T, X_T) \in L^1(\mathbb{Q})$  and consider the Dirichlet problem*

$$\begin{cases} (\sigma^2 \partial_{\mathfrak{o}} + b \partial_x + \frac{\sigma^2}{2} \partial_{xx}) u(\mathfrak{o}, x) = 0, & \text{on } \mathcal{D}_\Theta, \\ u(\mathfrak{o}, x) = \varphi(\mathfrak{o}, x), & \text{on } \partial \mathcal{D}_\Theta, \end{cases} \quad (45a)$$

$$\quad (45b)$$

If  $(\mathcal{O}, X)$  is a strong solution of (39a)–(39b),  $\mathbb{E}^\mathbb{Q}[\tau_\Theta] < \infty$ , and  $v \in \mathcal{C}^{1,2}(\mathcal{D})$  is a classical solution (45a)–(45b), then

$$v(\mathfrak{o}, x) = \mathbb{E}^\mathbb{Q}[\varphi(\mathcal{O}_{\tau_\Theta}^{\mathfrak{o},x}, X_{\tau_\Theta}^{\mathfrak{o},x})], \quad (\mathfrak{o}, x) \in \overline{\mathcal{D}_\Theta}. \quad (46)$$

The condition  $\mathbb{E}^\mathbb{Q}[\tau_\Theta] < \infty$  in Theorem 3.5 holds for instance if  $\sigma(\mathfrak{o}, x) \geq \underline{\sigma}$  for some constant  $\underline{\sigma} > 0$ . As  $\mathcal{O}_t(\mathbb{R}) = \langle X \rangle_t = \int_0^t \sigma(\mathcal{O}_s, X_s)^2 ds$ , it is then immediate that  $\tau_\Theta \leq \Theta / \underline{\sigma}^2$ .

**Remark 5.** When  $b \equiv 0$ , then (45a) reads  $\sigma^2(\partial_{\mathfrak{o}} + \frac{1}{2} \partial_{xx})u = 0$  which is equivalent to the heat equation (35a)–(35b) when  $\sigma$  is positive. This is not surprising since  $X$  is then a local martingale, hence a time-changed Brownian motion; see Remark 1 and Example 12.

We finish this section by stating Feynman-Kac's theorem for functionals of the calendar time occupation flow. To this end, consider

$$\begin{cases} d\tilde{\mathcal{O}}_t = \delta_{X_t} dt, & \tilde{\mathcal{O}}_0 \in \mathcal{M}, \\ dX_t = b(\tilde{\mathcal{O}}_t, X_t) dt + \sigma(\tilde{\mathcal{O}}_t, X_t) dW_t, & X_0 \in \text{supp}(\tilde{\mathcal{O}}_0). \end{cases} \quad (47a)$$

$$\quad (47b)$$

The wellposedness of (47a)–(47b) may be established through a straightforward adaptation of Theorem 3.3; see Theorem 4.2.14 in [81].

**Theorem 3.6.** (Feynman-Kac, calendar time) *Consider  $\varphi : \mathcal{D} \rightarrow \mathbb{R}$  such that  $\varphi(\tilde{\mathcal{O}}_T, X_T) \in L^1(\mathbb{Q})$  and the backward occupied PDE*

$$\begin{cases} (\partial_{\mathfrak{o}} + b \partial_x + \frac{\sigma^2}{2} \partial_{xx}) u(\mathfrak{o}, x) = 0, & \text{on } \mathcal{D}_T, \\ u(\mathfrak{o}, x) = \varphi(\mathfrak{o}, x), & \text{on } \partial \mathcal{D}_T, \end{cases} \quad (48a)$$

$$\quad (48b)$$

If (47a)–(47b) admits a strong solution and (48a)–(48b) has a classical solution  $v \in \mathcal{C}^{1,2}(\mathcal{D})$ , then

$$v(\mathfrak{o}, x) = \mathbb{E}^\mathbb{Q}[\varphi(\tilde{\mathcal{O}}_T^{\mathfrak{o},x}, X_T^{\mathfrak{o},x})], \quad (\mathfrak{o}, x) \in \overline{\mathcal{D}_T}. \quad (49)$$

The above results allows to characterize the pricing PDE of financial derivatives contingent on the calendar time occupation flow; see Section 4.1.

**Remark 6.** Similar to path-dependent PDEs, the occupied PDEs (45a)–(45b), (48a)–(48b) typically do not admit a classical solution. Fortunately, a viscosity theory can be effectively established, even in the fully nonlinear case; see the follow-up paper [78]. In particular, it is shown therein that, under mild assumptions, the value function  $v$  in (46) is the unique viscosity solution of (45a)–(45b).

## 4 Unified Markovian Lift of Financial Instruments

The next three sections demonstrate the broad range of financial applications offered by occupied processes. First, we show that occupation flows provide a unified way to express payoffs of financial derivatives while preserving the Markov property. Precisely, if  $X$  is the asset price process and  $\xi : \Omega \rightarrow \mathbb{R}$  a European style, path-dependent claim, a common approach in derivatives pricing consists of choosing a path-dependent feature  $F_t(\omega) = f(t, \omega) \in \mathfrak{F}$  where  $f : [0, T] \times \Omega \rightarrow \mathbb{R}$  is a non-anticipative functional (see Section 3.2.1), such that

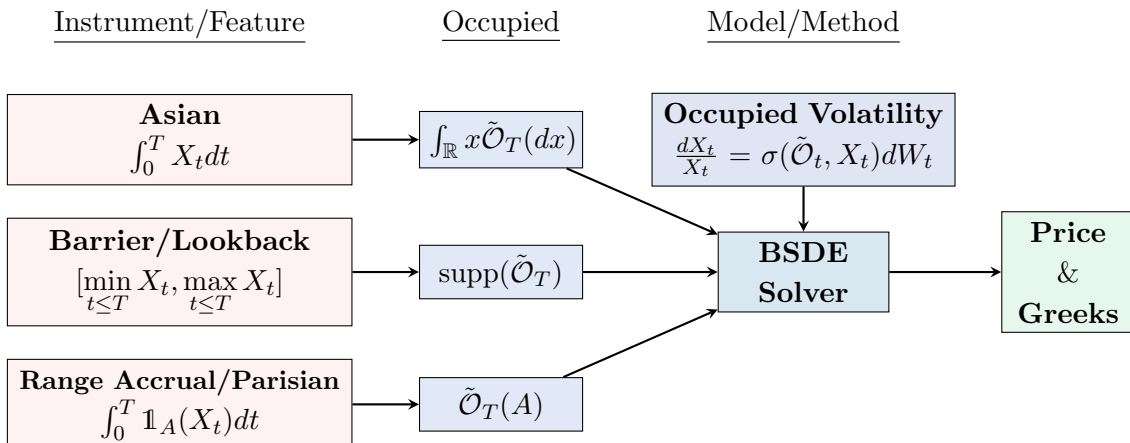
$$\xi(\omega) = \varphi(F_T, X_T)(\omega), \quad \varphi : \mathfrak{F} \times \mathbb{R} \rightarrow \mathbb{R}, \quad \omega \in \Omega, \quad (50)$$

while  $(F, X)$  is a Markov process. The feature space  $\mathfrak{F}$  is chosen to be "nicer" than  $\Omega$ , e.g., a finite-dimensional Euclidean space  $\mathfrak{F} = \mathbb{R}^d$  or  $\mathfrak{F} = \mathcal{M}$  in the case of occupation flows. Due to the Markov property, the derivatives price will be function of these variables as well, leading to tractable numerical methods to solve the corresponding pricing PDE in the projected space. When  $\mathfrak{F} = \mathcal{M}$ , we stress that the occupation flow needs to be discretized in the implementation, leading to a finite-dimensional Markovian lift given by finitely many occupation times. Setting  $F = \tilde{\mathcal{O}}$  or  $F = \mathcal{O}$  then leads to occupied pricing PDEs, allowing the underlying to include the occupation flow in its dynamics as well. The use of occupied SDEs in financial modeling will be discussed in Sections 5 and 6. It turns out that the relevant features in finance are very often expressible in terms of the occupation flow, either with respect to calendar time and variance time as shown next.

### 4.1 Exotic Options and Structured Products

We here gather many financial instruments whose payoff is function of the calendar time occupied process, that is  $\xi = \varphi(\tilde{\mathcal{O}}_T, X_T)$ . If  $\mathbb{Q}$  is a risk-neutral measure, then the time  $t$  European price of an exotic option with payoff  $\varphi$  is  $v(\tilde{\mathcal{O}}_t, X_t) = e^{-r(T-t)} \mathbb{E}^{\mathbb{Q}}[\varphi(\tilde{\mathcal{O}}_T, X_T) | \mathcal{F}_t]$  for some constant interest rate  $r \in \mathbb{R}$ . If the asset follows the dynamics of an occupied SDE as in (47b) (see also Section 5), we can then invoke Feynman-Kac's formula in Theorem 3.6 to deduce the corresponding pricing PDE. The latter is then integrated using a numerical solver, the *same* for all occupation-dependent derivatives, from which the initial price and sensitivities (Greeks) can be extracted. This unified approach is summarized in Fig. 3.

Figure 3: Unified Markovian lift for exotic options and structured products.



**Example 7.** *Asian options* are contingent upon the time average of the asset. One typically choose the running integral  $F_t = \int_0^t X_s ds$  as feature over the running average due to the simpler dynamics of the former. Clearly, the chronology of the path is here irrelevant, so we conclude from Theorem A.1 that  $F_t$  is function of  $\tilde{\mathcal{O}}_t$ . This is confirmed by the occupation time formula, namely  $\int_0^t X_s ds = \int_{\mathbb{R}} x d\tilde{\mathcal{O}}_t$ . Hence, Asian payoffs can be rewritten in terms of  $\tilde{\mathcal{O}}_T$  and the terminal asset price when need be. For instance, the payoff of an floating strike Asian call option reads

$$\xi = \left( X_T - \frac{1}{T} \int_0^T X_t dt \right)^+ = \left( X_T - \frac{1}{T} \int_{\mathbb{R}} x d\tilde{\mathcal{O}}_T \right)^+ = \varphi(\tilde{\mathcal{O}}_T, X_T).$$

The scaling factor  $\frac{1}{T}$  may also be written as  $\tilde{\mathcal{O}}_T(\mathbb{R})^{-1}$  in the occupation payoff, though the maturity is known from the contract's term sheet.

**Example 8.** The payoff of *barrier and lookback options* involves the range of the underlying asset. The relevant feature is thus given by

$$F_t = [\min_{s \leq t} X_s, \max_{s \leq t} X_s],$$

which coincides with the support of  $\tilde{\mathcal{O}}_t$  as seen in Example 3. Barrier options use the range to monitor whether the asset has breached a prescribed level—the barrier, which acts as a knock-in (creation) or or knock-out (termination) trigger. On the other hand, lookback derivatives mimic vanilla call/put payoffs by replacing the terminal value by the maximum/minimum price, or use the latter as a floating strike. E.g., the payoff of a floating lookback call options admits the form

$$\left( X_T - \min_{t \leq T} X_t \right)^+ = (X_T - \inf \text{supp}(\tilde{\mathcal{O}}_T))^+ = \varphi(\tilde{\mathcal{O}}_T, X_T).$$

We end this section with a popular class of contracts in the quantitative finance literature known as *occupation time derivatives*<sup>3</sup> [24, 62] [34, Chapter 7]. The generic form for the payoff of such options is

$$\varphi(\tilde{\mathcal{O}}_T, X_T) = \phi(\tilde{\mathcal{O}}_T(A), X_T), \quad \phi : \mathbb{R}^2 \rightarrow \mathbb{R}, \quad A \in \mathcal{B}(\mathbb{R}). \quad (51)$$

While it is technically sufficient to use the two-dimensional process  $(\tilde{\mathcal{O}}(A), X)$  for the payoff in (51), this minimal approach becomes impractical when a book of occupation time derivatives contingent on several Borel sets is given, calling for the more general occupation lift  $X_T \rightarrow (\tilde{\mathcal{O}}_T, X_T)$ . Moreover, the price of an occupation time derivative would be function of the three variables  $(t, \tilde{\mathcal{O}}_t(A), X_t)$  as the total mass cannot be extracted from a single occupation time (except when  $A = \mathbb{R}$ , where the payoff becomes vanilla anyway).

**Example 9.** *Range accruals* are popular hybrid products in fixed income and foreign exchange markets. The holder receives a floating interest payment based on the proportion of time the reference rate (e.g. SOFR) has stayed within a given range, say  $[x_1, x_2]$ . In other words, the paid amount is of the form  $\frac{C}{T} \int_0^T \mathbf{1}_{[x_1, x_2]}(X_t) dt$ , so the relevant feature is precisely the occupation time  $F_T = \tilde{\mathcal{O}}_T([x_1, x_2])$ .

<sup>3</sup>not to be confused with the occupation derivative in Definition 3!

Note that range accruals are linear in  $\tilde{\mathcal{O}}_T$ , so their price is theoretically known from vanilla options. Indeed, recall from Breeden and Litzenberger [19] that  $\mathbb{Q}(X_T \leq x) = \partial_K P(x, T)$ , with the undiscounted vanilla put price  $P(K, T) = \mathbb{E}^{\mathbb{Q}}[(K - X_T)^+]$ . Consequently, the expected calendar occupation time of  $X$  in  $[x_1, x_2]$  becomes

$$\mathbb{E}^{\mathbb{Q}}[\tilde{\mathcal{O}}_T([x_1, x_2])] = \int_0^T \mathbb{Q}(X_t \in [x_1, x_2]) dt = \int_0^T (\partial_K P(x_2, t) - \partial_K P(x_1, t)) dt, \quad (52)$$

assuming that  $\mathbb{Q} \circ X_T^{-1}$  has no atoms. However, only finitely many strikes and maturities are available in practice. Even when the range accrual is monitored daily, so the right side of (52) becomes a sum, options on the reference rate rarely expires on every business day. Hence, the valuation of range accruals would still benefit from the unified pricing and modeling framework in Fig. 3.

**Example 10.** *Parisian options* [24, 62] were introduced to relax the knock-in/out component of barrier options seen in Example 8. Precisely, the option is activated or terminated only once the asset has performed an excursion above/below the barrier of length at least  $\delta > 0$ , referred to as the *window*. A variant, called cumulative Parisian or *Parasian* option [57], requires that the cumulative time above/below the barrier exceeds the window. As the payoff of excursion-based Parisian options depends on the chronology of the path, the occupied lift can only be applied to the cumulative counterparts in view of Theorem A.1. For example, consider an asset-or-nothing, up-and-out cumulative Parisian call option with strike  $K$ , barrier  $B > K$ , and window  $\delta > 0$ , namely

$$\xi = \begin{cases} X_T, & \text{if } \int_0^T \mathbb{1}_{\{X_t \geq B\}} dt < \delta, \\ 0, & \text{otherwise.} \end{cases}$$

Letting  $A = [B, \infty)$ , we can rewrite the above payoff as  $\xi = X_T \mathbb{1}_{\{\tilde{\mathcal{O}}_T(A) < \delta\}}$ , which is indeed of the form (51). The relaxed knock-in/out feature is particularly appealing to the buyer of knock-out Parisian options as it (partially) prevents price manipulation from the seller to push the underlying towards the barrier, making the contracts worthless. From the seller's perspective, Parisian options are easier to hedge as the soft barrier effectively smoothen the Greeks. Other instruments exhibit a similar relaxation feature. One example is the soft call provision of convertible bonds, where the issuer discontinues (calls) the contract once the underlying has spent a prescribed amount of time above a threshold.

#### 4.1.1 Deep BSDE Solver

Back to the unified approach in Fig. 3, the occupation payoffs and calibrated model are then given to a numerical solver. We here present an adaptation of deep BSDE methods [43, 42, 63], which will be further discussed and tested in an accompanying paper [61]. Let  $W$  be Brownian motion and  $X$  denotes the asset price process adapted to  $W$ . Given a risk-neutral measure  $\mathbb{Q}$  and contingent claim  $\xi \in L^1(\mathbb{Q})$ , then the value process  $Y_t = \mathbb{E}_t^{\mathbb{Q}}[\xi]$  solves the backward SDE (BSDE),

$$Y_t = \xi - \int_t^T Z_s dW_s, \quad (53)$$

for some adapted process  $Z$ . Assuming a Markov structure, the deep BSDE method consists of parameterizing the  $Z$  process by a feedforward neural network, taking the state variable as

input. Among other applications, the deep BSDE method has shown impressive performance in derivatives pricing, especially when the state process is high-dimensional [43, 42, 63]. The increasing dimensionality may come from numerous underlying securities in multi-asset options or, perhaps of greater relevance in practice, from features to express exotic payoffs and path-dependent models as shown next.

Suppose that  $\xi = \varphi(\tilde{\mathcal{O}}_T, X_T)$  for some occupation payoff  $\varphi$  and that  $X$  has dynamics  $dX_t = X_t \sigma(\tilde{\mathcal{O}}_t, X_t) dW_t$ ; see Section 5. Since  $(\tilde{\mathcal{O}}, X)$  is Markovian, then  $Y_t = v(\mathcal{O}_t, X_t)$  for some price functional  $v : \mathcal{D} \rightarrow \mathbb{R}$ . Assuming that  $v$  is smooth, we conclude from Itô's formula (Theorem 3.1) that  $Z_t = \partial_x v(\mathcal{O}_t, X_t) \sigma(\mathcal{O}_t, X_t)$ . One then parameterizes the Delta  $\Delta = \partial_x v$ , or  $Z$ , by a feedforward neural network  $\Phi : \mathcal{D}_T \times \Theta \rightarrow \mathbb{R}$  for some parameter set  $\Theta \subseteq \mathbb{R}^p$ ,  $p \in \mathbb{N}$ . In the present context of pricing and hedging, it is more natural to approximate the Delta process, namely

$$\partial_x v(\tilde{\mathcal{O}}_t, X_t) \approx \Phi(\tilde{\mathcal{O}}_t, X_t; \theta) =: \Delta^\theta(\tilde{\mathcal{O}}_t, X_t). \quad (54)$$

Moreover, the unknown initial value  $Y_0$  is replaced by an extra parameter  $\pi \in \mathbb{R}$ , the price of the claim, leading to the parameterized value process  $Y_t^{\pi, \theta} = \pi + \int_0^t \Delta^\theta(\tilde{\mathcal{O}}_s, X_s) dX_s$ . In light of (53), the parameters  $\pi, \theta$  are trained so as to satisfy  $Y_T^{\pi, \theta} \approx \xi$ , e.g., by solving the following quadratic hedging problem using stochastic gradient descent,

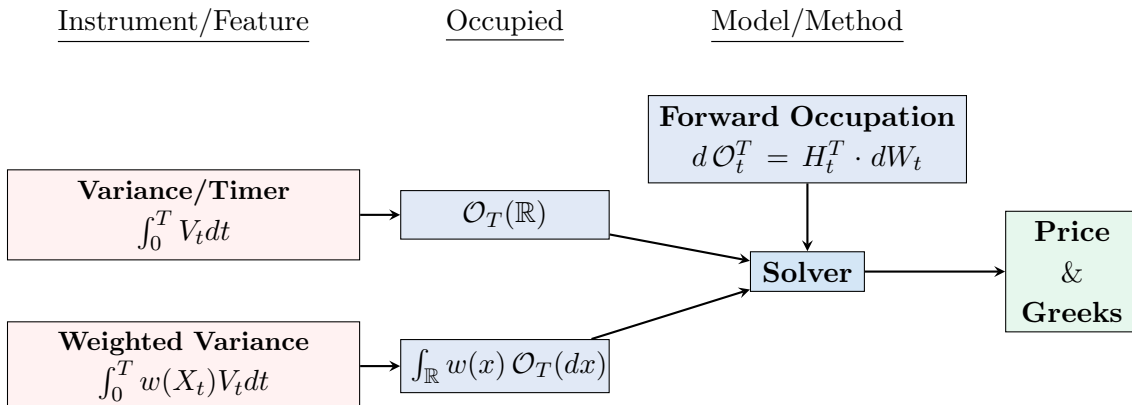
$$\inf_{\pi, \theta} \mathcal{L}(\pi, \theta), \quad \mathcal{L}(\pi, \theta) := \mathbb{E}^{\mathbb{Q}}[|\xi - Y_T^{\pi, \theta}|^2]. \quad (55)$$

Crucially, the control  $\Delta^\theta(\tilde{\mathcal{O}}_t, X_t)$  takes the state process as input, so can be parametrized by a single neural network across time. This is in stark contrast with path-dependent PDEs where the deep BSDE method is not available due to the lack of Markov structure. Instead, one may use recurrent neural networks, e.g. [76] extending the deep Galerkin method to PPDEs. However, the training and tuning of recurrent neural networks is much more involved and suffers from an explosion in input dimension when the number of time steps becomes large. Hence, it is less clear that such approach would be adopted by practitioners.

## 4.2 Variance Derivatives

Similarly, the occupation flow  $\mathcal{O}$  provides a unified lift for variance instruments as shown in the following examples and diagram below. The forward occupation model mentioned in Fig. 4 will be introduced in Section 6.

Figure 4: Unified Markovian lift for variance derivatives.



**Example 11.** *Corridor Variance Swaps* (CVS) are over-the-counter instruments providing exposure to the volatility of an asset when the latter lies within a prescribed range. They belong to the larger family of weighted variance swaps; see Bergomi [10, Chapter 5] and Lee [67]. For concreteness, if the log price of an asset has dynamics  $dX_t = -\frac{1}{2}V_t dt + \sqrt{V_t}dW_t$ , then the terminal profit and loss (P&L) for the buyer is given by

$$\text{P\&L} = \frac{1}{T} \int_0^T \mathbb{1}_{[x_1, x_2]}(X_t) V_t dt - K_{x_1, x_2}^2, \quad x_1 < x_2. \quad (56)$$

The levels  $x_1, x_2$  defines the corridor during which the instantaneous variance  $V_t$  is accumulated. Since  $V_t dt = d\langle X \rangle_t$ , the floating leg is proportional to the occupation time  $\mathcal{O}_T([x_1, x_2])$ . The *fair strike*  $K_{x_1, x_2}$  is set such that the swap has zero initial cost. By the law of one price, it is thus given by the (scaled) expected occupation time  $K_{x_1, x_2}^2 = \frac{1}{T} \mathbb{E}^{\mathbb{Q}}[\mathcal{O}_T([x_1, x_2])]$ . Hence, corridor variance can be viewed as the primitive securities associated to  $\mathcal{O}$  and will play a central role in the forward occupation models introduced in Section 6.

Corridor variance swaps offer several advantages over a standard variance swap which delivers the cumulative realized variance irrespective of the underlying price level. First, CVS's are less expensive the variance accumulated outside the prescribed corridor is simply discarded. Second, the holder may have some views on the market and can speculate a range on the asset's future levels by entering a suitable CVS. See [67, 68] for further details.

**Remark 7.** Towards a parallel with the stop local time problem (Section 7), we may envision a *floating American CVS* where the holder chooses when to receive the realized variance within a floating corridor around the spot price. That is,  $x_1 = X_\tau - \varepsilon$ ,  $x_2 = X_\tau + \varepsilon$ , in which case we have<sup>3</sup>

$$K^2(\varepsilon) = \sup_{\tau \leq T} \mathbb{E}^{\mathbb{Q}} \left[ \frac{1}{2\varepsilon} \int_0^\tau \mathbb{1}_{B_\varepsilon(X_\tau)}(X_t) V_t dt \right] = \sup_{\tau \leq T} \mathbb{E}^{\mathbb{Q}} [\varphi_\varepsilon(\mathcal{O}_\tau, X_\tau)], \quad (57)$$

with  $\varphi_\varepsilon$  seen in (97). As seen Section 7.4 that  $K^2(\varepsilon) = v_\varepsilon^*$  converges to the value of the spot local time problem (95). While these contracts are not traded in financial markets, their introduction could benefit investors seeking exposure to volatility around the asset price when it is exercised.

**Example 12.** Introduced by Société Générale [77], *timer options* differ from traditional derivatives by having a floating maturity determined by the asset's realized volatility [11] [55, Chapter 1]. Concretely, the payoff is delivered once the total variance exceeds a prescribed budget. This characteristic presents benefits for both parties: the buyer can save on the premium, typically positive, between implied and realized volatility, while the seller is less exposed, if exposed at all, to model risk arising from volatility, called Vega risk. This is because these contracts they are less sensitive, if not insensitive to volatility as explained next.

Let  $S$  be an asset with dynamics  $dS_t = \sigma_t S_t dW_t$ , with  $\sigma_t \geq \underline{\sigma}$  for some constant  $\underline{\sigma} > 0$ . Define also the log price  $X = \log S$ , quadratic variation process  $Q_t = \langle X \rangle_t = \int_0^t \sigma_s^2 ds$ , and stopping time  $\tau_q = \inf\{t \geq 0 : Q_t \geq q\}$ . Fix a variance budget  $\bar{q} > 0$  and payoff  $\varphi : \mathbb{R}_+ \rightarrow \mathbb{R}$  such that  $w(q, s) := \mathbb{E}^{\mathbb{Q}}[\varphi(S_{\tau_{\bar{q}-q}}) \mid S_0 = s]$  belongs to  $\mathcal{C}^{1,2}(\mathbb{R}_+^2)$ . Then, it is easily seen from

<sup>3</sup>Note that  $\mathcal{O}_T(\overline{B_\varepsilon(x)}) = \mathcal{O}_T(B_\varepsilon(x))$  as  $\mathcal{O}_T \ll \lambda \mathbb{Q}$ -a.s.

Itô's formula that  $w$  solves the PDE

$$\begin{cases} \left( \partial_q + \frac{s^2}{2} \partial_{ss} \right) u(q, s) = 0, & q < \bar{q}, \\ u(q, s) = \varphi(s) & q = \bar{q}. \end{cases} \quad (58a)$$

$$(58b)$$

The volatility does not appear in (58a) since it is absorbed by the quadratic variation process. Consequently, the value of the contract is insensitive to volatility. However, this conclusion does not hold anymore in the presence of (nonzero) interest rates or dividends; see [11].

Importantly,  $q$  plays the role of time in (58a)-(58b) as does the occupation flow, and one naturally expects a connection between the above PDE and the Dirichlet problem (45a)-(45b). Indeed, if  $\mathcal{O}$  is the occupation flow of  $X$ , then  $Q_t = \mathcal{O}_t(\mathbb{R})$ , and set  $v(\mathfrak{o}, x) := w(\mathfrak{o}(\mathbb{R}), e^x)$ . Hence  $v \in \mathcal{C}^{1,2}(\mathcal{D})$  with  $\partial_x v = s \partial_s w$ ,  $\partial_{xx} v = s^2 \partial_{ss} w$ , and  $\partial_{\mathfrak{o}} v = \partial_q w$  from Example 2. If the volatility process satisfies  $\sigma_t = \sigma(\mathcal{O}_t, X_t)$  for some map  $\sigma : \mathcal{D} \rightarrow [\underline{\sigma}, \infty)$ , then  $dX_t = -\frac{1}{2} \sigma(\mathcal{O}_t, X_t)^2 dt + \sigma(\mathcal{O}_t, X_t) dW_t$ , and according to Theorem 3.5,  $v$  solves the occupied PDE

$$\begin{cases} \left( \sigma^2 \partial_{\mathfrak{o}} - \frac{\sigma^2}{2} \partial_x + \frac{\sigma^2}{2} \partial_{xx} \right) u(\mathfrak{o}, x) = 0, & \text{on } \mathcal{D}_{\Theta}, \\ u(\mathfrak{o}, x) = \varphi(e^x) & \text{on } \partial \mathcal{D}_{\Theta}, \end{cases} \quad (59a)$$

$$(59b)$$

where  $\Theta = \bar{q}$ . Again, we can factor out  $\sigma^2$  from (59a), again confirming the irrelevance of the volatility to price the option.

## 5 Occupied Volatility

We here discuss some avenues with regards to financial modeling. Precisely, we would like to see how occupied SDEs (Section 3.4) can be used for this task. We start with deterministic clocks, while OSDEs with variance time will be discussed in Section 6. Recall the calendar time occupation flow  $\tilde{\mathcal{O}} = \int_0^\cdot \delta_{X_s} ds$  and assume that the price process  $X$  of an asset follows the dynamics,

$$\frac{dX_t}{X_t} = (r - q)dt + \sigma(\tilde{\mathcal{O}}_t, X_t) dW_t, \quad (60)$$

with interest rate  $r \in \mathbb{R}$  and dividend yield  $q \geq 0$ , both assumed to be constant for simplicity. The diffusion coefficient  $\sigma$  shall be termed *occupied volatility*. A special case is Dupire's local volatility model [38]. Indeed, if  $\sigma_{\text{loc}}$  denotes the local volatility function, then

$$\sigma(\mathfrak{o}, x) := \sigma_{\text{loc}}(\mathfrak{o}(\mathbb{R}), x) \implies \sigma(\tilde{\mathcal{O}}_t, X_t) = \sigma_{\text{loc}}(t, X_t). \quad (61)$$

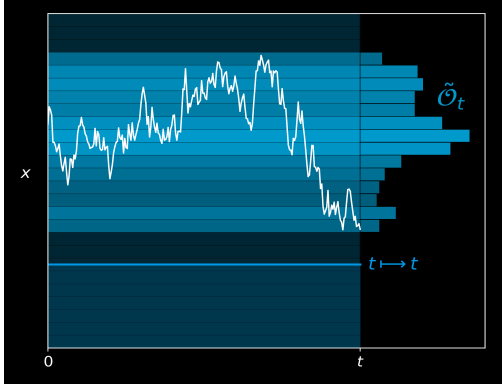
Hence (60) gives a sensible generalization of the local volatility model as long as  $\sigma$  satisfies the *smile calibration condition*,

$$\mathbb{E}^{\mathbb{Q}}[\sigma^2(\tilde{\mathcal{O}}_t, X_t) \mid X_t] = \sigma_{\text{loc}}^2(t, X_t). \quad (62)$$

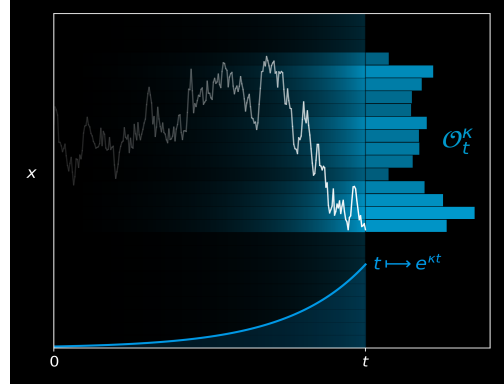
ensuring that vanilla call and put options are correctly priced; see, e.g., [20]. On the other hand, occupied volatility is a particular example of path-dependent volatility [20, 52, 53, 56, 59] and thus enjoys similar benefits. Notably, as the occupation flow is endogenous, the model remains complete, i.e., every contingent claim  $\xi$  can be perfectly replicated by dynamically trading the underlying  $X$ .

Figure 5: Occupation measure using calendar time ( $\tilde{\mathcal{O}}_t$ , left) compared with exponential time ( $\mathcal{O}^\kappa$ , right). As can be seen,  $\mathcal{O}^\kappa$  puts more emphasis on recent levels of the path.

(a) Calendar time. Preferred under  $\mathbb{Q}$ .



(b) Exponential time. Preferred under  $\mathbb{P}$ .



Back to the unified framework Fig. 3, we can then price any instrument contingent on  $(\tilde{\mathcal{O}}_T, X_T)$  in model Fig. 3, which can be done efficiently due to the Markov structure. From an econometric perspective, calendar time may not be the most realistic clock to model volatility, due to the chronology invariance of  $\tilde{\mathcal{O}}$  discussed in Section A. As an illustration, fix a one-year horizon, with current time  $t = 1$ , and consider two scenarios  $\omega^1, \omega^2$  such that  $X_1(\omega^1) = X_1(\omega^2)$  and  $\tilde{\mathcal{O}}_1(\omega^1) = \tilde{\mathcal{O}}_1(\omega^2)$ . Then  $\omega^1, \omega^2$  generate the same occupied volatility level. However, suppose that in the first (respectively second) scenario, a financial crash occurred a week (resp. a year) ago, while the market has been bullish otherwise. One would then expect much higher volatility in the first scenario.

The above example calls for a clock that captures a memory decay in past information. Among others, this is achieved through the *exponential time* occupation flow,

$$d\mathcal{O}_t^\kappa = \delta_{X_t} e^{\kappa t} dt, \quad \kappa \geq 0. \quad (63)$$

The calendar time occupation flow is recovered by setting  $\kappa = 0$ , so all the subsequent results will be presented in terms of the more general object  $\mathcal{O}^\kappa$ . Note that calendar time may still be preferred for pricing/hedging purposes due to the unified framework Fig. 3. In short, calendar time is preferred under  $\mathbb{Q}$  (pricing measure), while exponential time is preferred under  $\mathbb{P}$  (historical measure).

The volatility now takes the exponential time occupation flow as input, leading to

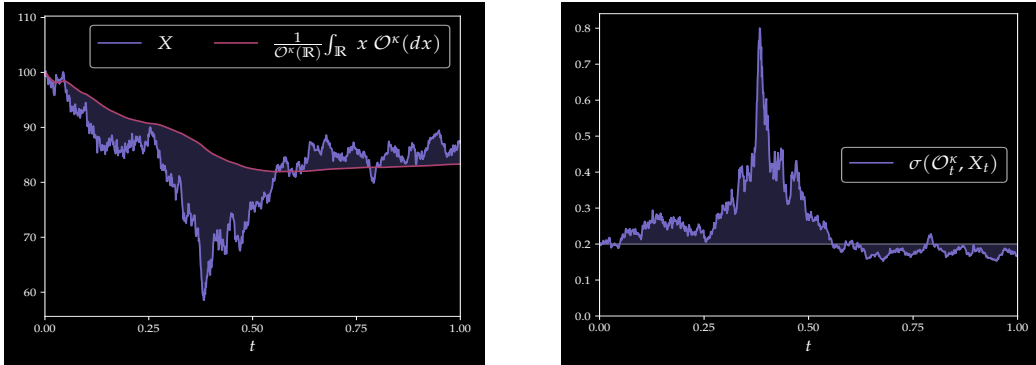
$$\frac{dX_t}{X_t} = (r - q)dt + \sigma(\mathcal{O}_t^\kappa, X_t)dW_t. \quad (64)$$

By increasing the exponential parameter  $\kappa$ , the exponential time occupation flow puts more emphasis on the present, thus making volatility more reactive to recent shocks. Crucially,  $(\mathcal{O}^\kappa, X)$  remains a Markov process when  $\kappa > 0$ , enabling efficient simulation of (64).

**Example 13.** (Guyon's toy volatility model) Consider the occupied volatility

$$\sigma(\mathcal{O}_t^\kappa, X_t) = \Sigma(\Upsilon(\mathcal{O}_t^\kappa, X_t)), \quad \Sigma(y) = -\frac{\alpha}{\beta} + \gamma y^{-\beta}, \quad (65)$$

Figure 6: Guyon's toy volatility model with  $\sigma$  given in (65). One simulations using the Euler-Maruyama scheme in Section 5.1. Parameters:  $x_0 = 100, T = 1, \kappa = 12$ , and  $(\alpha, \beta, \gamma) = (2.1, 1.2, 1.9)$ .



with parameters  $\alpha, \beta, \gamma > 0$ , and functional

$$\Upsilon(\mathcal{O}_t^\kappa, X_t) = \frac{X_t}{\frac{1}{\mathcal{O}_t^\kappa(\mathbb{R})} \int_{\mathbb{R}} x \mathcal{O}_t^\kappa(dx)}. \quad (66)$$

The ratio (66) characterizes the *trend* of the asset by noting that the barycenter of  $\mathcal{O}^\kappa$  coincide with the exponentially weighted moving average (EMA) of the asset, namely

$$\text{EMA}_t = \frac{1}{1 - e^{-\kappa t}} \int_0^t X_u \kappa e^{-\kappa(t-u)} du = \frac{1}{\mathcal{O}_t^\kappa(\mathbb{R})} \int x \mathcal{O}_t^\kappa(dx). \quad (67)$$

Then  $dX_t = \sigma(\mathcal{O}_t^\kappa, X_t) X_t dW_t$  is precisely Guyon's toy volatility model [53], further analyzed by Bonesini et al. [15]. Since  $\Sigma$  in (65) is decreasing, the volatility  $\sigma$  is inversely proportional to the trend of the asset. This is in line with the *leverage effect*, a stylized fact in equity markets stating that volatility tends to increase when the asset price drops.

Fig. 6 displays two realizations of  $(X, \sigma(\mathcal{O}^\kappa, X))$  where  $X_0 = 100, T = 1$  year,  $\kappa = 12$ , to reflect a one-month window for the weighted average (67), and parameters  $(\alpha, \beta, \gamma) = (2.1, 1.2, 1.9)$  taken from [53, page 25]. We indeed observe that the volatility shoots up when the asset falls far below the running average. The trajectories in Fig. 6 using the scheme in Section 5.1 with  $N = 1,000$  time steps and levels  $x_m = 50 + m, m = 0, \dots, 100$ .

## 5.1 Simulation of Occupied SDEs

The numerical integration of OSDEs inevitably requires a discretization of the occupation flow. Focusing on the occupied volatility model (64), a natural way consists of keeping track of finitely occupation times  $\mathcal{O}_t^\kappa(C_1), \dots, \mathcal{O}_t^\kappa(C_M)$ , where  $(C_m)$  forms a partition of  $\mathbb{R}_+$ . Concretely, let  $x_1 < \dots < x_M, M \in \mathbb{N}$ , and introduce the corridors,

$$C_m = [x_m - \varepsilon_{m-1}, x_m + \varepsilon_m), \quad \varepsilon_m = \frac{x_{m+1} - x_m}{2}, \quad (\varepsilon_0 = x_1, \varepsilon_M = \infty).$$

The nodes  $(x_m)$  are chosen so as to match the scale of  $X_0$  and OSDE coefficients. We then replace  $\mathcal{O}_t^\kappa$  by the discrete measure  $\sum_{m=1}^M \mathcal{O}_t^\kappa(C_m) \delta_{x_m}$ , and approximate OSDE (64) by the finite-dimensional system

$$\frac{dX_t}{X_t} = (r - q)dt + \sigma^M(\mathcal{O}_t^\kappa, X_t) dW_t, \quad d\mathcal{O}_{t,m}^\kappa = \mathbf{1}_{C_m}(X_t) e^{\kappa t} dt, \quad (68)$$

with  $O_t^\kappa = (\mathcal{O}_t^\kappa(C_1), \dots, \mathcal{O}_t^\kappa(C_M)) \in \mathbb{R}^M$ . In light of (68),  $(O^\kappa, X)$  is an  $M+1$ -dimensional Markov process. Moreover, the *projected volatility*

$$\sigma^M : \mathbb{R}^{M+1} \rightarrow \mathbb{R}, \quad \sigma^M(O_t^\kappa, X_t) = \sigma\left(\sum_{m=1}^M O_{t,m}^\kappa \delta_{x_m}, X_t\right),$$

converges to  $\sigma(\mathcal{O}_t^\kappa, X_t)$  when  $\sigma(\mathfrak{o}, x)$  is weakly continuous in  $\mathfrak{o}$ . We can then simulate  $X$  using standard numerical schemes for SDEs [65, 51]. To wit, consider a regular time grid  $t_n = n\delta t$ ,  $\delta t = \frac{T}{N}$ ,  $N \in \mathbb{N}$ . Given  $X_0 \in \mathbb{R}_+$  and  $O^{\text{tmp}} = 0 \in \mathbb{R}^M$ , we then generate sample paths from (68) as follows,

$$\begin{cases} O_m^{\text{tmp}} & \leftarrow O_m^{\text{tmp}} + e^{\kappa t_n} \delta t, & X_{t_n} \in C_m, \\ \sigma_{t_n} & = \sigma^M(O^{\text{tmp}}, X_{t_n}), \\ X_{t_{n+1}} & = X_{t_n} \exp\{\sigma_{t_n} \sqrt{\delta t} Z_n + (r - q - \frac{1}{2}\sigma_{t_n}^2)\delta t\}, \end{cases}$$

where  $Z_n \stackrel{i.i.d.}{\sim} \mathcal{N}(0, 1)$ ,  $n = 0, \dots, N-1$ . Note that the occupation measure is represented by the temporary variable  $O^{\text{tmp}}$  updated at each iteration. Indeed, it is not necessary (and costly) to store the occupation times  $O_{t_n}^\kappa$  for each  $n$ .

More generally, one may use a partition of unity  $\{f_m : \mathbb{R}_+ \rightarrow [0, 1]\}_{m \leq M}$ ,  $\sum_m f_m \equiv 1$ , leading to the *cylindrical projection*  $\sigma(\mathcal{O}_t^\kappa, X_t) \approx \sigma^M(f_1 \cdot \mathcal{O}_t^\kappa, \dots, f_M \cdot \mathcal{O}_t^\kappa, X_t)$ . The occupation time approximation is thus recovered by setting  $f_m = \mathbb{1}_{C_m}$ , and similarly to  $(C_m)$  being a partition, the property  $\sum_m f_m \equiv 1$  ensures that the total mass of  $\mathcal{O}^\kappa$  is preserved. A convergence analysis of cylindrical projections of OSDEs as  $M \rightarrow \infty$  is addressed in a forthcoming paper [82].

**Remark 8.** The simulation of fully path-dependent volatility models,

$$\frac{dX_t}{X_t} = (r - q)dt + \sigma(t, \omega)dW_t,$$

typically involves discretization of the form  $\sigma(t_n, \omega) \approx \sigma_n^N(X_{t_1}(\omega), \dots, X_{t_n}(\omega))$  for some function  $\sigma_n^N : \mathbb{R}^n \rightarrow \mathbb{R}$ . Note the input dimension of  $\sigma_n^N$  grows linearly with  $n$ , which becomes highly problematic when the total number of time steps  $N$  is large. In contrast, occupied SDEs decouple the dimensionality of the space and time discretization, allowing for efficient simulations as shown in Example 13 and Section 5.3.

## 5.2 Local Occupied Volatility (LOV) Model

Let us start with an autonomous path-dependent volatility model of the form

$$\frac{dX_t}{X_t} = (r - q)dt + \sigma(F_t, X_t)dW_t,$$

for some path-dependent feature  $F_t(\omega) = f(t, \omega) \in \mathfrak{F}$ ,  $f : [0, T] \times \Omega_T \rightarrow \mathfrak{F}$ . The linear feature space  $\mathfrak{F}$  may be finite-dimensional, e.g.,  $F_t \in \{\sup_{s \leq t} X_s, \int_0^t X_s ds\}$  in Brunick and Shreve [20], or infinite-dimensional in occupied volatility models where  $\mathfrak{F} = \mathcal{M}$ ; see Section 5.2.1. Recall the smile calibration condition

$$\sigma_{\text{loc}}^2(t, X_t) = \mathbb{E}^{\mathbb{Q}}[\sigma^2(F_t, X_t) \mid X_t], \quad (69)$$

and introduce the *projected feature*  $\hat{F}_t = \mathbb{E}^{\mathbb{Q}}[F_t|X_t] = \hat{f}(t, X_t)$  for some map  $\hat{f} : \mathbb{R}_+^2 \rightarrow \mathfrak{F}$ . If  $\sigma^2(F, X)$  were linear in  $F$ , then  $\mathbb{E}^{\mathbb{Q}}[\sigma^2(F_t, X_t)|X_t] = \sigma^2(\hat{F}_t, X_t)$ , and (69) would imply that  $\sigma_{\text{loc}}(t, X_t) = \sigma(\hat{f}(t, X_t), X_t)$ . In general, one would linearize  $F \mapsto \sigma^2(F, X)$  using a first order *Markovian expansion* around  $\hat{F}_t$ , namely

$$\sigma^2(F_t, X_t) \approx \sigma^2(\hat{F}_t, X_t) + D\sigma^2(\hat{F}_t, X_t) \cdot (F_t - \hat{F}_t), \quad (70)$$

with the Fréchet derivative  $D\sigma^2(\cdot, X_t) : \mathfrak{F} \rightarrow \mathfrak{F}^*$  and dual pairing  $\mathfrak{F}^* \times \mathfrak{F} \ni (\ell, F) \rightarrow \ell \cdot F$ . The derivative  $D\sigma^2(\hat{F}_t, X_t)$  is the sensitivity of variance with respect to path-dependent (or non-Markovian) shocks. Noting that  $\sigma^2(\hat{F}_t, X_t)$ ,  $D\sigma^2(\hat{F}_t, X_t)$  are functions of  $(t, X_t)$  and in light of (69), we can *postulate* the following local path-dependent volatility (LPDV) model,

$$\sigma^2(F_t, X_t) = \sigma_{\text{loc}}^2(t, X_t) + \ell(t, X_t) \cdot (F_t - \hat{F}_t), \quad \ell : \mathbb{R}_+^2 \rightarrow \mathfrak{F}^*. \quad (71)$$

In particular, the term  $\sigma^2(\hat{F}_t, X_t)$  in (70) has been replaced with the local variance. Since  $\mathbb{E}^{\mathbb{Q}}[F_t - \hat{F}_t|X_t] = 0$ , the above specification automatically satisfies the smile calibration condition (69) for any reasonable choice of  $\ell$ , e.g., such that  $\sigma^2(F_t, X_t)$  remains positive.

The LPDV model (71) is reminiscent of local stochastic volatility (LSV) models [54, 55] where one multiplies  $\sigma_{\text{loc}}$  by an exogenous stochastic processes  $\alpha_t$  and normalized such that (69) holds. The volatility process is thus of the form

$$\sigma_t = \sigma_{\text{loc}}(t, X_t) \frac{\alpha_t}{\sqrt{\mathbb{E}^{\mathbb{Q}}[\alpha_t^2|X_t]}}, \quad (72)$$

where the conditional expectation is typically estimated using the particle method of Guyon and Henry-Labordère [54]. It is a powerful family of models that is consistent with vanilla options and capable of producing more realistic spot-vol dynamics than the standard local volatility model. On the other hand, local path-dependent volatility models also preserve market completeness by explaining future volatility from the price history directly. Moreover, considering an additive correction term  $\ell(t, X_t) \cdot (F_t - \hat{F}_t)$  term is arguably preferred numerically over the fraction in (72) with distribution-dependent denominator. Indeed, any error introduced when computing  $\hat{F}_t$  is controlled in a linear way.

### 5.2.1 The LOV Model

Let us set  $F_t = \mathcal{O}_t^\kappa$ . The feature space is  $\mathfrak{F} = \mathcal{M}$ , and the Fréchet differential in (70) becomes the linear derivative  $\delta_{\mathbf{o}}$  from Section 3.1. Recalling the dual pairing  $\phi \cdot \mathbf{o} = \int_{\mathbb{R}} \phi(x) \mathbf{o}(dx)$ ,  $(\phi, \mathbf{o}) \in \mathcal{C}_b(\mathbb{R}) \times \mathcal{M}$ , we can then rewrite (70) as

$$\sigma^2(\mathcal{O}_t^\kappa, X_t) \approx \sigma^2(\hat{\mathcal{O}}_t^\kappa, X_t) + \int_{\mathbb{R}_+} \delta_{\mathbf{o}} \sigma^2(\hat{\mathcal{O}}_t^\kappa, X_t)(x) (\mathcal{O}_t^\kappa - \hat{\mathcal{O}}_t^\kappa)(dx). \quad (73)$$

The *occupation sensitivity*  $\delta_{\mathbf{o}} \sigma^2(\hat{\mathcal{O}}_t^\kappa, X_t)(x) = \frac{d}{dh} \sigma^2(\hat{\mathcal{O}}_t^\kappa + h\delta_x, X_t)|_{h=0}$  describes the change in variance when the asset spends *more time than expected* (captured by  $\hat{\mathcal{O}}_t^\kappa$ ) at level  $x$ . We then replace  $\sigma^2(\hat{\mathcal{O}}_t^\kappa, X_t)$  with the local variance, and rewrite the occupation sensitivity as

$$\delta_{\mathbf{o}} \sigma^2(\hat{\mathcal{O}}_t^\kappa, X_t)(x) = \gamma_t^\kappa \ell(t, X_t, x), \quad \gamma_t^\kappa = \mathcal{O}_t^\kappa(\mathbb{R})^{-1} = \frac{\kappa}{e^{\kappa t} - 1}, \quad \kappa > 0, \quad \gamma_t^0 = \frac{1}{t}.$$

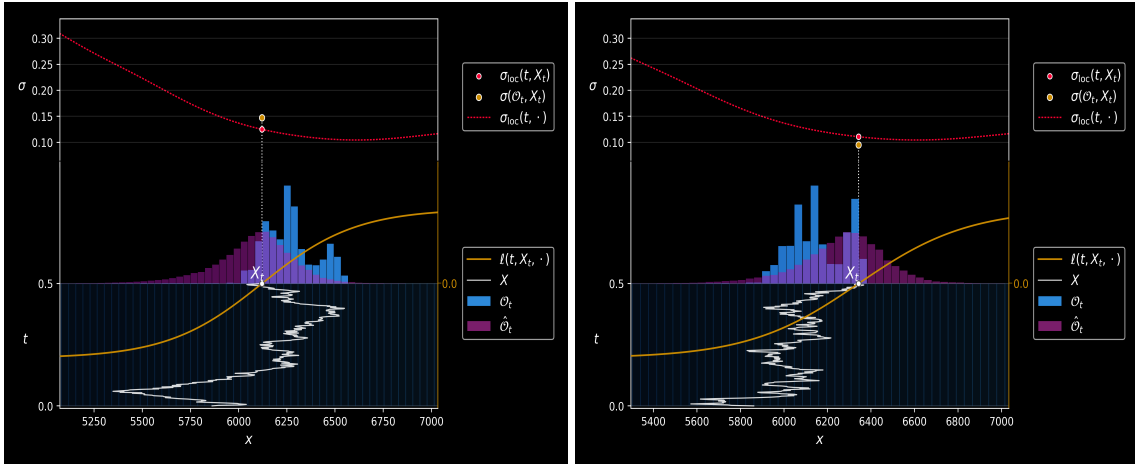
Altogether, we have derived the Local Occupied Volatility (LOV) model,

$$\frac{dX_t}{X_t} = (r - q)dt + \sigma(\mathcal{O}_t^\kappa, X_t)dW_t, \quad (74)$$

$$\sigma^2(\mathcal{O}_t^\kappa, X_t) = \sigma_{\text{loc}}^2(t, X_t) + \gamma_t^\kappa \int_{\mathbb{R}_+} \ell(t, X_t, x)(\mathcal{O}_t^\kappa - \hat{\mathcal{O}}_t^\kappa)(dx). \quad (75)$$

The factor  $\gamma_t^\kappa$  is introduced so as to maintain a constant magnitude of  $\ell$  over time, and allow to interpret the linear term as the average sensitivity of variance when the realized occupation measure  $\mathcal{O}_t^\kappa$  deviates from the implied one ( $\hat{\mathcal{O}}_t^\kappa$ ).

Figure 7: Local occupied volatility (yellow dot) compared with local volatility (red). The yellow curve is the local sensitivity function  $x \mapsto \ell(t, X_t, x)$ , which is integrated against the spread  $\mathcal{O}_t^\kappa - \hat{\mathcal{O}}_t^\kappa$  between the realized occupation measure (blue) and the expected one (purple).



Without careful specification of the sensitivity function ( $\ell$ ), the LOV model may produce negative variances because the path-dependent term in (75) is centered around zero. However, mild conditions on  $\ell$  can guarantee  $\sigma^2$  remains positive, as shown next.

**Proposition 5.** *Consider the LOV model with occupied volatility function  $\sigma : \mathcal{M} \times \mathbb{R}_+ \rightarrow \mathbb{R}$  given in (75). If  $|\ell(t, x', x)| < \frac{1}{2}\sigma_{\text{loc}}^2(t, x')$  for all  $t, x', x$ , then  $\sigma^2 > 0$  on  $\mathcal{M} \times \mathbb{R}_+$ .*

*Proof.* Let  $c(t, x') = \sup_x |\ell(t, x', x)|$ . Then  $c(t, x') < \frac{1}{2}\sigma_{\text{loc}}^2(t, x')$  by assumption, hence

$$\sigma^2(\mathcal{O}_t^\kappa, X_t) \geq \sigma_{\text{loc}}^2(t, X_t) - \gamma_t^\kappa \int_{\mathbb{R}} |\ell(t, X_t, x)|(\mathcal{O}_t^\kappa + \hat{\mathcal{O}}_t^\kappa)(dx) \geq \sigma_{\text{loc}}^2(t, X_t) - 2c(t, X_t) > 0.$$

□

Under the above assumption on  $\ell$ , the sensitivity function can nearly double the local variance or push it down to nearly zero. The path-dependent term in (75) thus offers a wide, yet controlled, range to adjust the local variance while ensuring positivity. Alternatively, one can rewrite the occupied variance in a multiplicative way, namely

$$\sigma^2(\mathcal{O}_t^\kappa, X_t) = \sigma_{\text{loc}}^2(t, X_t) \left( 1 + \gamma_t^\kappa \int_{\mathbb{R}_+} \tilde{\ell}(t, X_t, x)(\mathcal{O}_t^\kappa - \hat{\mathcal{O}}_t^\kappa)(dx) \right), \quad (76)$$

where the condition  $|\tilde{\ell}(t, X_t, x)| < \frac{1}{2}$  ensures positivity of  $\sigma^2$ .

**Example 14.** (one-factor LOV) Consider the multiplicative version (76), with  $\tilde{\ell}(t, X_t, x) = \beta \mathbb{1}_A(x)$ ,  $A \in \mathcal{B}(\mathbb{R}_+)$ , and  $|\beta| < 1/2$ . Then,

$$\sigma^2(\mathcal{O}_t^\kappa, X_t) = \sigma_{\text{loc}}^2(t, X_t) \left( 1 + \beta \gamma_t^\kappa (\mathcal{O}_t^\kappa - \hat{\mathcal{O}}_t^\kappa)(A) \right).$$

In view of Proposition 5,  $\sigma^2 > 0$ . Recalling that  $\gamma_t^\kappa = \mathcal{O}_t^\kappa(\mathbb{R}_+)^{-1} = \hat{\mathcal{O}}_t^\kappa(\mathbb{R}_+)^{-1}$ , the local variance is thus rescaled according to the fraction of time  $\gamma_t^\kappa \mathcal{O}_t^\kappa(A)$  spent by the asset in  $A$  compared to what is expected. Here, the occupied volatility depends only on  $t, X_t$ , and the occupation time  $\mathcal{O}_t^\kappa(A)$ . As  $(\mathcal{O}^\kappa(A), X)$  is a two-dimensional Markov process, trajectories from the LOV model can thus be effectively simulated under this simple specification. In Algorithm 1, this would correspond to choosing  $M = 1$  corridor.

Examples for  $A$  include the upside corridor  $A^+ = [X_0, \infty)$ , where a positive parameter  $\beta$  would be consistent with the leverage effect. Alternatively, one can consider a narrow corridor around the money, e.g.,  $A = [0.9X_0, 1.1X_0]$ , where high values for  $\mathcal{O}_t^\kappa(A)$  indicate some mean reversion of the recent path toward the initial value. This mean reversion would, in turn, translate into lower volatilities than  $\sigma_{\text{loc}}$  by choosing  $\beta < 0$ .

**Example 15.** (EMA LOV) Suppose that  $\ell(t, X_t, x) = \beta \log x$  for some parameter  $\beta \in \mathbb{R}$ . Then, using (67), we can rewrite the local occupied volatility (75) as

$$\sigma^2(\mathcal{O}_t, X_t) = \sigma_{\text{loc}}^2(t, X_t) + \beta(\text{EMA}_t - \widehat{\text{EMA}}_t),$$

$$\text{EMA}_t = \frac{1}{1 - e^{-\kappa t}} \int_0^t \log X_u \kappa e^{-\kappa(t-u)} du, \quad \widehat{\text{EMA}}_t = \mathbb{E}^\mathbb{Q}[\text{EMA}_t \mid X_t].$$

The trend  $\text{EMA}_t - \widehat{\text{EMA}}_t$  is similar to the first offset process of Hobson and Rogers [59], where the projected EMA is replaced by the log spot  $\log X_t$ . Note that choosing  $\beta > 0$  makes the path-dependent correction term consistent with the leverage effect.

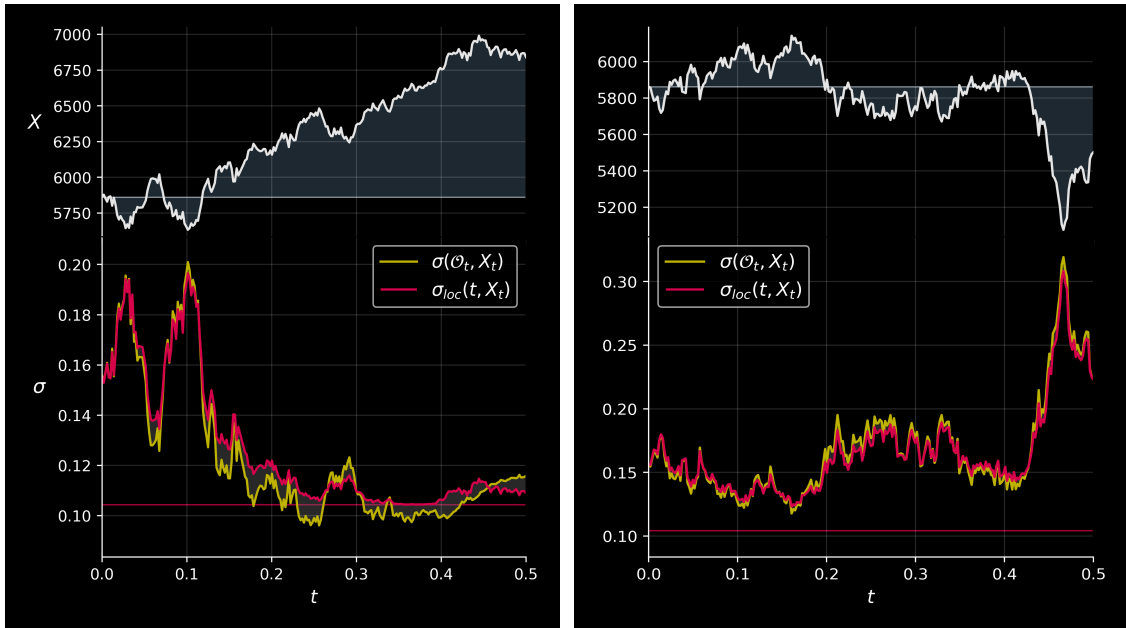
**Example 16.** Consider a time-homogeneous local volatility function given by the Markov projection  $\sigma_{\text{loc}}(x) = \mathbb{E}^\mathbb{Q}[\sigma^2(\mathcal{O}_t^\kappa, X_t) \mid X_t = x]^{1/2}$ ,  $t \approx 0.5$ , displayed in Fig. 11. The occupied volatility  $\sigma$  is calibrated to options on the S&P 500 Index (SPX); see Section 5.3. Assume that  $\ell(t, X_t, \cdot)$  is time-homogeneous, and nondecreasing in  $x$ . For simplicity, consider the following (scaled) hyperbolic tangent of the moneyness  $x/X_t$ ,

$$\ell(t, X_t, x) = \frac{1}{4} \underline{\sigma}^2 \tanh(\alpha x / X_t), \quad \underline{\sigma} = \inf_x \sigma_{\text{loc}}^2(x) > 0, \quad \alpha > 0.$$

According to Proposition 5, the occupied variance remains positive. Fig. 8 shows two sample paths of the asset and volatilities with  $\kappa = 12$  (one month window), and  $T = 0.5$ , aligned with the last option's expiry from Section 5.3. The right panel illustrates that local volatility is typically floored (by  $\underline{\sigma}$ ). This undesirable property is overcome with the local occupied volatility due to its path-dependent correction term.

Fig. 7 displays the occupation measures and sensitivity function  $x \mapsto \ell(t, X_t, x)$  (yellow curve) at  $t = T$ , together with the local and occupied volatility. As can be seen, the local volatility is adjusted up or down according to the difference between the realized and implied occupation measures  $\mathcal{O}_t^\kappa, \hat{\mathcal{O}}_t^\kappa$ . In the left panel of Fig. 7, the recent path has spent more time above the spot than *expected*, namely  $\mathcal{O}_t^\kappa(dx) > \hat{\mathcal{O}}_t^\kappa(dx)$  for almost every  $x > X_t$ , indicating

Figure 8: Simulated price path and volatility in the Local Occupied Volatility (LOV) model, with sensitivity function given in Example 16.



a possibly large drawdown resulting in higher volatility. Since the sensitivity function is positive above the spot and negative otherwise, the occupied volatility in the LOV model will be greater than the local volatility, further capturing the leverage effect. The right panel of Fig. 7 shows the opposite situation, where the spot is close to the asset's recent high, which typically translates into lower volatilities.

### 5.2.2 Simulation

We sample trajectories from (74)-(75) through an extension of the algorithm in Section 5.1. Specifically, the projected flow  $\hat{O}^\kappa$  is estimated using the particle method [54]. Concretely, the projected occupation times  $\hat{O}_m(\omega_j)$  in Step III.2. is estimated by the Nadaraya-Watson estimator,

$$\hat{O}_m^\kappa(\omega_j) = \frac{\sum_{j'} \psi_{j,j'} O_m^\kappa(\omega_{j'})}{\sum_{j'} \psi_{j,j'}}, \quad \psi_{j,j'} = \psi(X_{t_n}(\omega_j) - X_{t_n}(\omega_{j'})),$$

where  $\psi : \mathbb{R} \rightarrow \mathbb{R}_+$  is a kernel. In our numerical experiments, we use the quartic kernel  $\psi(\delta) = \frac{15}{16}(1 - (\delta/h)^2)^2/h$ , and set the bandwidth  $h$  following the guidelines in [55, Chapter 11]. The complete simulation scheme is provided in Algorithm 1.

**Algorithm 1** (LOV Model, Simulation)

---

$T > 0$ ,  $N \in \mathbb{N}$  (# time steps),  $M$  (# corridors),  $J \in \mathbb{N}$  (# simulations)

---

I. **Initialize**  $O^\kappa = 0 \in \mathbb{R}^M$ ,  $X_0 = x_0$

II. **Generate** Gaussian random variates  $Z_n(\omega_j) \stackrel{i.i.d.}{\sim} \mathcal{N}(0, 1)$

III. **For**  $n = 0, \dots, N - 1$ : (with  $t_n = n\delta t$ ,  $\delta t = \frac{T}{N}$ )

1. **Update**  $O^\kappa$ :  $O_m^\kappa(\omega_j) \leftarrow O_m^\kappa(\omega_j) + e^{\kappa t_n} \delta t$ ,  $X_{t_n}(\omega_j) \in C_m$

2. **Compute**  $\hat{O}^\kappa$  using the particle method:

$$\hat{O}_m^\kappa(\omega_j) = \frac{\sum_{j'} \psi_{j,j'} O_m^\kappa(\omega_{j'})}{\sum_{j'} \psi_{j,j'}}, \quad \psi_{j,j'} = \psi(X_{t_n}(\omega_j) - X_{t_n}(\omega_{j'}))$$

3. **Update**  $\sigma$ :  $\sigma_{t_n}^2(\omega_j) = \left( \sigma_{\text{loc}}^2(t_n, X_{t_n}) + \gamma_{t_n}^\kappa \sum_{m=1}^M \ell(t_n, X_{t_n}, x_m) (O_m^\kappa - \hat{O}_m^\kappa) \right) (\omega_j)$

4. **Update**  $X$ :  $X_{t_{n+1}}(\omega_j) = X_{t_n} \exp \left\{ \sigma_{t_n} \sqrt{\delta t} Z_n + \left( r - q - \frac{1}{2} \sigma_{t_n}^2 \right) \delta t \right\} (\omega_j)$

---

### 5.3 Market Implied Occupation Sensitivity

Let us gain insights into the LOV model (74)–(75) under the risk-neutral measure ( $\mathbb{Q}$ ), where we shall extract the sensitivity function  $\ell^\mathbb{Q}$  implied by options market data. To this end, we first go back to the general occupied volatility (64) and parameterize  $\sigma$  by a feedforward neural network, that is

$$\sigma(O_t^\kappa, X_t) \approx \sigma_\theta(O_t^\kappa, X_t) := \Phi(O_t^\kappa, X_t; \theta), \quad \Phi: \mathbb{R}^M \times \mathbb{R}_+ \times \Theta \rightarrow \mathbb{R}_+, \quad (77)$$

with the occupation times  $O_t^\kappa = (O_t^\kappa(C_1), \dots, O_t^\kappa(C_M)) \in \mathbb{R}^M$ . The asset price process thus evolves according to the following neural occupied SDE,

$$\frac{dX_t^\theta}{X_t^\theta} = (r - q)dt + \sigma_\theta(O_t^{\kappa,\theta}, X_t^\theta) dW_t, \quad dO_{t,m}^{\kappa,\theta} = \mathbf{1}_{C_m}(X_t^\theta) e^{\kappa t} dt. \quad (78)$$

The parameters  $\theta \in \Theta$  are then calibrated to market quotes of vanilla call and put options (see Algorithm 2). Note that a single neural network is used in (77) for all time points, which presents present significant benefits in terms of computational cost and smoothness in the time variable; see [74]. The optimization is also done on the full horizon at all once, often called global-in-time approach [60].

Neural networks offer an effective and flexible way to parametrize high-dimensional functions, at the cost of losing a clear interpretation of the parameters. Nevertheless, one way to understand the link between input (spot and occupation times) and output (volatility) is to compute sensitivities of the neural network, readily available through automatic differentiation; see e.g., [36, Chapter 5]. In our context, we can extract the partial derivatives of variance with respect to the occupation times  $O_t^{\kappa,\theta}(C_m)$ , and retrieve the implied sensitivity  $\ell^\mathbb{Q}$  through

$$\gamma_t^\kappa \ell^\mathbb{Q}(t, X_t^\theta, x) = \delta_o \sigma^2(O_t^{\kappa,\theta}, X_t)(x) \approx \partial_m \sigma_\theta^2(O_t^{\kappa,\theta}, X_t^\theta), \quad x \in C_m, \quad (79)$$

where  $\partial_m$  denotes the partial derivative with respect to  $O_m$ . Illustrations of  $\ell^{\mathbb{Q}}$  will be given in Section 5.3.3.

### 5.3.1 Calibration

Consider a collection of  $I \in \mathbb{N}$  quoted vanilla contracts with payoffs  $(\eta_i(X_{T_i} - K_i))^+$ ,  $i = 1, \dots, I$ , where  $T_i$  is the maturity,  $K_i$  is the strike price, and  $\eta \in \{\pm\}$  specifies the option type ( $\eta = 1$ : call, and  $\eta = -1$ : put). The market bid/ask price and Black-Scholes implied volatility of the  $i$ -th contracts is denoted by  $\pi_i^{\text{bid}}, \pi_i^{\text{ask}}$  and  $\sigma_i^{\text{bid}}, \sigma_i^{\text{ask}}$ , respectively. We recall that the Black-Scholes bid/ask implied volatility is defined through the equation  $\pi_i^{\text{bid/ask}} = \pi^{\text{BS}}(K, T, \eta, \sigma_i^{\text{bid/ask}})$ , where  $\pi^{\text{BS}}(K, T, \eta, \sigma)$  is the price of a vanilla contract with characteristics  $(K, T, \eta)$  in the Black-Scholes model with volatility  $\sigma$ .

We then train the parameters of the neural volatility  $\sigma_\theta$  in (78) so that the model prices,

$$\pi_i^\theta := e^{-rT_i} \mathbb{E}^{\mathbb{Q}}[(\eta_i(X_{T_i}^\theta - K_i))^+],$$

lie between the bid and ask market prices  $\pi_i^{\text{bid}}, \pi_i^{\text{ask}}$  for all  $i = 1, \dots, I$ . Training loop is summarized in Algorithm 2. In Step V., the calibration is deemed complete when the loss has stabilized and remains below the following bid/ask threshold (see also [5])

$$\alpha = \left( \frac{1}{I} \sum_{i=1}^I |w_i(\pi_i^{\text{bid/ask}} - \pi_i^{\text{mid}})|^2 \right)^{1/2} = \frac{1}{2} \left( \frac{1}{I} \sum_{i=1}^I |w_i(\pi_i^{\text{ask}} - \pi_i^{\text{bid}})|^2 \right)^{1/2}.$$

**Remark 9.** (Calibration weights) Similar to Ben Hamida and Cont [5], we use the inverse Black-Scholes Vega in (80) to translate prices into implied volatilities. Indeed, if  $\sigma_i^\theta, \sigma_i^{\text{mid}}$  is respectively the Black-Scholes implied volatility associated to  $\pi_i^\theta, \pi_i^{\text{mid}}$ , then a first order Taylor expansion of  $\sigma \mapsto \pi^{\text{BS}}(K_i, T_i, \eta_i, \sigma)$  gives

$$|\pi_i^\theta - \pi_i^{\text{mid}}| = |\pi^{\text{BS}}(K_i, T_i, \eta_i, \sigma_i^\theta) - \pi^{\text{BS}}(K_i, T_i, \eta_i, \sigma_i^{\text{mid}})| \approx \vartheta_i^{\text{mid}} |\sigma_i^\theta - \sigma_i^{\text{mid}}|.$$

As the Vega becomes arbitrarily small for out-of-the-money options and short maturities, we also cap the weights by setting instead  $(\vartheta_i^{\text{mid}} \vee \varepsilon)^{-1}$  in (80) with, e.g.,  $\varepsilon = 10^{-2}$ ; see also [5]. Moreover, the bid-ask ratio  $\frac{\sigma_i^{\text{bid}}}{\sigma_i^{\text{ask}}}$  gives greater weight to liquid contracts, i.e., those with tighter percentage bid-ask spread  $1 - \frac{\sigma_i^{\text{bid}}}{\sigma_i^{\text{ask}}}$ . Although one could directly use the implied volatility errors  $|\sigma_i^\theta - \sigma_i^{\text{mid}}|$  in the loss function, this would necessitate the computation of the model implied volatilities  $(\sigma_i^\theta)_{i=1}^I$  at every training step, which is prohibitively costly for large  $I$ . Note in contrast that the bid-ask ratios  $\frac{\sigma_i^{\text{bid}}}{\sigma_i^{\text{ask}}}$  can be computed offline.

### 5.3.2 Market Data and Results

We consider the market quotes of the front six-month SPX monthly options as of 2025/02/27, 4pm EST. The close price of the SPX Index that day was  $X_0 = 5,861.57$ . The expiration dates are given by

$$2025/\text{mm}/\text{dd}, \quad \text{mm}/\text{dd} \in \{03/21, 04/18, 05/16, 06/20, 07/18, 08/15\}.$$

We consider a moneyness range of [80%, 120%], roughly corresponding to the strike range [4,700, 7000]. This gives a total of  $I = 2,667$  instruments to calibrate our neural occupied

**Algorithm 2** (Calibration of Neural Occupied Volatility)

$J \in \mathbb{N}$  (batch size),  $I \in \mathbb{N}$  (# instruments),  $\pi_i^{\text{bid}}, \pi_i^{\text{ask}}$  (bid/ask quotes),  $(K_i, T_i, \eta_i) \in \mathbb{R}_+^2 \times \{\pm 1\}$  (option parameters),  $w_i \in \mathbb{R}_+$  (calibration weights)

I. **Generate** paths  $X^\theta(\omega_1), \dots, X^\theta(\omega_J)$  from the neural occupied SDE (78)

II. **Estimate** the model prices through Monte Carlo:  $\pi_i^\theta = e^{-rT_i} \frac{1}{J} \sum_{j=1}^J (\eta_i (X_{T_i}^\theta(\omega_j) - K_i))^+$

III. **Compute** the loss function given by the weighted root mean-squared error,

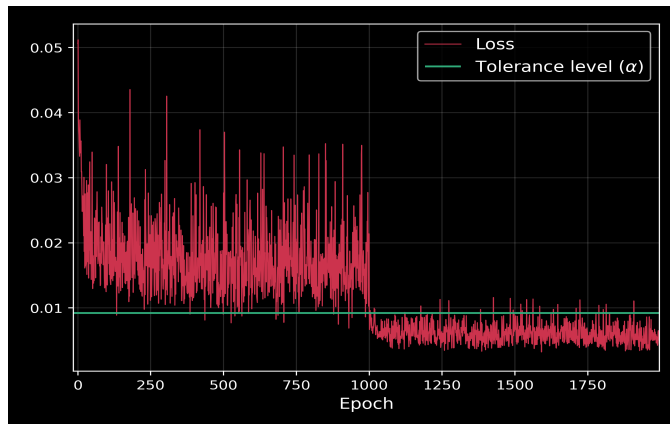
$$\mathcal{L}(\theta) = \left( \frac{1}{I} \sum_{i=1}^I |w_i (\pi_i^\theta - \pi_i^{\text{mid}})|^2 \right)^{1/2}, \quad w_i = (\vartheta_i^{\text{mid}})^{-1} \cdot \frac{\sigma_i^{\text{bid}}}{\sigma_i^{\text{ask}}}, \quad (80)$$

with the mid price  $\pi_i^{\text{mid}} = \frac{\pi_i^{\text{bid}} + \pi_i^{\text{ask}}}{2}$  and Black-Scholes Vega  $\vartheta_i^{\text{mid}}$ ; see Remark 9

IV. **Update** parameters:  $\theta \leftarrow \theta - \zeta \nabla \mathcal{L}(\theta)$ , with learning rate  $\zeta$  from the Adam optimizer

V. **Repeat** above steps until calibration is complete

Figure 9: Calibration loss  $\mathcal{L}(\theta)$  versus epochs.



volatility model. We also set  $r = 4.35\%$  and  $q = 0.5\%$ , aligned respectively with short-term U.S. treasury rates and SPX implied dividend yields as of 02/27/2025. All market data was sourced from Bloomberg.

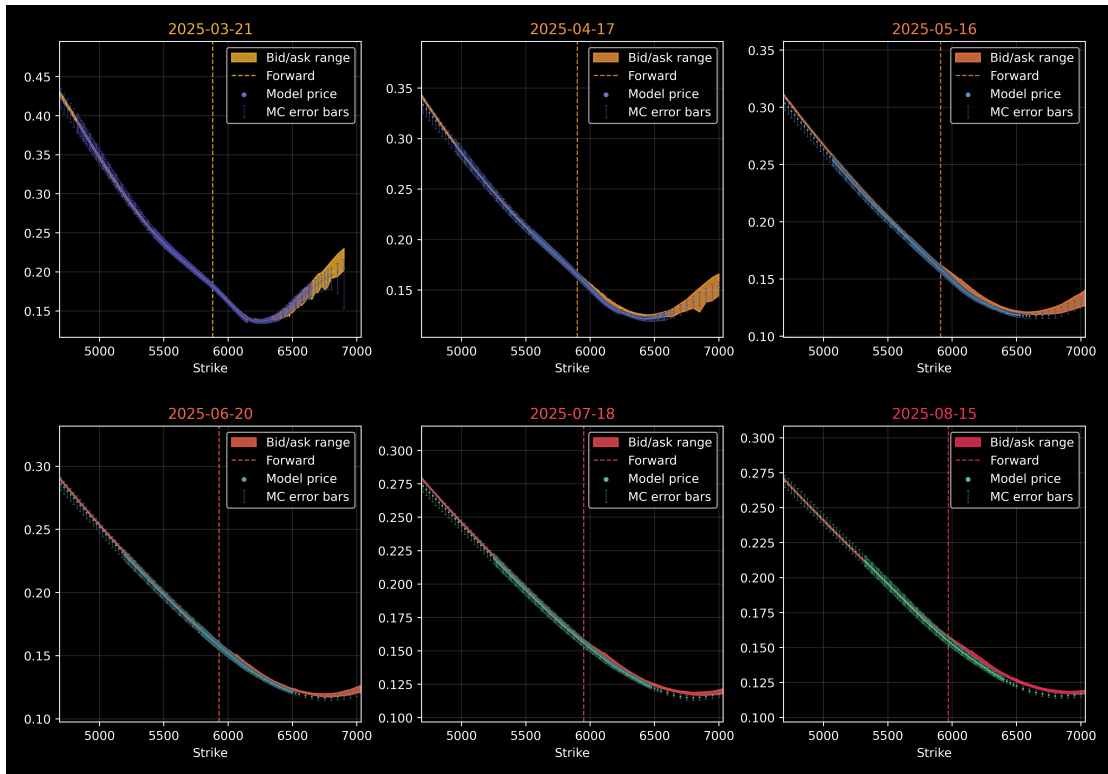
We sample  $2^8$  pairs of antithetic paths (hence  $J = 2^9$ ) for each training iteration, which is increased to  $2^{12}$  pairs after 1,000 epochs. In Step I., the occupied SDE is discretized using  $\delta t = \frac{1}{252}$  (daily time step) and  $M = 2^6 - 1 = 63$  bins centered at equally spaced nodes between  $X_0^T \pm 2\sigma_{\text{ATMF}}^T$ , where  $X_0^T = \mathbb{E}^{\mathbb{Q}}[X_T] \approx 6,000$  is the market implied forward price from the six-month options (hence  $T \approx 0.5$ ) and  $\sigma_{\text{ATMF}}^T$  is the associated at-the-money forward implied volatility. We also choose calendar time parameter ( $\kappa = 0$ ) so the calibrated model could be used to price/manage exotic options according to the unified framework Fig. 3. The neural network  $\Phi$  contains two hidden layers containing  $2^6 = 64$  nodes, with the ReLU and softplus activation function for the hidden and output layers, respectively.

Although the loss reaches the tolerance level  $\alpha$  around the milestone of 1,000 epochs,

we train longer to make sure the loss has stabilized as shown in Fig. 9. Once the training is complete, all model prices are computed using the same Monte Carlo paths, consisting of  $2^{15}$  antithetic pairs. The training phase and pricing take respectively about 30 minutes and 10 seconds on an Apple Macbook pro M3 using CPUs only. In practice, the training can be accelerated using GPU clusters and/or using fewer instruments across the strike dimension.

The implied volatility skews are displayed in Fig. 10, where it is observed that the model implied volatilities are all within, or close to, the market bid-ask range. The bars represent the Monte Carlo pricing errors (one standard deviation) converted into volatilities.

Figure 10: Model implied volatility skews for SPX monthly options compared to market bid and ask quotes. The bars show the Monte Carlo pricing error, transformed into volatilities.

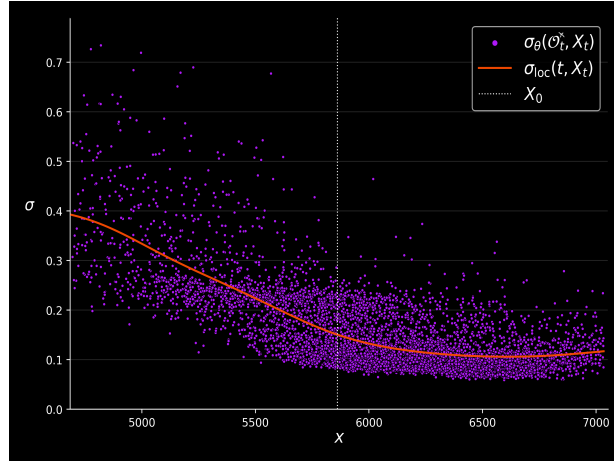


### 5.3.3 Implied Sensitivity Function

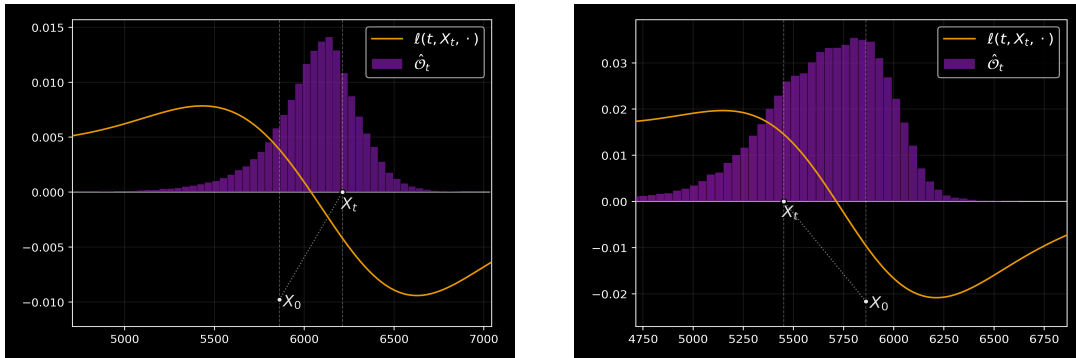
First, we check that the calibrated volatility contains some path dependence. Indeed, it is a priori sufficient to use the local volatility model to match the vanilla prices, which is recovered if  $\sigma(\mathcal{O}_t^\kappa, X_t) = \sigma_{\text{loc}}(\varsigma(\mathcal{O}_t^\kappa(\mathbb{R})), X_t)$ , where  $\varsigma(u) = \frac{1}{\kappa} \log(1 + u\kappa)$  is the inverse of the total mass function  $\mathcal{O}_t^\kappa(\mathbb{R}) = \frac{e^{\kappa t} - 1}{\kappa}$ . However, local volatility is by far not the unique model that calibrates to vanillas, especially when finitely strikes and maturities are given.

Fig. 11 Displays the volatility values  $\sigma_\theta(\mathcal{O}_t^{\kappa, \theta}, X_t^\theta)$  against the spot  $X_t^\theta$  for  $2^{10}$  trajectories on the full calibration horizon ( $t \approx 0.5$ ). Observe that the dots do not lie on a one-dimensional manifold, confirming the presence of path dependence in  $\sigma_\theta$ . Moreover, the volatility level typically increases as  $X_t^\theta$ , in line with the leverage effect. Note also that  $\hat{\sigma}^\theta$  is a smooth approximation of the local volatility  $\sigma_{\text{loc}}$  since the neural occupation volatility has been calibrated to vanilla options.

Back to the LOV model, we can finally visualize the implied sensitivity function  $\ell^{\mathbb{Q}}(t, X_t, x)$

Figure 11: Neural and local volatility versus spot.  $2^{10}$  samples.

using formula (79). Fig. 12 displays two scenarios where the spot as of 2025/08/15 ends respectively above and below the initial value. As can be seen, the shape of the sensitivity function (yellow) remains consistent across scenarios, suggesting that  $\ell^{\mathbb{Q}}$  may be chosen to depend on  $X_t, x$  primarily through the ratio  $x/X_t$ , aligned with Example 16. However, a notable discrepancy is the *decreasing* sensitivity function near the spot. This is the opposite of the behavior expected under the historical measure  $\mathbb{P}$ , where an increasing function is typical for capturing the leverage effect (recall Fig. 7). This pattern has been consistently observed over multiple calibration runs with varied neural network initializations.

Figure 12: Implied sensitivity function  $\ell^{\mathbb{Q}}(t, X_t, \cdot)$  (yellow) and projected occupation measure  $\hat{\mathcal{O}}_t^\kappa = \mathbb{E}^{\mathbb{Q}}[\mathcal{O}_t^\kappa | X_t]$  (purple).

## 5.4 Joint Calibration

To better pinpoint the sensitivity function, further work includes the calibration of occupied volatility to other instruments, such as VIX, exotic, or American options. Indeed, while the local volatility function guarantees perfect calibration to European vanilla options, the sensitivity function  $\ell^{\mathbb{Q}}$  can be tuned so as to match the price of other instruments, as summarized below:

$$\sigma^2(\mathcal{O}_t^\kappa, X_t) = \underbrace{\sigma_{\text{loc}}^2(t, X_t)}_{\text{European vanillas}} + \gamma_t^\kappa \int_{\mathbb{R}_+} \underbrace{\ell^{\mathbb{Q}}(t, X_t, x)}_{\substack{\text{VIX, exotic} \\ \text{American}}} (\mathcal{O}_t^\kappa - \hat{\mathcal{O}}_t^\kappa)(dx).$$

Also, from our experiments, the sensitivity function seems critical to build a model consistent with American-style vanilla options on U.S. single names, where one should typically go beyond local volatility for this task. One interesting case arises when the underlying does not pay dividends, such as Amazon.com, Inc. (AMZN). Indeed, the price of American call options coincides with their European counterparts [70], so the local volatility is uniquely characterized by the call options through Dupire's formula. On the other hand, assuming positive interest rates, American put options carry an early exercise premium, and the local volatility model is not guaranteed to perfectly replicate the market prices of these options. The author is currently investigating the application of the LOV model to this *joint American/European calibration* problem.

## 6 Forward Occupation Models

This section introduces a generalization of *forward variance models* [10, 49] that uses the information content of vanilla options not only through the forward variance curve, but through all forward occupation times.<sup>4</sup> Consider a standard Brownian motion  $W = (W^1, \dots, W^d)$  in  $\mathbb{R}^d$ ,  $d \geq 1$ , and denote its natural filtration by  $(\mathcal{F}_t)$ . Assume that the log price  $X = \log S$  of an asset has dynamics

$$dX_t = -\frac{1}{2}V_t dt + \sqrt{V_t} dW_t^1,$$

where the instantaneous variance  $V$  may depend on every component of  $W$ . Forward variance models [10, 49] rely on the following embedding  $V_t \hookrightarrow \xi_t^T$ , with the instantaneous forward variance curve  $\xi_t^T = \mathbb{E}_t^{\mathbb{Q}}[V_T] := \mathbb{E}^{\mathbb{Q}}[V_T | \mathcal{F}_t]$ , with  $V_t = \xi_t^t$ . Then  $\xi^T$  is a  $\mathbb{Q}$ -martingale on  $[0, T]$ , and one typically specifies a dynamics for the forward variance curve of the form

$$d\xi_t^T = \eta(t, T, \xi_t^\tau) \cdot dW_t = \sum_{i=1}^d \eta_i(t, T, \xi_t^\tau) dW_t^i, \quad (81)$$

where  $\tau \geq 0$  depends on  $t, T$ . In Bergomi models [10],  $\tau = T$  with  $\eta(t, T, \xi_t^T)$  linear in  $\xi_t^T$ , while in affine forward variance models [49],  $\tau = t$ , namely  $\eta(t, T, \xi_t^t) = \eta(t, T, V_t)$ . See Examples 17 and 18. Given a variance swap that delivers the realized variance on  $[0, T]$ , then the value of its (unannualized) floating leg at time  $t \in [0, T]$  can then be written as

$$\text{VS}_t^T := \mathbb{E}_t^{\mathbb{Q}}\left[\int_0^T V_s ds\right] = \underbrace{\int_0^t V_s ds}_{\text{realized}} + \underbrace{\int_t^T \xi_t^s ds}_{\text{implied}}. \quad (82)$$

Note that  $\text{VS}^T$  is also a  $\mathbb{Q}$ -martingale, starting at the fair strike  $\text{VS}_0^T$  and delivering the (unannualized) realized variance at  $t = T$ . Shifting gears, one can embed the forward variance curve into the *instantaneous forward occupation measure*,

$$\xi_t^T \hookrightarrow \mathfrak{o}_t^T(A) = \mathbb{E}_t^{\mathbb{Q}}[\mathbf{1}_A(X_T)V_T], \quad A \in \mathcal{B}(\mathbb{R}), \quad (83)$$

where  $\xi_t^T = \mathfrak{o}_t^T(\mathbb{R})$  and also  $V_t = \xi_t^t = \mathfrak{o}_t^t(\mathbb{R})$ . Alternatively,  $\mathfrak{o}_t^T$  can be seen as a surface in strikes and maturities, namely  $(K, T) \rightarrow \mathbb{E}_t^{\mathbb{Q}}[\delta_K(X_T)V_T]$ , an object initially introduced by Dupire [39]. Integrating  $\mathfrak{o}_t^s$  for fixed  $t$  gives the forward occupation measure

$$\mathcal{O}_t^T(A) = \int_0^T \mathfrak{o}_t^s(A) ds = \mathbb{E}_t^{\mathbb{Q}}\left[\int_0^T \mathbf{1}_A(X_s)V_s ds\right] = \mathbb{E}_t^{\mathbb{Q}}[\mathcal{O}_T(A)], \quad (84)$$

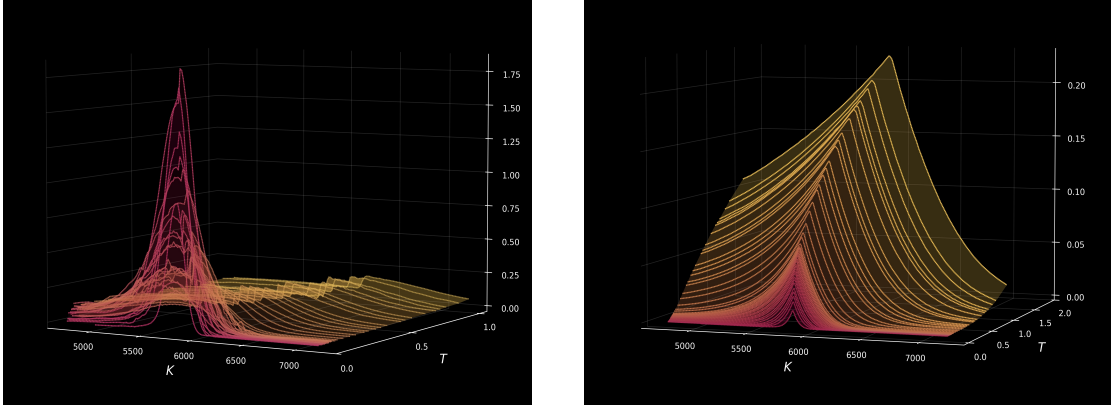
<sup>4</sup>I would like to thank an anonymous referee for suggesting this promising direction.

which is equivalently described by the local time surface  $(K, T) \mapsto \mathbb{E}_t^{\mathbb{Q}}[L_T^K]$ ; see Fig. 13. When  $A = [x_1, x_2]$ , then  $\mathcal{O}_T^T(A) = \mathcal{O}_T(A)$  is the (unannualized) floating leg of the associated corridor variance swap (Example 11), while  $\mathcal{O}_0^T(A) = \mathbb{E}^{\mathbb{Q}}[\mathcal{O}_T(A)]$  is its fair strike. Classically, the latter can be statically replicated using vanilla options as follows,

$$\mathcal{O}_0^T(A) = 2 \int_A \text{OTM}(K, T) \frac{dK}{K^2},$$

where  $\text{OTM}(K, T)$  is the initial price of the corresponding out-of-the-money vanilla contract (put if  $K < S_t$  and call otherwise). As  $\mathfrak{o}_0^T = \partial_T \mathcal{O}_0^T$ , the instantaneous forward occupation surface can be extracted from the weighted sum of calendar spreads  $\mathfrak{o}_0^T(A) = 2 \int_A \partial_T \text{OTM}(K, T) \frac{dK}{K^2}$ . An illustration is given in Fig. 13 for SPX options. In conclusion, one can add granularity to forward variance models by including all the forward occupation times  $\mathcal{O}_\circ(A)$ , which are tradeable quantities as well.

Figure 13: Forward occupation surfaces of SPX Options as of 2025/02/27, 4pm EST. Left:  $\mathfrak{o}_0^T$  (instantaneous). Right:  $\mathcal{O}_0^T = \int_0^T \mathfrak{o}_0^s ds$  (cumulative).



## 6.1 Dynamics of Forward Occupation Flows

The forward occupation time process  $t \mapsto \mathfrak{o}_t^T(A)$  is a martingale for all  $A \in \mathcal{B}(\mathbb{R})$  adapted to the filtration of  $W$ . Consequently, it admits the martingale representation

$$\mathfrak{o}_t^T(A) = \mathfrak{o}_0^T(A) + \int_0^t \eta_u^T(A) \cdot dW_u, \quad t \leq T, \quad (85)$$

for some adapted process  $\eta^T(A)$  living in  $\mathbb{R}^d$ . Moreover, for disjoint Borel sets  $A, A' \in \mathcal{B}(\mathbb{R})$ ,

$$\eta_t^T(A \cup A') \cdot dW_t = d\mathfrak{o}_t^T(A \cup A') = d\mathfrak{o}_t^T(A) + d\mathfrak{o}_t^T(A') = (\eta_t^T(A) + \eta_t^T(A')) \cdot dW_t.$$

Hence  $\eta_t^T(A \cup A') = \eta_t^T(A) + \eta_t^T(A')$  for all  $t \leq T$ , by uniqueness of the martingale representation. Similarly, one can show that  $\eta_t^T$  is  $\sigma$ -additive, hence a signed random measure. We can then write the dynamics of the instantaneous forward occupation flow as

$$d\mathfrak{o}_t^T = \eta_t^T \cdot dW_t = \sum_{i=1}^d \eta_{t,i}^T dW_t^i, \quad (86)$$

where  $\eta_t^T \in \mathcal{M}^d$  is a vector-valued measure. Similar to the forward variance model (81), suppose that  $\eta_t^T = \eta(t, T, \mathfrak{o}_t^T)$  for some map  $\eta : \mathbb{R}_+^2 \times \mathcal{M} \rightarrow \mathcal{M}^d$  and time  $\tau = \tau(t, T)$ . When

$t \geq T$ , we set  $\eta_t^T = 0$  since  $\mathfrak{o}_t^T$  is constant after  $T$  (equal to  $\delta_{X_T} V_T$ ). Moreover, the forward occupation measure  $\mathcal{O}_t^T$  has  $t$ -dynamics,

$$d\mathcal{O}_t^T = d\left(\int_0^T \mathfrak{o}_t^s ds\right) = d\left(\int_t^T \mathfrak{o}_t^s ds\right) = H_t^T \cdot dW_t,$$

with volatility  $H_t^T = \int_t^T \eta_t^s ds = \int_t^T \eta(t, s, \mathfrak{o}_t^{\tau(t,s)}) ds \in \mathcal{M}^d$ . Unlike  $\mathcal{O}$ , the forward occupation flow  $\mathcal{O}^T$  does not play the role of time since its total mass process, the variance swap rate  $VS^T$ , is of infinite variation. Moreover, by leveraging the tools in Section 3, we obtain the following chain rule for functionals of  $\mathcal{O}^T$ ,

$$df(\mathcal{O}_t^T) = (\delta_{\circ} f(\mathcal{O}_t^T) \cdot H_t^T) \cdot dW_t + \frac{1}{2} \delta_{\circ\circ} f(\mathcal{O}_t^T) \cdot (H_t^T)^{\otimes 2} dt, \quad f \in \mathcal{C}^2(\mathcal{M}), \quad (87)$$

where  $\phi \cdot H = \int_{\mathbb{R}} \phi dH \in \mathbb{R}^d$  if  $\phi = \delta_{\circ} f(\mathcal{O}_t^T) \in \mathcal{C}(\mathbb{R})$ ,  $H \in \mathcal{M}^d$ , and when  $\phi = \delta_{\circ\circ} f(\mathcal{O}_t^T) \in \mathcal{C}(\mathbb{R}^2)$ , we set

$$\phi \cdot H^{\otimes 2} = \int_{\mathbb{R}^2} \phi(x, x') H(dx) \cdot H(dx') = \sum_{i=1}^d \int_{\mathbb{R}^2} \phi(x, x') H_i(dx) H_i(dx') \in \mathbb{R}.$$

As expected, a second-order term appears due to the martingality of  $\mathcal{O}^T$ , further confirming that  $\mathcal{O}^T$  differs from the time variable.

Promising directions for future research include the development of an Itô formula in this context, and numerical methods for the associated occupied PDEs. The latter could then be used to price variance derivatives contingent on the terminal occupation measure  $\mathcal{O}_T$ . While weighted variance swaps are readily available from the prices of vanilla options, the proposed model would allow to introduce and efficiently price weighted variance derivatives, which do not seem to be traded *yet*. For instance, it seems relevant to popularize vanilla options on downside/upside variance, namely

$$\varphi(\mathcal{O}_T) = (\mathcal{O}_T(A^{\pm}) - K)^+, \quad A^- = (-\infty, X_0], \quad A^+ = (X_0, \infty).$$

One could also envision options on *weighted VIX indexes*, whose square is defined by the forward increment

$$\frac{1}{\Delta} w \cdot (\mathcal{O}_T^{T+\Delta} - \mathcal{O}_T) = \mathbb{E}_T^{\mathbb{Q}} \left[ \frac{1}{\Delta} \int_T^{T+\Delta} w(X_s) V_s ds \right], \quad w : \mathbb{R} \rightarrow \mathbb{R}, \quad \Delta > 0.$$

In particular, a downside/upside VIX indexes would be obtained using  $w = \mathbb{1}_{A_{\pm}}$ .

We finally gather some examples.

**Example 17.** Inspired by Bergomi [10], let  $\tau = T$ ,  $\kappa : \mathbb{R}_+ \rightarrow \mathbb{R}_+^d$  be a vector-valued kernel, and choose  $\eta(t, T, \mathfrak{o}_t^T) = \eta_0 \kappa(T - t) \mathfrak{o}_t^T$ , that is

$$\mathfrak{o}_t^T(A) = \mathfrak{o}_0^T(A) \exp \left\{ \eta_0 Z_t - \frac{1}{2} \eta_0^2 \mathbb{E}^{\mathbb{Q}}[Z_t^2] \right\}, \quad (88)$$

with the Gaussian Volterra process  $Z_t = \int_0^t \kappa(t - s) \cdot dW_s$  and constant  $\eta_0 > 0$ . Note that  $\eta(t, T, \mathfrak{o}_t^T)$  is indeed a measure, possibly vector-valued when  $d \geq 2$ , and  $\mathfrak{o}_t^T(A)$  remains nonnegative. When  $A = \mathbb{R}$ , we recover the Bergomi model  $d\xi_t^T / \xi_t^T = \eta_0 \kappa(T - t) \cdot dW_t$ .

**Example 18.** (Affine forward occupation) Let  $\tau = t$  and choose  $\eta(t, T, \mathbf{o}_t^t) = \eta_0 \sqrt{\mathbf{o}_t^t} \kappa(T - t)$ ,  $\kappa : \mathbb{R}_+ \rightarrow \mathbb{R}_+^d$ , namely  $\eta_t^T(A) = \mathbb{1}_A(X_t) \eta_0 \sqrt{V_t} \kappa(T - t)$ . When  $A = \mathbb{R}$ , we recover the affine forward model of Gatheral and Keller-Ressel [49],

$$d\mathbf{o}_t^T(\mathbb{R}) = d\xi_t^T = \eta_0 \sqrt{V_t} \kappa(T - t) \cdot dW_t.$$

Note that the log price  $X$  is still an affine process since it depends on  $\mathbf{o}_t^T$  only through its total mass  $\mathbf{o}_t^T(\mathbb{R}) = \xi_t^T$ , and  $(X, \xi)$  admits an affine cumulant generating function as shown in [49]. The volatility of  $\mathcal{O}_t^T = \int_0^T \mathbf{o}_t^s ds$  is given by

$$H_t^T = \delta_{X_t} \eta_0 \sqrt{V_t} K(t, T), \quad K(t, T) = \int_t^T \kappa(s - t) ds \in \mathbb{R}^d. \quad (89)$$

Consequently, the chain rule (87) simplifies to

$$df(\mathcal{O}_t^T) = \partial_{\mathbf{o}} f(\mathcal{O}_t^T, X_t) \eta_0 \sqrt{V_t} K(t, T) \cdot dW_t + \frac{1}{2} \partial_{\mathbf{o}\mathbf{o}} f(\mathcal{O}_t^T, X_t) \eta_0^2 V_t |K(t, T)|^2 dt,$$

with the second order occupation derivative  $\partial_{\mathbf{o}\mathbf{o}} f(\mathbf{o}, x) = \delta_{\mathbf{o}\mathbf{o}} f(\mathbf{o})(x, x)$ . It would be interesting to see if one can describe the characteristic function of the forward occupation times  $\mathcal{O}_t^T(A)$ , e.g. using the forest expansion in Friz and Gatheral [48]. This would give access to Fourier methods for variance derivatives contingent on  $w \cdot \mathcal{O}_T = \int_0^T w(X_t) V_t dt$ , the floating leg of weighted variance swaps. Alternatively, one may adapt the deep-learning algorithm of Jacquier and Oumgari [64] for curve-dependent PDEs to price weighted variance derivatives using finitely many forward occupation curves  $T \rightarrow \mathbf{o}_t^T(A)$ .

## 7 Stopping Spot Local Time

This section intends to study the spot local time  $L_t^{X_t}$  in more depth, particularly in the context of optimal stopping (OS). We dwell on this problem as we believe it is highly challenging both theoretically and numerically. Hence, the stopping of spot local time can be used as a benchmark for algorithms solving path-dependent OS problems. For instance, it would be worth checking the performance on this example of recent methods involving deep learning and/or the path signature [2, 3, 4]. See Section 7.3 for further numerical considerations.

### 7.1 Optimal Stopping

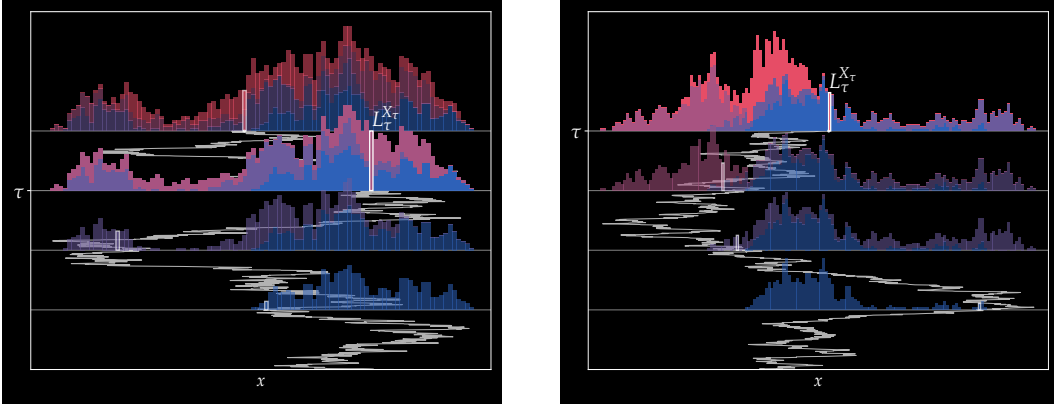
Let us first adapt standard results in optimal stopping to occupied processes. Suppose that  $X$  is Brownian motion and refer to Remark 1 for the general semimartingale case. Given a reward functional  $\varphi : \mathcal{D} \rightarrow \mathbb{R}_+$  such that  $\sup_{t \leq T} \varphi(\mathcal{O}_t, X_t) \in L^1(\mathbb{Q})$  and exercise dates  $\mathcal{T} \subseteq [0, T]$  containing  $T$ , consider the *optimal stopping (OS) problem* [72],

$$\sup_{\tau \in \vartheta(\mathcal{T})} \mathbb{E}^{\mathbb{Q}}[\varphi(\mathcal{O}_\tau, X_\tau)], \quad (90)$$

where  $\vartheta(\mathcal{T})$  is the set of  $\mathcal{T}$ -valued  $(\mathbb{F}, \mathbb{Q})$ -stopping times. Define the *value function*,

$$v(\mathbf{o}, x) = \sup_{\tau \in \vartheta(\mathcal{T}_t)} \mathbb{E}_{\mathbf{o}, x}^{\mathbb{Q}}[\varphi(\mathcal{O}_\tau, X_\tau)], \quad \mathcal{T}_t = \mathcal{T} \cap [t, T], \quad t = \mathbf{o}(\mathbb{R}). \quad (91)$$

The *stopping region* is traditionally defined as the coincidence set  $\mathcal{S}_T = \{(\mathbf{o}, x) \in \mathcal{D}_T : v(\mathbf{o}, x) = \varphi(\mathbf{o}, x)\}$ . In particular,  $\partial \mathcal{S} = \partial \mathcal{D}_T$  since  $T \in \mathcal{T}$ . As it is challenging to represent

Figure 14: Occupation flow  $\mathcal{O}$  and stopped spot local time  $L_\tau^{X_\tau}$ . Two simulations.

$\mathcal{S}$  either mentally or visually, we can regard the stopping region as a subset of  $\mathbb{R}$  for a given occupation measure, i.e.,  $\mathcal{S}(\mathbf{o}) = \{x \in \text{supp}(\mathbf{o}) : (\mathbf{o}, x) \in \mathcal{S}\}$ . For every  $t \in [0, T]$ , this gives the pathwise partition

$$\{X_s : s \leq t\} = \text{supp}(\mathcal{O}_t) = \mathcal{S}(\mathcal{O}_t) \cup \mathcal{C}(\mathcal{O}_t),$$

with the *continuation region*  $\mathcal{C}(\mathbf{o}) = \{x \in \text{supp}(\mathbf{o}) : v(\mathbf{o}, x) > \varphi(\mathbf{o}, x)\}$ . See Fig. 15 and [34, Chapter 7] for a related comment.

The Dynamic Programming Principle (DPP) states that for all  $\varsigma \in \vartheta(\mathcal{T}_t)$ ,

$$v(\mathbf{o}, x) = \sup_{\tau \in \vartheta(\mathcal{T}_t)} \mathbb{E}_{\mathbf{o}, x}^{\mathbb{Q}}[\varphi(\mathcal{O}_\tau, X_\tau)\mathbf{1}_{\{\tau < \varsigma\}} + v(\mathcal{O}_\varsigma, X_\varsigma)\mathbf{1}_{\{\tau \geq \varsigma\}}]. \quad (92)$$

Let us recall how to derive the dynamic programming equation satisfied by  $v$ . If  $v \in \mathcal{C}^{1,2}(\mathcal{D})$  and  $Y_t := v(\mathcal{O}_t, X_t)$  denotes the *Snell envelope* of  $\varphi$ , then Itô's formula (Theorem 3.1) gives

$$dY_t = \left( \partial_{\mathbf{o}} + \frac{1}{2} \partial_{xx} \right) v(\mathcal{O}_t, X_t) dt + \partial_x v(\mathcal{O}_t, X_t) dX_t. \quad (93)$$

It is classical that the Snell envelope  $Y$  is the smallest supermartingale dominating  $\varphi$  [72]. In particular, the drift in (93) is  $\mathbb{Q}$ -a.s. non-positive and equal to zero outside of the stopping region  $\mathcal{S}$ . This leads to the *dynamic programming equation*,

$$\begin{cases} \left( \partial_{\mathbf{o}} + \frac{1}{2} \partial_{xx} \right) v = 0 & \text{on } \mathcal{D}_T, \\ v = \varphi & \text{on } \mathcal{S}_T \cup \partial \mathcal{D}_T. \end{cases} \quad (94a) \quad (94b)$$

The present discussion is of course formal as the value function is typically not regular enough to be a classical solution of (94a)–(94b). Nevertheless, one can adapt the arguments from our companion paper [78] to show that  $v$  is the unique viscosity solution of the obstacle problem (94a)–(94b).

## 7.2 Spot Local Time and Early Exercise Premium

We are now set to study the OS problem,

$$\text{maximize } v(\tau) := \mathbb{E}^{\mathbb{Q}}[L_\tau^{X_\tau}] \quad \text{over } \tau \in \vartheta(\mathcal{T}). \quad (95)$$

The spot local time corresponds to the reward  $\varphi(o, x) = \frac{d\varrho}{d\lambda}(x)$  which is defined on  $\mathcal{D}^\lambda$ , namely those elements  $(o, x)$  of  $\mathcal{D}$  such that  $o \in \mathcal{M}^\lambda$ . Clearly,  $\sup_{t \leq T} \varphi(\mathcal{O}_t, X_t) \in L^1(\mathbb{Q})$  since  $\varphi(\mathcal{O}_t, X_t) \leq \|\mathcal{O}_T\|_\infty = \sup_{x \in \mathbb{R}} L_T^x$  which is bounded in  $L^p(\mathbb{Q})$  for all  $p \geq 1$  [1]. Hence the above OS problem is well-defined. Within the family of metrics  $\{\mathfrak{m}_p : p \in [1, \infty]\}$  introduced in Section 2.4, note that  $\varphi$  is continuous *only* with respect to  $\mathfrak{m}_\infty$ .

It is intuitive that (95) has a positive *early exercise premium* when  $\mathcal{T} \neq \{T\}$  (recall our assumption  $T \in \mathcal{T}$ ). See also Fig. 14. In other words, there exists  $\tau \in \vartheta(\mathcal{T})$  such that  $v(\tau)$  strictly dominates  $v(T) = \mathbb{E}^\mathbb{Q}[L_T^{X_T}]$ . First, let us compute the latter explicitly.

**Proposition 6.** *Let  $X$  be Brownian motion and  $T > 0$ . Then  $\mathbb{E}^\mathbb{Q}[L_T^{X_T}] = \mathbb{E}^\mathbb{Q}[L_T^0] = \sqrt{\frac{2}{\pi}}T$ .*

*Proof.* Consider the time reversed process  $\overleftarrow{X}_s = X_{T-s} - X_T$ ,  $s \in [0, T]$  and denote its local time at 0 by  $\overleftarrow{L}_T^0$ . By the chronology invariance of occupation functionals (Theorem A.1), then  $L_T^{X_T} = \overleftarrow{L}_T^0$  pathwise. Moreover, it is classical that  $\overleftarrow{X}$  is also Brownian motion with respect to its own filtration, hence  $\mathbb{E}^\mathbb{Q}[L_T^{X_T}] = \mathbb{E}^\mathbb{Q}[\overleftarrow{L}_T^0] = \mathbb{E}^\mathbb{Q}[L_T^0]$ . The last equality in the statement follows from the standard result from Paul Lévy that  $L_T^0$  and  $|X_T|$  have the same law.  $\square$

Next, we verify the existence of an early exercise premium in the minimal case  $\mathcal{T} = \{t, T\}$ . Invoking the dynamic programming principle (92) with  $\varsigma = T$ , then  $Y_t := v(\mathcal{O}_t, X_t) = L_t^{X_t} \vee C_t$  with the continuation value  $C_t = \mathbb{E}^\mathbb{Q}[L_T^{X_T} | \mathcal{F}_t]$  derived in Example 6, namely

$$C_t = \int_{\mathbb{R}} L_t^y \phi_{T-t}(y - X_t) dy + \mathbb{E}^\mathbb{Q}[L_{T-t}^0], \quad \phi_s(x) = \frac{e^{-\frac{x^2}{2s}}}{\sqrt{2\pi s}}. \quad (96)$$

We can finally approximate the initial value  $Y_0 = \mathbb{E}^\mathbb{Q}[Y_t]$  using Monte Carlo simulations. For the numerical computation of the local times in (96), see Remark 10. The optimal strategy is classically to stop at  $t$  if the intrinsic value  $L_t^{X_t}$  is greater than or equal to  $C_t$ ; see Fig. 15. As the heat kernel  $\phi_{T-t}$  concentrates around zero (especially when  $T - t$  is small), we gather from (96) that the field  $(L_t^x)_{x \in \mathbb{R}}$  is relevant for the stopping decision *only* in a neighborhood of the spot. This observation is crucial in Section 7.3 when truncating the occupation measure.

Table 1 summarizes the results in the case  $T = 2t = 1$ . We simulate  $2^{14} = 16,384$  Monte Carlo paths on a regular time grid with  $N = 400$  steps and set  $\varepsilon = \sqrt{T/N} = 0.05$ ; see Remark 10. The early exercise premium is indeed significantly positive.

Table 1: Existence of an early exercise premium. Value of the OS problem (95) with  $\mathcal{T} = \{0.5, 1\}$  and  $\mathcal{T} = \{1\}$ .  $N = 400$ ,  $\varepsilon = 0.05$ , and  $2^{14}$  Monte Carlo (MC) simulations.

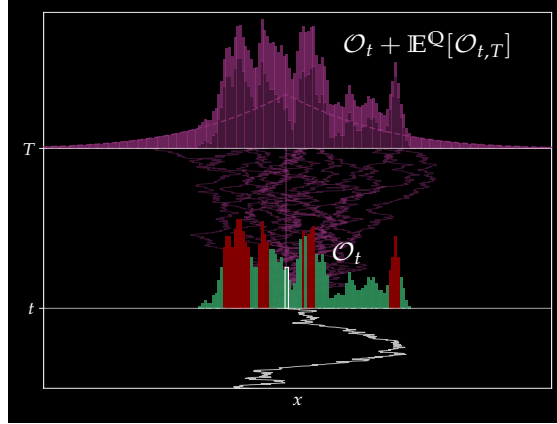
Exercise dates	Value	MC Error
$\mathcal{T} = \{0.5, 1\}$	0.8455	0.0050
$\mathcal{T} = \{1\}$	0.7979	-

**Remark 10.** (Numerical approximation of Brownian local time) Define

$$\varphi^\varepsilon(\mathcal{O}_t, x) := \frac{\mathcal{O}_t(B_\varepsilon(x))}{2\varepsilon} = \frac{1}{2\varepsilon} \int_0^t \mathbb{1}_{\{|X_s - x| \leq \varepsilon\}} ds. \quad (97)$$

In light of (12),  $\varphi^\varepsilon(\mathcal{O}_t, x)$  converges to  $L_t^x$  pathwise. In the present context of optimal stopping, we shall also see in Section 7.4 that estimating local time with narrow corridors is

Figure 15: Spot local time OS problem with  $\mathcal{T} = \{t, T\}$ . Stopping region (red) and continuation region (green) at  $t$  depending whether the intrinsic value  $L_t^x$  (if  $X_t = x$ ) exceeds the continuation value given in (96).



legitimate in the sense that the value of the OS problem (90) with  $\varphi = \varphi^\varepsilon$  converges to the value of (95). If  $X$  is a simulated Brownian path on a regular time grid  $t_n = n\delta t$ ,  $\delta t = \frac{T}{N}$ , we then discretize the integral in (97) to obtain  $L_t^x \approx \frac{1}{2\varepsilon} \sum_{n=1}^N \mathbb{1}_{\{|X_{t_n} - x| \leq \varepsilon\}} \delta t$ . This estimate induces constraints on  $\varepsilon$  once  $\delta t$  is fixed. Intuitively,  $\varepsilon \gg \delta t$ , and from our experiments, adequate choices are  $\varepsilon = c\sqrt{\delta t}$ , e.g.  $c = 1$ , matching the scale of Brownian motion.

### 7.3 Numerical Resolution in the case $\mathcal{T} = [0, T]$

We now turn to the case  $\mathcal{T} = [0, T]$ . As the backward induction in the previous section does not apply when  $|\mathcal{T}| > 2$  due to path-dependence, alternative methods must be considered. First, we outline a simple stopping rule giving a lower bound on the value of (95).

For fixed  $\iota \in [0, T]$ , interpreted as an inspection date, define<sup>5</sup>

$$\tau_\iota = \inf\{t \in [\iota, T] : X_t = X_\iota^*\} \wedge T, \quad X_\iota^* = \operatorname{argmax}_x L_\iota^x.$$

In other words, it is the hitting time after  $\iota$  of the level which maximizes local time on  $[0, \iota]$ . If  $\sigma^* = \sup\{s \in [0, T] : X_s = X_\iota^*\} \wedge 0$  denotes the last visit of the optimal level  $X_\iota^*$ , then on  $\{\sigma^* \geq \iota\}$ , the reward  $L_{\tau_\iota}^{X_\iota^*}$  is precisely  $L_\iota^{X_\iota^*} = \sup_x L_\iota^x$ . This gives the decomposition,

$$\mathbb{E}^\mathbb{Q}[L_{\tau_\iota}^{X_\iota^*}] = p_\iota \mathbb{E}^\mathbb{Q}[\sup_x L_\iota^x \mid \sigma^* \geq \iota] + (1 - p_\iota) \mathbb{E}^\mathbb{Q}[L_T^{X_\iota^*} \mid \sigma^* < \iota], \quad p_\iota = \mathbb{Q}(\sigma^* \geq \iota).$$

There is a clear tradeoff between the reward  $\sup_x L_\iota^x$  (increasing in  $\iota$ ) and the probability  $p_\iota$  to hit the level  $X_\iota^*$  again (decreasing in  $\iota$ ). Table 2 summarizes the numerical results for values of  $\iota$ . We use  $T = 1$  and  $2^{14} = 16,384$  simulated Brownian trajectories on a regular time grid with 400 steps. To compute  $X_\iota^*$ , we use a regular space grid of  $[-2, 2]$  with 200 subintervals. Despite the simplicity of the present stopping rule, a significant premium is observed. Note that the inspection date  $\iota = 0.7$  yields nearly a 40% improvement over the case  $\mathcal{T} = \{T\}$  seen in Table 1.

Next, we implement an approach à la Longstaff-Schwartz where we refer to the original paper [69] and Section C.1 for further details. Given the time grid  $t_n = n\delta t$ ,  $\delta t = \frac{T}{N}$ , a

<sup>5</sup>It is easy to show that the maximum of  $x \mapsto L_\iota^x$  is attained and  $\mathbb{Q}$ -almost surely unique.

Table 2: Value of the stopping rule  $\tau_\iota = \inf\{t \in [\iota, T] : X_t = X_\iota^*\}$ ,  $X_\iota^* = \operatorname{argmax}_x L_\iota^x$  for varying inspection date  $\iota$  and parameters  $T = 1$ ,  $N = 400$ ,  $\varepsilon = 0.05$ .

Inspection date	Value	Monte Carlo Error
$\iota = 0.5$	1.0404	0.0035
$\iota = 0.6$	1.0897	0.0040
$\iota = 0.7$	1.1116	0.0046
$\iota = 0.8$	1.0892	0.0052
$\iota = 0.9$	1.0182	0.0056

crucial step in [69] is the computation of the continuation value  $C_{t_n} = \mathbb{E}^{\mathbb{Q}}[Y_{t_{n+1}} | \mathcal{F}_{t_n}]$  where  $Y = v(\mathcal{O}, X)$  denotes the Snell envelope of  $L^X$ . Although we can write  $C_{t_n} = c(\mathcal{O}_{t_n}, X_{t_n})$ ,  $c : \mathcal{D} \rightarrow \mathbb{R}$ , using the Markov property of  $(\mathcal{O}, X)$  (Proposition 2), it is naturally challenging to estimate  $c$  as the occupation measure is infinite-dimensional. Therefore, we carry out a space discretization to summarize  $\mathcal{O}$  with finitely many features.

Given  $\nu = \frac{1}{6}(\delta_{-\sqrt{3}} + 4\delta_0 + \delta_{\sqrt{3}})$  matching the first five moments of  $\mathcal{N}(0, 1)$ , introduce the random walk  $X_{t_{n+1}} = X_{t_n} + Z_{n+1}\sqrt{\delta t}$ ,  $Z_{n+1} \sim \nu$ , taking values on a trinomial tree with nodes  $x_m = m\sqrt{3\delta t}$  and  $|m| \leq n$  at time  $t_n$ . In this model, the occupation measure becomes finite-dimensional, namely

$$\mathcal{O}_{t_n} = (L_{t_n}^{x_{-n}}, \dots, L_{t_n}^{x_n}), \quad L_{t_n}^{x_m} = \frac{\mathcal{O}_{t_n}(B_\varepsilon(x_m))}{2\varepsilon} := \frac{1}{2\varepsilon} \sum_{i=1}^n \mathbb{1}_{\{X_{t_i} = x_m\}} \delta t. \quad (98)$$

where  $\varepsilon = \frac{x_{m+1} - x_m}{2} = \frac{\sqrt{3\delta t}}{2}$  in line with Remark 10. The above expression for  $L_{t_n}^{x_m}$  also reveals our motivation behind the chosen trinomial structure: the local time process may accumulate at every step instead of every other step in a (recombining) binomial tree.

Notice that the dimension of  $\mathcal{O}_{t_n}$  in (98) still expands with time, which becomes problematic for large  $N$ . Therefore, we introduce the truncation  $\mathcal{O}_{t_n}^{\bar{m}} = (L_{t_n}^{x_{m-\bar{m}}}, \dots, L_{t_n}^{x_{m+\bar{m}}})$ ,  $\bar{m} \in \mathbb{N}$ , around the spot  $x_m = X_{t_n}$ . The resulting pair  $(\mathcal{O}_{t_n}^{\bar{m}}, X_{t_n})$  is of dimension  $2\bar{m} + 2$ , hence a least square approach can be implemented for small values of  $\bar{m}$  (say, less than 5). Note that this is tailored to the payoff  $L^X$ : similar to (96), the continuation value primarily depends on the local time close to the spot. Evidently, other rewards may lead to other truncations.

We then follow the least square Monte Carlo method [69], expounded in Algorithm 3 for completeness. We perform an offline and online phase as in [55, Remark 6.8] consisting of  $2^{11}$  and  $2^{14}$  simulations, respectively. See also Section C.1 for other implementation details. The results are given in Table 3. Note that adding the local time of adjacent nodes ( $\bar{m} = 1$ ) is indeed beneficial, while the value improves slowly beyond that. Comparing with Table 2, we also see that the least square Monte Carlo approach indeed outperforms the more naive inspection strategy.

## 7.4 Shrinking the Corridor

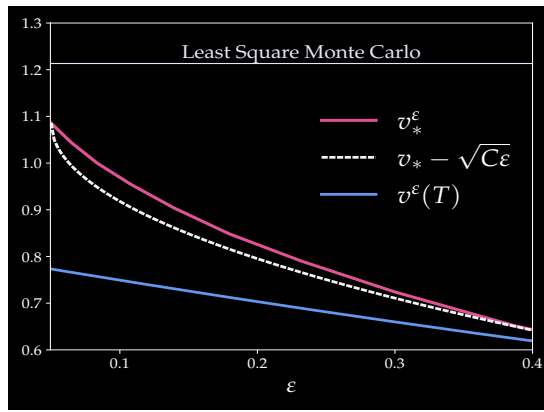
Let  $\varphi^\varepsilon(\mathfrak{o}, x) = \frac{\mathfrak{o}(B_\varepsilon(x))}{2\varepsilon}$ ,  $\varepsilon > 0$  as in (97). Hence  $\varphi^\varepsilon(X_t, \mathcal{O}_t)$  is a pathwise approximation of the spot local time  $L_t^{X_t}$ . We aim to show that the value  $v_*^\varepsilon$  of the optimal stopping problem

$$\text{maximize } v^\varepsilon(\tau) := \mathbb{E}^{\mathbb{Q}}[\varphi^\varepsilon(\mathcal{O}_\tau, X_\tau)] \quad \text{over } \tau \in \vartheta(\mathcal{T}), \quad (99)$$

Table 3: Value of OS problem (95) with  $\mathcal{T} = \{n/N : n = 1, \dots, N\}$ ,  $N = 400$ , using Least square Monte Carlo for varying truncation level  $\bar{m}$ .

Truncation level ( $\bar{m}$ )	Value	MC Error	Run time
0	1.1916	0.0044	182 sec.
1	1.2180	0.0031	187 sec.
2	1.2252	0.0030	194 sec.
3	1.2277	0.0030	197 sec.
5	1.2296	0.0030	210 sec.

Figure 16: Verification of Proposition 7 and Corollary 1 with  $T = 1$ . Estimate of  $\varepsilon \mapsto v_*^\varepsilon$  using the inspection strategy (Section 7.3),  $N = 400$  time intervals and  $2^{14}$  simulations.



converges to the value  $v_*$  of (95) in the extreme cases  $\mathcal{T} = \{T\}$  and  $\mathcal{T} = [0, T]$ . We start with the former, where  $v_*^\varepsilon = v^\varepsilon(T)$  and  $v_* = v(T)$ .

**Proposition 7.** *We have  $v^\varepsilon(T) \uparrow v(T)$  as  $\varepsilon \downarrow 0$ . Precisely,  $v^\varepsilon(T) = v(T) - \frac{\varepsilon}{2} + \frac{\varepsilon^2}{\sqrt{18\pi T}}(1 + r_\varepsilon)$  with  $\lim_{\varepsilon \downarrow 0} r_\varepsilon = 0$ .*

*Proof.* See Section B.5. □

We gather from Proposition 7 that the function  $\varepsilon \mapsto v^\varepsilon(T)$  is essentially linear for small values of  $\varepsilon$ . This will be confirmed in Fig. 16. In the next results, we prove that the convergence rate of  $v^\varepsilon(\tau)$  for general stopping times and  $v_*^\varepsilon$  when  $\mathcal{T} = [0, T]$  is at least  $1/2$ . In fact, this lower bound seems tight according to Fig. 16.

**Proposition 8.** *There exists a constant  $C \in (0, \infty)$  such that for all  $0 < \varepsilon \leq 1$ ,*

$$\left\| \varphi^\varepsilon(\mathcal{O}_\tau, X_\tau) - L_\tau^{X_\tau} \right\|_{L^2(\mathbb{Q})} \leq \sqrt{C\varepsilon} \quad \forall \tau \in \vartheta(\mathcal{T}). \quad (100)$$

*In particular,  $|v^\varepsilon(\tau) - v(\tau)| \leq \sqrt{C\varepsilon}$  for all  $\tau \in \vartheta(\mathcal{T})$ .*

*Proof.* See Section B.6. □

**Corollary 1.** *Let  $v_*^\varepsilon, v_*$  be respectively the value of the OS problem (99) and (95) with  $\mathcal{T} = [0, T]$ . Then  $|v_*^\varepsilon - v_*| \leq \sqrt{C\varepsilon}$ , with  $C$  as in Proposition 8. In particular,  $\lim_{\varepsilon \rightarrow 0} v_*^\varepsilon = v_*$ .*

*Proof.* This is immediate: let  $\gamma > 0$  be arbitrary and  $\tau_\gamma$  such that  $v(\tau_\gamma) \geq v_* - \gamma$ . Then

$$v_* - \gamma \leq v(\tau_\gamma) \leq v^\varepsilon(\tau_\gamma) + \sqrt{C\varepsilon} \leq v_*^\varepsilon + \sqrt{C\varepsilon},$$

so  $v_* - v_*^\varepsilon \leq \sqrt{C\varepsilon}$  as  $\gamma \rightarrow 0$ . The inequality  $v_*^\varepsilon - v_* \leq \sqrt{C\varepsilon}$  is shown mutatis mutandis.  $\square$

Fig. 16 displays the optimal value of (95) as function of  $\varepsilon$  in the case  $\mathcal{T} = \{1\}$  and  $\mathcal{T} = [0, 1]$ . The highest value from Table 3 using the least square Monte Carlo approach is also reported. We use the inspection strategy laid out in Section 7.3 to estimate the value in the case  $\mathcal{T} = [0, 1]$ . Note that the early exercise premium (spread between the magenta and blue lines) is significant and increases as the corridor width shrinks to zero. This is because peaks in the local time field  $x \mapsto L_t^x$  can be captured more accurately as  $\varepsilon$  gets smaller.

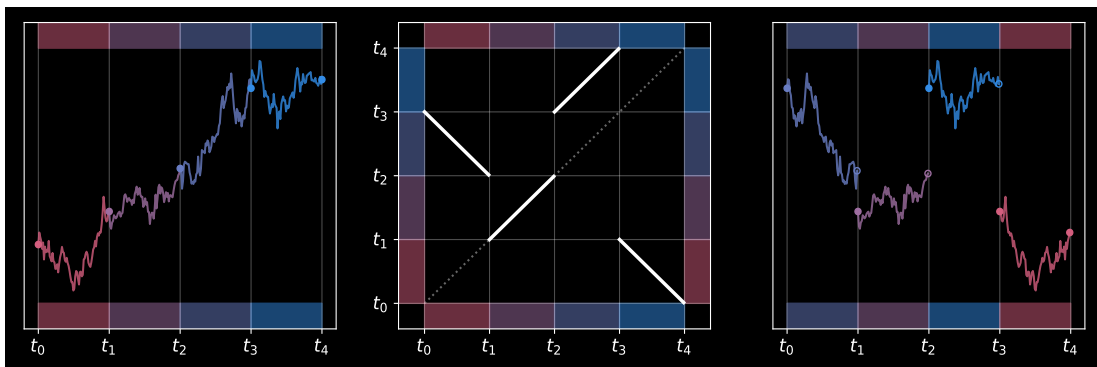
## A Chronology Invariance

Intuitively, the chronology of a path has no impact on its calendar time occupation measure. Indeed, given  $A \in \mathcal{B}(\mathbb{R})$  and  $T > 0$ , then  $\tilde{\mathcal{O}}_T(A)$ , tells us how much time  $X$  has spent in  $A$  up to  $T$ , but not *when*. We can therefore "shuffle" pieces of the path while leaving the occupation measure unchanged. This invariance carries over to occupation functionals  $f(\tilde{\mathcal{O}}_T)$ . We here provide some insights by adopting the pathwise setting from Section 3.2.1. Let  $\Omega_T = \{\omega : [0, T] \rightarrow \mathbb{R}, \text{càdlàg}\}$  as in Section 3.2.1, and  $\text{Sym}(A)$  denote the symmetric group of some arbitrary set  $A$ . Consider the partition  $\{t_n = \frac{nT}{N} : n = 0, \dots, N\}$  of  $[0, T]$  and the subgroup  $\mathfrak{S}_T^N$  of  $(\text{Sym}([0, T]), \circ)$  containing the time permutations

$$\psi(s) = t_{\sigma(n)-\xi_n^+} + \xi_n(s - t_{n-1}), \quad t \in I_n := [t_{n-1}, t_n] \quad (I_N = [t_{N-1}, T]), \quad (101)$$

where  $\xi \in \{\pm 1\}^N$  and  $\sigma \in \text{Sym}(\{1, \dots, N\})$ . The transformations consists of two steps: (i) permute the intervals  $I_n$  according to  $\sigma$  (ii) use  $\xi_n$  to determine if the restriction  $\omega|_{I_{\sigma(n)}}$  is run forward ( $\xi_n = 1$ ) or backward ( $\xi_n = -1$ ). See Fig. 17. Next, consider the action  $(\psi, \omega) \mapsto \omega \circ \psi \in \Omega_T$  and set also  $\mathfrak{S}_T := \bigcup_{N \geq 1} \mathfrak{S}_T^N$ .

Figure 17: Original path  $\omega$  (left), time permutation  $\psi$  defined in (101) with  $\xi = (-1, 1, 1, -1)$  and  $\sigma((1, 2, 3, 4)) = (3, 2, 4, 1)$  (middle) and transformed path  $\omega \circ \psi$  (right).



**Definition 4.** A path functional  $f : \Omega_T \rightarrow \mathbb{R}$  is called *chronology-invariant* if  $f(\omega \circ \psi) = f(\omega)$  for all  $\omega \in \Omega_T$ ,  $\psi \in \mathfrak{S}_T$ .

The next Theorem finally connects chronology invariance functionals with occupation functionals.

**Theorem A.1.** *The following are equivalent:*

- I.  $f : \Omega_T \rightarrow \mathbb{R}$  is chronology-invariant.
- II. There exists  $f : \mathcal{M} \rightarrow \mathbb{R}$  such that  $f(\omega) = f(\tilde{\mathcal{O}}_T(\omega))$ .

In finance, the above equivalence comes as a useful tool to check if an exotic payoff is function of the calendar time occupation measure; see Section 4.1.

*Proof.* Clearly, II. implies I. as the occupation measure is chronology invariant. For completeness, fix  $\omega \in \Omega_T$ ,  $\psi \in \mathfrak{S}_T^N$  with permutation  $\sigma$  and sign vector  $\xi \in \{\pm 1\}^N$ . First, we may assume that  $\xi_n = 1$  for all  $n$  as clearly  $\tilde{\mathcal{O}}_T(\overleftarrow{\omega}) = \tilde{\mathcal{O}}_T(\omega)$ , where  $\overleftarrow{\omega}_t := \omega_{T-t}$ . From the additivity of  $\tilde{\mathcal{O}}_T$ , we conclude that

$$\tilde{\mathcal{O}}_T(\omega \circ \psi) = \sum_{n=1}^N \int_{I_n} \delta_{\omega_{\psi(s)}} ds = \sum_{n=1}^N \int_{I_{\sigma(n)}} \delta_{\omega_s} ds = \tilde{\mathcal{O}}_T(\omega).$$

To prove I.  $\implies$  II. , introduce the equivalence relation

$$\omega \sim \omega' \iff \tilde{\mathcal{O}}_T(\omega) = \tilde{\mathcal{O}}_T(\omega').$$

We then construct a representative for the equivalence classes in  $\Omega_T / \sim$  by characterizing the pre-image of  $\tilde{\mathcal{O}}_T : \Omega_T \rightarrow \mathcal{M}$ . Given  $\mathfrak{o} = \tilde{\mathcal{O}}_T(\omega) \in \mathcal{M}$  for some  $\omega \in \Omega_T$ , let  $\omega^\circ \in \Omega_T$  defined as

$$\omega_t^\circ = \sup\{x \in \mathbb{R} : \mathfrak{o}((-\infty, x]) \leq t\}, \quad t \leq T. \quad (102)$$

Noting  $\omega_t^\circ \leq x \iff \mathfrak{o}((-\infty, x]) \geq t$  by construction, it is then easily seen that  $\tilde{\mathcal{O}}_T(\omega^\circ) = \mathfrak{o}$ . We can therefore define the representation map  $\mathcal{R} : \mathcal{M} \rightarrow \Omega_T / \sim$ ,  $\mathcal{R}(\mathfrak{o}) = \omega^\circ$  and projection  $\pi : \Omega_T \rightarrow \Omega_T / \sim$  as  $\pi = \mathcal{R} \circ \tilde{\mathcal{O}}_T$ . In short,

$$\pi : \Omega_T \ni \omega \xrightarrow{\tilde{\mathcal{O}}_T} \mathfrak{o} \xrightarrow{\mathcal{R}} \omega^\circ \in \Omega_T / \sim.$$

Next, fix a chronology-invariant functional  $f : \Omega_T \rightarrow \mathbb{R}$  and  $\omega \in \Omega_T$ . If  $\omega$  is constant in each subinterval of the partition  $\{\frac{nt}{N} : n \leq N\}$  for some  $N \in \mathbb{N}$ , then  $\mathfrak{o} = \tilde{\mathcal{O}}_T(\omega)$  is a discrete measure so the representative  $\omega^\circ$  is piecewise constant as well. Thus, there exists a sorting permutation  $\psi \in \mathfrak{S}_T^N$  such that  $\omega \circ \psi$  is non-decreasing, and as  $\tilde{\mathcal{O}}_T(\omega \circ \psi) = \tilde{\mathcal{O}}_T(\omega) = \mathfrak{o}$ , we gather that  $\pi(\omega) = \omega^\circ = \omega \circ \psi$ . For general càdlàg  $\omega$ , the same reasoning can be applied by first taking a piecewise constant approximation of  $\omega$  as seen in Section A, followed by a passage to the limit. To conclude, set  $f := f \circ \mathcal{R} : \mathcal{M} \rightarrow \mathbb{R}$ ,  $\omega \in \Omega$ , and  $\psi \in \mathfrak{S}_T$  such that  $\pi(\omega) = \omega \circ \psi$ . Hence,

$$f(\tilde{\mathcal{O}}_T(\omega)) = (f \circ \mathcal{R} \circ \tilde{\mathcal{O}}_T)(\omega) = (f \circ \pi)(\omega) = f(\omega \circ \psi) = f(\omega).$$

□

## B Proofs

### B.1 Theorem 3.1

*Proof.* Let  $\Pi^N = \{s = t_0 < \dots < t_N = t\}$  be a sequence of partitions with mesh size  $\|\Pi^N\| = \max_n(t_{n+1} - t_n)$  decreasing to zero as  $N \rightarrow \infty$ . Writing  $Y_t = f(\mathcal{O}_t, X_t)$ , then,

$$\begin{aligned} Y_t - Y_s &= \sum_{t_n \in \Pi^N} (Y_{t_{n+1}} - Y_{t_n}) \quad (t_{N+1} := t) \\ &= \sum_{t_n \in \Pi^N} (Y_{t_{n+1}} - f(\mathcal{O}_{t_n}, X_{t_{n+1}})) \end{aligned} \quad (103)$$

$$+ \sum_{t_n \in \Pi^N} (f(\mathcal{O}_{t_n}, X_{t_{n+1}}) - Y_{t_n}). \quad (104)$$

From the classical Itô's formula, (104) converges to

$$\int_s^t \partial_x f(\mathcal{O}_u, X_u) dX_u + \int_s^t \frac{1}{2} \partial_{xx} f(\mathcal{O}_u, X_u) d\langle X \rangle_u,$$

since the occupation measure each summand of (104) is "frozen" at time  $t_n$ . We now compute the limit of (103) as  $N \rightarrow \infty$ . In light of the definition of  $\delta_o$  (Definition 2), we set  $\Delta_n = \mathcal{O}_{t_n, t_{n+1}} = \mathcal{O}_{t_{n+1}} - \mathcal{O}_{t_n}$  for simplicity (note that  $\Delta_n$  depends on  $N$ ) and rewrite the summands in (103) as

$$Y_{t_{n+1}} - f(\mathcal{O}_{t_n}, X_{t_{n+1}}) = \int_0^1 \delta_o f(\mathcal{O}_{t_n} + \eta \Delta_n, X_{t_{n+1}}) \cdot \Delta_n d\eta = \delta_o f(\mathcal{O}_{t_n} + \eta_n \Delta_n, X_{t_{n+1}}) \cdot \Delta_n,$$

for some  $\eta_n \in [0, 1]$  by the mean value theorem. Next, the occupation time formula (11) yields

$$\begin{aligned} \sum_{t_n \in \Pi^N} (Y_{t_{n+1}} - f(\mathcal{O}_{t_n}, X_{t_{n+1}})) &= \sum_{t_n \in \Pi^N} \delta_o f(\mathcal{O}_{t_n} + \eta_n \Delta_n, X_{t_{n+1}}) \cdot \Delta_n \\ &= \sum_{t_n \in \Pi^N} \int_{t_n}^{t_{n+1}} \delta_o f(\mathcal{O}_{t_n} + \eta_n \Delta_n, X_{t_{n+1}})(X_u) d\langle X \rangle_u \\ &= \int_s^t Z_u^N d\langle X \rangle_u, \end{aligned}$$

with the step process

$$Z_u^N = \sum_{t_n \in \Pi^N} \delta_o f(\mathcal{O}_{t_n} + \eta_n \Delta_n, X_{t_{n+1}})(X_u) \mathbb{1}_{[t_n, t_{n+1})}(u), \quad [t_N, t_{N+1}) = \{t\}.$$

Recalling that  $\|\Pi^N\| = \max_n(t_{n+1} - t_n)$ , then for every  $n$  and  $u \in [t_n, t_{n+1})$ ,

$$\frac{1}{2} \mathbf{m}_1(\mathcal{O}_u, \mathcal{O}_{t_n} + \eta_n \Delta_n) \leq \frac{\|\mathcal{O}_{t_n, u}\|_1 + \|\Delta_n\|_1}{2} \leq \|\Delta_n\|_1 = \langle X \rangle_{t_{n+1}} - \langle X \rangle_{t_n} \leq \varrho(\|\Pi^N\|),$$

where  $\varrho = \varrho(\omega)$  is the modulus of continuity of  $\langle X \rangle$  on the compact  $[s, t]$ . Similarly,  $|X_u - X_{t_{n+1}}| \leq \rho(\|\Pi^N\|)$  for all  $u \in [t_n, t_{n+1})$ , where  $\rho = \rho(\omega)$  is the modulus of continuity of  $X$  on  $[s, t]$ . Since  $(o, x, y) \mapsto \delta_o f(o, x)(y)$  is jointly continuous and  $\lim_{N \rightarrow \infty} \|\Pi^N\| = 0$ ,

$$Z_u^N \rightarrow Z_u^\infty = \delta_o f(\mathcal{O}_u, X_u)(X_u) = \partial_o f(\mathcal{O}_u, X_u), \text{ uniformly on } [s, t], \mathbb{Q}\text{-a.s.}$$

Hence,  $\lim_{N \rightarrow \infty} \int_s^t Z_u^N d\langle X \rangle_u = \int_s^t \partial_o f(\mathcal{O}_u, X_u) d\langle X \rangle_u$ ,  $\mathbb{Q}$ -a.s. which completes the proof.  $\square$

## B.2 Proposition 4

*Proof.* First, the additivity property of  $\mathcal{O}$  gives

$$\mathcal{O}_T(\omega + h\mathbb{1}_{[t,T]}) = \mathcal{O}_t(\omega) + \int_t^T \delta_{\omega_s+h} ds = \mathcal{O}_t(\omega) + \mathcal{O}_{t,T}^h(\omega), \quad \forall A \in \mathcal{B}(\mathbb{R}),$$

where  $\mathcal{O}_{t,T}^h(\omega)(A) = \mathcal{O}_{t,T}(\omega)(A - h)$ . That is, parallel shifts of  $\omega$  in  $[t, T]$  translate into translations of the increment occupation measure  $\mathcal{O}_{t,T}$ . Writing  $\Delta_{t,T}^h = \mathcal{O}_{t,T}^h - \mathcal{O}_{t,T}$ , then from the definition of  $\delta_{\circ}$  and  $\mathfrak{f}$ , we have

$$\mathfrak{f}(\omega + h\mathbb{1}_{[t,T]}) - \mathfrak{f}(\omega) = \int_0^1 (\delta_{\circ} f(\mathcal{O}_T + \eta \Delta_{t,T}^{t,h}) \cdot \Delta_{t,T}^h)(\omega) d\eta = (\delta_{\circ} f(\mathcal{O}_T + \eta^h \Delta_{t,T}^{t,h}) \cdot \Delta_{t,T}^h)(\omega),$$

for some  $\eta^h \in [0, 1]$ . Formally, note that  $\lim_{h \rightarrow 0} \frac{\Delta_{t,T}^h(A)}{h} = \lim_{h \rightarrow 0} \int_A \frac{L_{t,T}^{x-h} - L_{t,T}^x}{h} dx = - \int_A \partial_x L_{t,T}^x dx$  (omitting the dependence on  $\omega$ ), hence

$$D_t f(\mathcal{O}_T) = - \int_{\mathbb{R}} \delta_{\circ} f(\mathcal{O}_T)(x) \partial_x L_{t,T}^x dx = \int_{\mathbb{R}} \partial_{x_0} f(\mathcal{O}_T, x) L_{t,T}^x dx = \int_t^T \partial_{x_0} f(\mathcal{O}_T, X_s) ds,$$

using integration by parts and the occupation time formula. Although local time of Brownian motion is  $\mathbb{Q}$ -a.s. nowhere differentiable (e.g. as a consequence of the first Ray-Knight theorem [75, Chapter XI]), this heuristics turns out to be correct. Indeed, for all  $\phi \in \mathcal{C}^1(\mathbb{R})$ , we have using the occupation time formula that

$$\frac{1}{h} (\phi \cdot \Delta_{t,T}^h) = \int_t^T \frac{\phi(X_s + h) - \phi(X_s)}{h} ds \longrightarrow \int_t^T \partial_x \phi(X_s) ds.$$

Noting that  $\delta_{\circ} f(\mathcal{O}_T + \eta^h \Delta_{t,T}^h) = \delta_{\circ} f(\mathcal{O}_T) + \varepsilon_h$ ,  $\lim_{h \rightarrow 0} \varepsilon_h = 0$ , we can apply the above limit to  $\phi = \delta_{\circ} f(\mathcal{O}_T) \in \mathcal{C}^1(\mathbb{R})$  and obtain (34).  $\square$

## B.3 Theorem 3.2

*Proof.* The first assertion follows from the fact that  $v(\mathcal{O}, X)$  is an  $(\mathbb{F}, \mathbb{Q})$ -martingale, as a consequence of (35a) and Itô's formula (Theorem 3.1) applied to  $v \in \mathcal{C}^{1,2}(\mathcal{D})$ . Hence  $v(\mathfrak{o}, x) = \mathbb{E}_{\mathfrak{o}, x}^{\mathbb{Q}}[v(\mathcal{O}_T, X_T)]$ , which is (36) in light of the terminal condition (35b).

For the second part, it is enough to verify that  $v \in \mathcal{C}_2^2(\mathcal{D})$  as the uniqueness then follows from the previous assertion. For all  $\mathfrak{o}, \mathfrak{o}' \in \mathcal{M}$ ,  $\Delta = \mathfrak{o}' - \mathfrak{o}$ , and condition (23), observe that

$$\begin{aligned} v(\mathfrak{o}', x) - v(\mathfrak{o}, x) &= \mathbb{E}^{\mathbb{Q}}[\varphi(\mathfrak{o}' + \mathcal{O}_{T-t}^x, x + X_{T-t}) - \varphi(\mathfrak{o} + \mathcal{O}_{T-t}^x, x + X_{T-t})] \\ &= \mathbb{E}^{\mathbb{Q}} \left[ \int_0^1 \delta_{\circ} \varphi(\mathfrak{o} + \mathcal{O}_{T-t}^x + \eta \Delta, x + X_{T-t}) \cdot \Delta d\eta \right] \\ &= \int_0^1 w(\mathfrak{o} + \eta \Delta, x, \cdot) \cdot \Delta d\eta, \end{aligned}$$

$$w(\mathfrak{o}, x, y) = \mathbb{E}^{\mathbb{Q}}[\delta_{\circ} \varphi(\mathfrak{o} + \mathcal{O}_{T-t}^x, x + X_{T-t})(y)].$$

Clearly, the joint continuity of  $(\mathfrak{o}, x, y) \mapsto \delta_{\circ} \varphi(\mathfrak{o}, x)(y)$  carries over to  $w$ . Moreover, defining  $C := \sup_{(\mathfrak{o}, x) \in \mathcal{D}, y \in \mathbb{R}} \frac{|\delta_{\circ} \varphi(\mathfrak{o}, x)(y)|}{1 + |y|^2}$  which is finite as  $\varphi \in \mathcal{C}_2^2(\mathcal{D})$ , we have from Jensen's inequality

that  $|w(\mathbf{o}, x, y)| \leq C(1 + |y|^2)$ , uniformly in  $(\mathbf{o}, x)$ . Hence  $\delta_{\mathbf{o}}v = w$  in light of Definition 2, which implies that  $v \in \mathcal{C}^{1,0}(\mathcal{D})$ . Next, it is easily seen that

$$\delta_{\mu\mu}v(\mathbf{o}, x)(y, y') = \delta_{\mathbf{o}}w(\mathbf{o}, x, y)(y') = \mathbb{E}^{\mathbb{Q}}[\delta_{\mu\mu}\varphi(\mathbf{o} + \mathcal{O}_{T-t}^x, x + X_{T-t})(y, y')],$$

which is, similar to  $\varphi$ , continuous in  $(\mathbf{o}, x)$ , twice differentiable with respect to  $(y, y')$  and satisfies the quadratic growth condition II. in Definition 2 (with respect to  $y'$ ).

Moving to the space derivatives, observe that for every  $f \in \mathcal{C}^1(\mathcal{M})$  such that  $y \mapsto \delta_{\mathbf{o}}f(\mathbf{o})(y) \in \mathcal{C}^1(\mathbb{R})$ , we have  $\frac{d}{dh}f(\mathbf{o} + \mathcal{O}_s^{x+h}) = \partial_y\delta_{\mathbf{o}}f(\mathbf{o} + \mathcal{O}_s^x) \cdot \mathcal{O}_s^x$  using similar arguments as in the proof of Proposition 4; see Section B.2. Thus, the chain rule and bounded convergence theorem yields

$$\partial_x v(\mathbf{o}, x) = \underbrace{\mathbb{E}^{\mathbb{Q}}[\partial_x\varphi(\mathbf{o} + \mathcal{O}_{T-t}^x, x + X_{T-t})]}_{=: w_1^{\varphi}(\mathbf{o}, x)} + \underbrace{\mathbb{E}^{\mathbb{Q}}[\partial_y\delta_{\mathbf{o}}\varphi(\mathbf{o} + \mathcal{O}_{T-t}^x, x + X_{T-t}) \cdot \mathcal{O}_{T-t}^x]}_{=: w_2^{\varphi}(\mathbf{o}, x)},$$

which is jointly continuous. Next, it is immediate that  $\partial_x w_1^{\varphi} = w_1^{\partial_x\varphi} + w_2^{\partial_x\varphi} \in \mathcal{C}(\mathcal{D})$ . For  $w_2^{\varphi}$ , we compute

$$\begin{aligned} \partial_x w_2^{\varphi}(\mathbf{o}, x) &= \mathbb{E}^{\mathbb{Q}}[(\partial_x + \partial_y)\partial_y\delta_{\mathbf{o}}\varphi(\mathbf{o} + \mathcal{O}_{T-t}^x, x + X_{T-t}) \cdot \mathcal{O}_{T-t}^x], \\ &\quad + \mathbb{E}^{\mathbb{Q}}[\partial_{y'y}\delta_{\mu\mu}\varphi(\mathbf{o} + \mathcal{O}_{T-t}^x, x + X_{T-t}) \cdot (\mathcal{O}_{T-t}^x \otimes \mathcal{O}_{T-t}^x)] \end{aligned}$$

where  $\phi \cdot (\mathbf{o} \otimes \mathbf{o}') = \int_{\mathbb{R}^2} \phi(y, y')\mathbf{o}(dy)\mathbf{o}'(dy')$ ,  $\phi : \mathbb{R}^2 \rightarrow \mathbb{R}$ , and using [21, Lemma 2.2.4.] to rewrite  $\partial_{y'y}\delta_{\mathbf{o}}\partial_y\delta_{\mathbf{o}}$  more compactly as  $\partial_{y'y}\delta_{\mu\mu}$ . Given our assumptions on  $\varphi$ , we conclude that  $\partial_x w_2^{\varphi} \in \mathcal{C}(\mathcal{D})$  and thus  $v \in \mathcal{C}^2(\mathcal{D})$ .  $\square$

#### B.4 Theorem 3.3

*Proof.* We use a fixed point argument similar to [75, Chapter IX]. Let  $\mathcal{R}$  consist of all the pairs  $(\mathcal{O}, X)$ , where  $\mathcal{O}$  (resp.  $X$ ) is a continuous measure-valued (resp. real-valued)  $\mathbb{F}$ -adapted process. Note that  $\mathcal{O}$  need not be the occupation flow of  $X$ . Moreover, let  $\|\mathcal{O}\|_t := \|\mathcal{O}_t^*\|_{L^2(\mathbb{Q})}$ ,  $X_t^* = \sup_{s \in [0, t]} |X_s|$ , and define the unit ball  $\mathcal{R}_1 \subset \mathcal{R}$  as

$$(\mathcal{O}, X) \in \mathcal{R}_1 \iff \|(\mathcal{O}, X)\| := \|\varrho(\mathcal{O}, X)\|_T \leq 1, \quad (105)$$

with  $\varrho(\mathcal{O}, X) = (\varrho(\mathcal{O}_t, X_t))_{t \in [0, T]}$ . Next, set  $\mathcal{O}_0 = X_0 = 0$  in (39a)–(39a) for simplicity and introduce the map  $\Psi = (\Psi_{\mathbf{o}}, \Psi_x) : \mathcal{R} \rightarrow \mathcal{R}$ , with

$$\begin{aligned} \Psi_{\mathbf{o}}(\mathcal{O}, X)_t &= \int_0^t \delta_{X_s}\sigma(\mathcal{O}_s, X_s)^2 ds \in \mathcal{M}, \\ \Psi_x(\mathcal{O}, X)_t &= \int_0^t b(\mathcal{O}_s, X_s) ds + \int_0^t \sigma(\mathcal{O}_s, X_s) dW_s. \end{aligned}$$

We show that  $\Psi$  admits a unique fixed point in  $\mathcal{R}_1$  using the contraction mapping theorem. *Step 1* ( $\Psi(\mathcal{R}_1) \subseteq \mathcal{R}_1$ ). Let  $(\mathcal{O}, X) \in \mathcal{R}_1$  and write  $(\bar{\mathcal{O}}, \bar{X}) = \Psi(\mathcal{O}, X)$ . If  $f_t = f(\mathcal{O}_t, X_t)$ ,  $f \in \{b, \sigma\}$ , we obtain from Cauchy-Schwarz inequality that  $\frac{1}{2}|\bar{X}_t|^2 \leq t \int_0^t b_s^2 ds + M_t^2$ , where  $M_t := \int_0^t \sigma_s dW_s$  is a true martingale due to the growth condition (41) satisfied by  $\sigma$ . Hence

$\|M\|_T \leq 2\|M_T\|_{L^2(\mathbb{Q})}$  from Doob's inequality. Next, Itô isometry gives

$$\begin{aligned} \frac{1}{2}\|\bar{X}\|_T^2 &\leq \left\| \sup_{t \in [0, T]} \int_0^t b_s^2 ds \right\|_{L^2(\mathbb{Q})}^2 + 4\|M_T\|_{L^2(\mathbb{Q})}^2 \\ &\leq \int_0^T \left[ T\|b_t\|_{L^2(\mathbb{Q})}^2 + 8\|\sigma_t\|_{L^2(\mathbb{Q})}^2 \right] dt \\ &\leq K^2(T+8) \int_0^T (1 + \|\varrho(\mathcal{O}_t, X_t)\|_{L^2(\mathbb{Q})}^2) dt \\ &\leq K^2 T(T+8)(1 + \|(\mathcal{O}, X)\|^2), \end{aligned}$$

using that  $\|\sigma_t\|_{L^2(\mathbb{Q})}^2 \leq K^2(1 + \|\varrho(\mathcal{O}_t, X_t)\|_{L^1(\mathbb{Q})}) \leq 2K^2(1 + \|\varrho(\mathcal{O}_t, X_t)\|_{L^2(\mathbb{Q})}^2)$ , which follows from (41) and the elementary inequality  $1 + \rho \leq 2(1 + \rho^2)$ . Recalling that  $\|(\mathcal{O}, X)\| \leq 1$ , we thus obtain  $\|\bar{X}\|_T^2 \leq 4K^2 T(T+8)$ . Next, observe that  $\sup_{t \in [0, T]} |\bar{\mathcal{O}}_t|_{\text{BL}} = |\bar{\mathcal{O}}_T|_{\text{BL}}$  since the flow  $\bar{\mathcal{O}}$  is nonnegative and nondecreasing. Then, for a bounded Lipschitz function  $\phi$  with  $\|\phi\|_{\text{BL}} \leq 1$ , the occupation time formula (11) and (41) yield

$$\phi \cdot \bar{\mathcal{O}}_T = \int_0^T \phi(X_t) \sigma_t^2 dt \leq K^2 \|\phi\|_{\infty} \int_0^T (1 + \varrho(\mathcal{O}_t, X_t)) dt,$$

$$\implies |\mathcal{O}_T|_{\text{BL}} = \sup\{\phi \cdot \bar{\mathcal{O}}_T : \|\phi\|_{\text{BL}} \leq 1\} \leq K^2 \int_0^T (1 + \varrho(\mathcal{O}_t, X_t)) dt.$$

Thus  $\| |\mathcal{O}_T|_{\text{BL}} \|_{L^1(\mathbb{Q})} \leq 2K^2 T$ , and  $\Psi(\mathcal{R}_1) \subseteq \mathcal{R}_1$  for all  $T$  that satisfies  $C_1(T) := 2K^2 T(2T + 17) \leq 1$ .

*Step 2* (Contraction property of  $\Psi$ ). Let  $(\mathcal{O}, X), (\mathcal{O}', X') \in \mathcal{R}_1$  and write  $(\bar{\mathcal{O}}, \bar{X}) = \Psi(\mathcal{O}, X)$ ,  $(\bar{\mathcal{O}}', \bar{X}') = \Psi(\mathcal{O}', X')$ . Using condition (42), then

$$\begin{aligned} \frac{1}{2}\|\bar{X} - \bar{X}'\|_T^2 &\leq \int_0^T T\|b_t' - b_t\|_{L^2(\mathbb{Q})}^2 + 4\|\sigma_t' - \sigma_t\|_{L^2(\mathbb{Q})}^2 dt \\ &\leq K^2 T(T+4)\|(\mathcal{O}' - \mathcal{O}, X' - X)\|^2. \end{aligned}$$

We now provide an estimate of  $|\bar{\mathcal{O}}_t' - \bar{\mathcal{O}}_t|_{\text{BL}}$ . For any bounded Lipschitz function  $\phi$  such that  $\|\phi\|_{\text{BL}} \leq 1$ , the occupation time formula (11) yields

$$\phi \cdot (\bar{\mathcal{O}}_t' - \bar{\mathcal{O}}_t) = \int_0^t (\phi(X_s')(\sigma_s')^2 - \phi(X_s)\sigma_s^2) ds \leq \int_0^t \left| \phi(X_s')(\sigma_s')^2 - \phi(X_s)\sigma_s^2 \right| ds.$$

Moreover, the conditions (41)–(42) give for all  $(\mathfrak{o}, x), (\mathfrak{o}', x') \in \mathcal{D}$ ,

$$\begin{aligned} \frac{|\phi(x')\sigma(\mathfrak{o}', x')^2 - \phi(x)\sigma(\mathfrak{o}, x)^2|}{\varrho(\mathfrak{o}' - \mathfrak{o}, x' - x)} &\leq \underbrace{\frac{|\phi(x') - \phi(x)|}{|x' - x|}}_{\leq 1} |\sigma(\mathfrak{o}', x')|^2 \\ &\quad + \underbrace{|\phi(x)|}_{\leq 1} \frac{|\sigma(\mathfrak{o}', x')^2 - \sigma(\mathfrak{o}, x)^2|}{\varrho(\mathfrak{o}' - \mathfrak{o}, x' - x)} \\ &\leq K^2(1 + \varrho(\mathfrak{o}', x')) + K(|\sigma(\mathfrak{o}', x')| + |\sigma(\mathfrak{o}, x)|) \\ &\leq K^2 \underbrace{[3 + 2\varrho(\mathfrak{o}', x') + \varrho(\mathfrak{o}, x)]}_{=: \Xi(\mathfrak{o}, \mathfrak{o}', x, x')} \end{aligned}$$

using the coarse estimate  $\sqrt{1+\varrho} \leq 1+\varrho$  in the last inequality. Defining  $\xi_s := \Xi(\mathcal{O}'_s, \mathcal{O}_s, X'_s, X_s)$ ,  $\varrho_s := \varrho(\mathcal{O}'_s - \mathcal{O}_s, X'_s - X_s)$ , then

$$|\bar{\mathcal{O}}'_t - \bar{\mathcal{O}}_t|_{\text{BL}} \leq \int_0^t \xi_s \varrho_s ds \leq T \xi^* \varrho^*,$$

with  $\xi^* = \sup_{t \in [0, T]} \xi_t$  and similarly for  $\varrho^*$ . Since  $(\mathcal{O}, X), (\mathcal{O}', X') \in \mathcal{R}_1$ , we obtain that  $\|\xi^*\|_{L^2(\mathbb{Q})}^2 \leq 3K^4 [9 + 4\|(\mathcal{O}', X')\|^2 + \|(\mathcal{O}, X)\|^2] \leq 42K^4$ , hence

$$\frac{1}{T} \mathbb{E}^{\mathbb{Q}} \left[ \sup_{t \in [0, T]} |\bar{\mathcal{O}}'_t - \bar{\mathcal{O}}_t|_{\text{BL}} \right] \leq \|\xi^*\|_{L^2(\mathbb{Q})} \|\varrho^*\|_{L^2(\mathbb{Q})} \leq \sqrt{42} K^2 \|(\mathcal{O}' - \mathcal{O}, X' - X)\|.$$

Altogether, we conclude that  $\|\Psi(\mathcal{O}', X') - \Psi(\mathcal{O}, X)\|^2 \leq C_2(T) \|(\mathcal{O}', X') - (\mathcal{O}, X)\|$ , with  $C_2(T) = K^2 T(T + 4 + \sqrt{42}) < C_1(T)$ . When  $C_1(T) < 1$ ,  $\Psi$  is thus a contraction from  $\mathcal{R}_1$  into itself and admits a unique fixed point, i.e., a strong solution of (39a)–(39b). When  $C_1(T) \geq 1$ , we split  $[0, T]$  into  $N \in \mathbb{N}$  intervals of length  $\delta T = \frac{T}{N}$  with  $C_1(\delta T) < 1$  and successively concatenate the strong solutions from each interval.  $\square$

## B.5 Proposition 7

*Proof.* Let  $\overleftarrow{X}_s = X_{T-s} - X_T$  and denote its flow of occupation measures by  $\overleftarrow{\mathcal{O}}$  and local time field by  $\overleftarrow{L}$ . Then,  $L_T^{X_T+z} = \overleftarrow{L}_T^z$  for all  $z \in \mathbb{R}$ , which implies that

$$\varphi^\varepsilon(\mathcal{O}_T, X_T) = \int_{B_\varepsilon} L_T^{X_T+z} dz = \int_{B_\varepsilon} \overleftarrow{L}_T d\lambda = \varphi^\varepsilon(\overleftarrow{\mathcal{O}}_T, 0).$$

Thus,

$$v^\varepsilon(T) = \mathbb{E}^{\mathbb{Q}}[\varphi^\varepsilon(\overleftarrow{\mathcal{O}}_T, 0)] = \int_{B_\varepsilon} \mathbb{E}^{\mathbb{Q}}[\overleftarrow{L}_T] d\lambda = \int_{[0, \varepsilon]} \mathbb{E}^{\mathbb{Q}}[L_T^x] dx \uparrow \mathbb{E}^{\mathbb{Q}}[L_T^0],$$

where we used that  $\text{Law}_{\mathbb{Q}}(\overleftarrow{L}_T^x) = \text{Law}_{\mathbb{Q}}(L_T^x)$  and  $\partial_x \mathbb{E}^{\mathbb{Q}}[L_T^x] < 0 \ \forall x > 0$  to prove the monotone convergence. Finally, recall from Proposition 6 that  $\mathbb{E}^{\mathbb{Q}}[L_T^0] = v(T)$ . For the second assertion, notice from Tanaka's formula that  $\mathbb{E}^{\mathbb{Q}}[L_T^x] = 2c(T, x)$ , where  $c(T, x) = \mathbb{E}^{\mathbb{Q}}[(X_T - x)^+]$  is the price of a call option struck at  $x$  with maturity  $T$  in a Bachelier model with unit volatility. Similar to [19], we have  $\partial_x c(T, x) = \mathbb{Q}(X_T \leq x) - 1 = \Phi_T(x) - 1$  and  $\partial_{xx} c(T, x) = \phi_T(x)$ , where  $\Phi_T, \phi_T$  is the CDF and PDF of  $\mathcal{N}(0, T)$ , respectively. Hence, a second order Taylor expansion of  $x \mapsto c(T, x)$  at  $x = 0$  yields

$$v^\varepsilon(T) = \frac{2}{\varepsilon} \int_0^\varepsilon c(T, x) dx = v(T) - \frac{\varepsilon}{2} + \frac{\varepsilon^2/3}{\sqrt{2\pi T}}(1 + r_\varepsilon), \quad \lim_{\varepsilon \downarrow 0} r_\varepsilon = 0.$$

$\square$

## B.6 Proposition 8

*Proof.* For every stopping time  $\tau \in \vartheta(\mathcal{T})$ ,  $x \in \mathbb{R}$ , we have by Jensen's inequality that

$$|\varphi^\varepsilon(\mathcal{O}_\tau, x) - L_\tau^x|^2 = \left| \int_{B_\varepsilon} (L_\tau^{x+z} - L_\tau^x) dz \right|^2 \leq \int_{B_\varepsilon} |L_\tau^{x+z} - L_\tau^x|^2 dz.$$

Moreover, there exists  $C > 0$  (to be determined) such that

$$\left\| \sup_{(t,x) \in [0,T] \times \mathbb{R}} |L_t^{x+z} - L_t^x| \right\|_{L^2(\mathbb{Q})}^2 \leq C|z|, \quad |z| \leq 1.$$

Indeed, writing  $L^x(Y)$  for the local time of some process  $Y$  at  $x$  and  $\|Y\| := \|\sup_{t \in [0,T]} Y_t\|_{L^2(\mathbb{Q})}$ , we can apply Theorem 6.5 in Barlow and Yor [1] with  $\gamma = 2$  to the continuous martingales  $M = X - z$ ,  $N = X$ . This yields

$$\begin{aligned} \left\| \sup_{(t,x) \in [0,T] \times \mathbb{R}} |L_t^{x+z} - L_t^x| \right\|_{L^2(\mathbb{Q})}^2 &= \left\| \sup_{(t,x) \in [0,T] \times \mathbb{R}} |L_t^x(M) - L_t^x(N)| \right\|_{L^2(\mathbb{Q})}^2 \\ &\leq C_2^2 (\|M\| + \|N\|) \underbrace{\|M - N\|}_{=|z|} \max \left( \log \frac{\|M\| + \|N\|}{\|M - N\|}, 1 \right) \\ &\leq 2C|z|, \end{aligned}$$

with  $C = 2C_2^2 \sqrt{T+1} \max(\log 4\sqrt{T+1}/|z|, 1)$ <sup>6</sup> and  $C_2$  as in [1, Theorem 6.5]. Thus,

$$\left\| \varphi^\varepsilon(X_\tau, \mathcal{O}_\tau) - L_\tau^{X_\tau} \right\|_{L^2(\mathbb{Q})}^2 \leq \int_{B_\varepsilon} \left\| L_\tau^{X_\tau+z} - L_\tau^{X_\tau} \right\|_{L^2(\mathbb{Q})}^2 dz \leq 2C \int_{B_\varepsilon} |z| dz = C\varepsilon, \quad \forall \varepsilon \leq 1.$$

The second assertion follows from Jensen's inequality.  $\square$

## C Algorithms

### C.1 Least Square Monte Carlo for Spot Local Time

Algorithm 3 summarizes the Least Square Monte Carlo approach seen in Section 7.3. Notice the exponential transformation of the discrete Brownian in step IV.2. so that all variables are nonnegative. We choose a family of functions on  $\mathbb{R}_+$ , namely the Laguerre polynomials  $(p_k)$ , up to degree 3, which are orthonormal in the weighted Hilbert space  $L^2(\mathbb{R}_+, w d\lambda)$ ,  $w(x) = e^{-x}$ . The basis functions  $\phi_k$  in Algorithm 3 then corresponds to evaluations of the feature variables  $\mathcal{O}_{t_n}^{\bar{m}}, \bar{X}_{t_n}$  through the polynomials. Note that  $p_1(\mathcal{O}_{t_n}^{\bar{m}}) := (p_1(L_{t_n}^{x_{m-\bar{m}}}), \dots, p_1(L_{t_n}^{x_{m+\bar{m}}}))$  contains the intrinsic value  $L_{t_n}^{X_{t_n}}$  itself (up to a constant) which is of course valuable information. One can also choose instead, as in [69], the better-behaved Laguerre polynomials weighted by  $\sqrt{w}$ , yielding similar results.

In both phases, we use antithetic sampling, i.e., we simulate  $X(\omega_j)$  for  $j = 1, \dots, J/2$  (provided that  $J$  is even) and set  $X(\omega_j) = -X(\omega_{j-J/2})$  for  $j = J/2+1, \dots, J$ ,  $J \in \{J_{\text{off}}, J_{\text{on}}\}$ .

<sup>6</sup>note that  $\frac{1}{4}\|N\|^2 \leq \frac{1}{4}\|M\|^2 \leq \|X_T - z\|_{L^2(\mathbb{Q})}^2 = T + |z|^2 \leq T + 1$  using Doob's inequality and  $|z| \leq 1$ . Hence  $\|M\| + \|N\| \leq 4\sqrt{T+1}$ .

**Algorithm 3** (Least Square Monte Carlo, Spot Local Time)

$T > 0$ ,  $N \in \mathbb{N}$ ,  $\bar{m} \ll N$  (truncation level),  $J_{\text{off}}$  (# simulations, offline phase),  $J_{\text{on}}$  (# simulations, online phase),  $\{\phi_k : k = 1, \dots, K\}$  (basis functions)

**OFFLINE**

I. **Space-time grid**  $\begin{cases} t_n = n\delta t, & n = 0, \dots, N, \quad \delta t = \frac{T}{N}, \\ x_m = m\sqrt{3\delta t}, & m = -N, \dots, N \end{cases}$

II. **Generate paths**  $X(\omega_j)$ ,  $j = 1, \dots, J_{\text{off}}$ , where

$$X_{t_{n+1}} = X_{t_n} + Z_{n+1}\sqrt{\delta t}, \quad X_0 = 0, \quad Z_1, \dots, Z_N \stackrel{i.i.d.}{\sim} \nu = \frac{1}{6} \left( \delta_{-\sqrt{3}} + 4\delta_0 + \delta_{\sqrt{3}} \right)$$

III. **Terminal value**  $Y_T = L_T^{X_T} = \frac{1}{2\varepsilon} \sum_{n=1}^N \mathbb{1}_{\{X_{t_n} = X_T\}} \delta t$ ,  $\varepsilon = \frac{x_{m+1} - x_m}{2} = \frac{\sqrt{3\delta t}}{2}$ .

IV. **For**  $n = N - 1, \dots, \bar{m}$ :

1. **Let**  $\mathcal{J} = \{j = 1, \dots, J_{\text{off}} : X_{t_n}(\omega_j) = x_m, |m| \leq n - \bar{m}\}$
2. **Feature variables:**  $\bar{X}_{t_n} = e^{X_{t_n}}$ ,  $\mathcal{O}_{t_n}^{\bar{m}} = (L_{t_n}^{x_{m-\bar{m}}}, \dots, L_{t_n}^{x_{m+\bar{m}}})$ ,  $x_m = X_{t_n}$ .
3. **Regression:**  $\hat{\beta}^n = \operatorname{argmin}_{\beta} \sum_{j \in \mathcal{J}} \left| Y_{t_{n+1}} - \sum_{k=1}^K \beta_k \phi_k(\mathcal{O}_{t_n}^{\bar{m}}, \bar{X}_{t_n}) \right|^2 (\omega_j)$ .
4. **Continuation value:**  $C_{t_n} = \sum_{k=1}^K \hat{\beta}_k^n \phi_k(\mathcal{O}_{t_n}^{\bar{m}}, \bar{X}_{t_n})$ .
5. **Update:**  $Y_{t_n}(\omega_j) = \begin{cases} Y_{t_{n+1}}(\omega_j), & C_{t_n}(\omega_j) > L_{t_n}^{X_{t_n}}(\omega_j) \text{ or } j \notin \mathcal{J}, \\ L_{t_n}^{X_{t_n}}(\omega_j), & \text{otherwise.} \end{cases}$

**ONLINE**

I'. **Generate paths**  $X(\omega_j)$ ,  $j = 1, \dots, J_{\text{on}}$  as in II.

II'. **Repeat** steps III., IV.1, 2, 4, 5 using  $\hat{\beta}^{N-1}, \dots, \hat{\beta}^{\bar{m}}$  from IV.3.

III'. **Return**  $Y_0 = \frac{1}{J_{\text{on}}} \sum_{j=1}^{J_{\text{on}}} Y_{t_1}(\omega_j)$ .

**References**

- [1] M. Barlow and M. Yor. Semi-martingale inequalities via the Garsia-Rodemich-Rumsey lemma, and applications to local times. *Journal of Functional Analysis*, 49(2):198–229, 1982.
- [2] C. Bayer, P. P. Hager, S. Riedel, and J. Schoenmakers. Optimal stopping with signatures. *The Annals of Applied Probability*, 33(1):238 – 273, 2023.
- [3] E. Bayraktar, Q. Feng, and Z. Zhang. Deep signature algorithm for multidimensional path-dependent options. *SIAM Journal on Financial Mathematics*, 15(1):194–214, 2024.
- [4] S. Becker, P. Cheridito, and A. Jentzen. Deep optimal stopping. *Journal of Machine Learning Research*, 20(74):1–25, 2019.

- [5] S. Ben Hamida and R. Cont. Recovering volatility from option prices by evolutionary optimization. *Journal of Computational Finance*, 8(4):43–76, 1997. ISSN 1755-2850.
- [6] M. Benaïm and O. Raimond. Self-interacting diffusions II: convergence in law. *Annales de l'Institut Henri Poincaré (B) Probability and Statistics*, 39(6):1043–1055, 2003.
- [7] M. Benaïm and O. Raimond. Self-interacting diffusions. III. symmetric interactions. *The Annals of Probability*, 33(5):1716–1759, 2005.
- [8] M. Benaïm and O. Raimond. Self-interacting diffusions IV: Rate of convergence. *Electronic Journal of Probability*, 16:1815–1843, 2011.
- [9] M. Benaïm, M. Ledoux, and O. Raimond. Self-interacting diffusions. *Probability Theory and Related Fields*, 122:1–41, 2002.
- [10] L. Bergomi. *Stochastic Volatility Modeling*. Chapman and Hall/CRC Financial Mathematics Series. CRC Press, 2016.
- [11] C. Bernard and Z. Cui. Pricing timer options. *Journal of Computational Finance*, 15, 08 2010.
- [12] L. Béthencourt, R. Catellier, and E. Tanré. Brownian particles controlled by their occupation measure. *SIAM Journal on Control and Optimization*, 63(2):1286–1313, 2025.
- [13] A. G. Bhatt and V. S. Borkar. Occupation measures for controlled markov processes: Characterization and optimality. *The Annals of Probability*, 24(3):1531–1562, 1996.
- [14] R. M. Blumenthal and R. K. Gettoor. Local times for markov processes. *Zeitschrift für Wahrscheinlichkeitstheorie und Verwandte Gebiete*, 3:50–74, 1964.
- [15] O. Bonesini, A. Jacquier, and C. Lacombe. A theoretical analysis of Guyon’s toy volatility model. *SIAM Journal on Financial Mathematics*, 16(2):271–309, 2025.
- [16] G. P. Boswell and F. A. Davidson. Modelling hyphal networks. *Fungal Biology Reviews*, 26(1):30–38, 2012. ISSN 1749-4613. Hyphal networks: mechanisms, modelling and ecology.
- [17] B. Bouchard and X. Tan. On the regularity of solutions of some linear parabolic path-dependent PDEs. *arXiv:2310.04308*, 2023.
- [18] G. Bouveret, R. Dumitrescu, and P. Tankov. Mean-field games of optimal stopping: A relaxed solution approach. *SIAM Journal on Control and Optimization*, 58(4):1795–1821, 2020.
- [19] D. T. Breeden and R. H. Litzenberger. Prices of state-contingent claims implicit in option prices. *The Journal of Business*, 51(4):621–651, 1978.
- [20] G. Brunick and S. Shreve. Mimicking an Itô process by a solution of a stochastic differential equation. *The Annals of Applied Probability*, 23(4):1584 – 1628, 2013.

- [21] P. Cardaliaguet, F. Delarue, J.-M. Lasry, and P.-L. Lions. *The Master Equation and the Convergence Problem in Mean Field Games:(AMS-201)*, volume 201. Princeton University Press, 2019.
- [22] R. Carmona and F. Delarue. *Probabilistic Theory of Mean Field Games with Applications I-II*. Probability Theory and Stochastic Modelling. Springer International Publishing, 2018.
- [23] J.-F. Chassagneux and G. Pagès. Computing the invariant distribution of mckean-vlasov sdes by ergodic simulation. *arXiv:2406.13370*, 2025.
- [24] M. Chesney, M. Jeanblanc-Picqué, and M. Yor. Brownian excursions and Parisian barrier options. *Advances in Applied Probability*, 29(1):165–184, 1997.
- [25] R. Cont. Functional Itô calculus and functional Kolmogorov equations. In V. Bally, L. Caramellino, and R. Cont, editors, *Stochastic Integration by Parts and Functional Itô Calculus*. Advanced Courses in Mathematics - CRM Barcelona, Birkauer, 2016.
- [26] R. Cont and D.-A. Fournié. Change of variable formulas for non-anticipative functionals on path space. *Journal of Functional Analysis*, 259(4):1043–1072, 2010.
- [27] A. M. G. Cox and S. Källblad. Model-independent bounds for asian options: A dynamic programming approach. *SIAM Journal on Control and Optimization*, 55(6):3409–3436, 2017.
- [28] A. M. G. Cox, S. Källblad, M. Larsson, and S. Svaluto-Ferro. Controlled measure-valued martingales: a viscosity solution approach. *arXiv:2109.00064*, 2021.
- [29] M. Cranston and Y. Le Jan. Self attracting diffusions: Two case studies. *Mathematische Annalen*, 303:87–93, 1995. doi: 10.1007/BF01460980.
- [30] C. Cuchiero, M. Larsson, and S. Svaluto-Ferro. Probability measure-valued polynomial diffusions. *Electronic Journal of Probability*, 24:1 – 32, 2019.
- [31] C. Cuchiero, F. Guida, L. di Persio, and S. Svaluto-Ferro. Measure-valued affine and polynomial diffusions. *arXiv:2112.15129*, 2021.
- [32] D. A. Dawson. Stochastic evolution equations and related measure processes. *Journal of Multivariate Analysis*, 5(1):1–52, 1975.
- [33] D. A. Dawson. Measure-valued Markov processes. In *École d’Été de Probabilités de Saint-Flour XXI—1991*, volume 1541 of *Lecture Notes in Math.*, pages 1–260. Springer, Berlin, 1993.
- [34] J. Detemple. *American-Style Derivatives: Valuation and Computation*. Chapman and Hall/CRC Financial Mathematics Series. CRC Press, 2005.
- [35] G. Di Nunno, B. Øksendal, and F. Proske. *Malliavin Calculus for Lévy Processes with Application to Finance*. Springer, 2009.
- [36] M. Dixon, I. Halperin, and P. Bilokon. *Machine Learning in Finance: From Theory to Practice*. Springer International Publishing, 2020. ISBN 9783030410674.

- [37] K. Du, Y. Jiang, and J. Li. Empirical approximation to invariant measures for McKean–Vlasov processes: Mean-field interaction vs self-interaction. *Bernoulli*, 29(3):2492–2518, Aug. 2023.
- [38] B. Dupire. Pricing with a smile. *Risk*, 7(1), 1994.
- [39] B. Dupire. A unified theory of volatility. In P. Carr, editor, *Derivatives Pricing: The Classic Collection*. Risk Books, London, 2004. Reprint of a 1996 working paper from Paribas Capital Markets.
- [40] B. Dupire. Functional Itô calculus. *SSRN*, 2009. Republished in *Quantitative Finance*, 19(5):721–729, 2019.
- [41] R. Durrett and L. Rogers. Asymptotic behavior of Brownian polymers. *Probability Theory and Related Fields*, 92(3):337–349, 1992.
- [42] W. E, J. Han, and A. Jentzen. Deep learning-based numerical methods for high-dimensional parabolic partial differential equations and backward stochastic differential equations. *Commun. Math. Stat.*, 5, 2017.
- [43] W. E, J. Han, and A. Jentzen. Solving high-dimensional partial differential equations using deep learning. *Proc. Natl. Acad. Sci.*, 115(34), 2018.
- [44] I. Ekren, C. Keller, N. Touzi, and J. Zhang. On viscosity solutions of path dependent PDEs. *The Annals of Probability*, 42(1):204 – 236, 2014.
- [45] W. H. Fleming and H. M. Soner. *Controlled Markov Processes and Viscosity Solutions*, volume 25 of *Stochastic Modelling and Applied Probability*. Springer, 2 edition, 2006.
- [46] W. H. Fleming and D. Vermes. Generalized solutions in the optimal control of diffusions. *stochastic control theory and applications (Minneapolis, Minn., 1986)*, pages 119–127, 1988.
- [47] W. H. Fleming and M. Viot. Some measure-valued Markov processes in population genetics theory. *Indiana University Mathematics Journal*, 28(5):817–843, 1979.
- [48] P. K. Friz and J. Gatheral. The forest expansion of forward variance models. In C. Bayer, P. K. Friz, M. Fukasawa, J. Gatheral, A. Jacquier, and M. Rosenbaum, editors, *Rough Volatility*, pages 183–198. SIAM, 2023. doi: 10.1137/1.9781611977783.ch9. URL <https://epubs.siam.org/doi/10.1137/1.9781611977783.ch9>.
- [49] J. Gatheral and M. Keller-Ressel. Affine forward variance models. *Finance and Stochastics*, 23(1):501 – 533, 2019.
- [50] D. Geman and J. Horowitz. Occupation Densities. *The Annals of Probability*, 8(1):1 – 67, 1980.
- [51] P. Glasserman. *Discretization Methods*, pages 339–376. Springer New York, New York, NY, 2003.
- [52] J. Guyon. Path-dependent volatility. *Risk*, 2014.

- [53] J. Guyon. Path-dependent volatility: practical examples. *Global Derivatives Conference*, 2017.
- [54] J. Guyon and P. Henry-Labordère. Being particular about calibration. *Risk*, 25:88–93, January 2012.
- [55] J. Guyon and P. Henry-Labordère. *Nonlinear Option Pricing*. Chapman and Hall/CRC Financial Mathematics Series. CRC Press, 2013.
- [56] J. Guyon and J. Lekeufack. Volatility is (mostly) path-dependent. *Quantitative Finance*, 23(9):1221–1258, 2023.
- [57] S. Haber, P. J. Schönbucher, and P. Wilmott. Pricing parisian options. *The Journal of Derivatives*, 6(3):71–79, 1999.
- [58] L. G. Hanin. An extension of the kantorovich norm. *Contemporary Mathematics*, 226: 113–130, 1999. ISSN 0271-4132.
- [59] D. G. Hobson and L. C. G. Rogers. Complete Models with Stochastic Volatility. *Mathematical Finance*, 8(1):27–48, 1998.
- [60] R. Hu and M. Laurière. Recent developments in machine learning methods for stochastic control and games. *Numerical Algebra, Control and Optimization*, 14(3):435–525, 2024.
- [61] Y. Huang, V. Tisot-Daguette, and X. Zhang. Deep BSDE solver for occupied pricing PDEs. *In preparation*.
- [62] J.-N. Hugonnier. The Feynman–Kac formula and pricing occupation time derivatives. *International Journal of Theoretical and Applied Finance*, 02(02):153–178, 1999.
- [63] C. Huré, H. Pham, and X. Warin. Deep backward schemes for high-dimensional nonlinear pdes. *Mathematics of Computation*, 89(324):1785–1821, 2020. doi: 10.1090/mcom/3514.
- [64] A. Jacquier and M. Oumgari. Deep curve-dependent PDEs for affine rough volatility. *SIAM Journal on Financial Mathematics*, 14(2):353–382, 2023.
- [65] P. Kloeden and E. Platen. *Numerical Solution of Stochastic Differential Equations*. Springer Berlin, 1992.
- [66] J.-M. Lasry and P.-L. Lions. Mean field games. *Japanese Journal of Mathematics*, 2: 229–260, 03 2007.
- [67] R. Lee. Weighted variance swap. *Encyclopedia of Quantitative Finance*, 2010.
- [68] P. Lieberman and A. Omprakash. Corridor variance swaps: A cheaper way to buy volatility? *BNP Paribas, U.S. Equities and Derivatives Strategy*, 2007. White paper.
- [69] F. A. Longstaff and E. S. Schwartz. Valuing American options by simulation: a simple least-squares approach. *The Review of Financial Studies*, 14(1):113–147, 2001.
- [70] R. C. Merton. Theory of rational option pricing. *The Bell Journal of Economics and Management Science*, 4(1):141–183, 1973.

- [71] S. Peng and F. Wang. BSDE, path-dependent PDE and nonlinear Feynman-Kac formula. *Science China Mathematics*, 08 2011.
- [72] G. Peskir and A. Shiryaev. Optimal stopping and free-boundary problems. *Basel: Birkhäuser Verlag*, 2006.
- [73] O. Raimond. Self-attracting diffusions: Case of the constant interaction. *Probability Theory and Related Fields*, 107:177–196, 1997.
- [74] A. Reppen, H. Soner, and Tissot-Daguette. Deep stochastic optimization in finance. *Digital Finance*, 5, 2023.
- [75] D. Revuz and M. Yor. *Continuous Martingales and Brownian Motion*. Springer Berlin, Heidelberg, 1999.
- [76] Y. F. Saporito and Z. Zhang. Path-dependent deep Galerkin method: A neural network approach to solve path-dependent partial differential equations. *SIAM Journal on Financial Mathematics*, 12(3):912–940, 2021.
- [77] N. Sawyer. SG CIB launches timer options. <https://www.risk.net/derivatives/structured-products/1506473/sg-cib-launches-timer-options>, 2007. *Risk*. Accessed 10/25/2023.
- [78] H. M. Soner, V. Tissot-Daguette, and J. Zhang. Controlled occupied processes and viscosity solutions. *arXiv:2411.12080*, 2024.
- [79] M. Talbi, N. Touzi, and J. Zhang. Dynamic programming equation for the mean field optimal stopping problem. *SIAM Journal on Control and Optimization*, 61(4):2140–2164, 2023.
- [80] M. Talbi, N. Touzi, and J. Zhang. Viscosity solutions for obstacle problems on wasserstein space. *SIAM Journal on Control and Optimization*, 61(3):1712–1736, 2023.
- [81] V. Tissot-Daguette. *Free boundaries, functional expansions, and occupied processes*. PhD thesis, Princeton University, 2024. Available at [ProQuest Dissertations & Theses Global](#).
- [82] V. Tissot-Daguette and X. Zhang. Cylindrical projections of occupied diffusions. *In preparation*, 2025.
- [83] M. Tomašević, V. Bansaye, and A. Véber. Ergodic behaviour of a multi-type growth-fragmentation process modelling the mycelial network of a filamentous fungus. *ESAIM: Probability and Statistics*, 26:397–435, 2022.
- [84] F. Viens and J. Zhang. A martingale approach for fractional Brownian motions and related path dependent PDEs. *The Annals of Applied Probability*, 29(6):3489 – 3540, 2019.
- [85] J. Zhang. *Backward Stochastic Differential Equations: From Linear to Fully Nonlinear Theory*. Probability Theory and Stochastic Modelling. Springer New York, 2017.